The Arctic Ocean in a Fresh and Warm Future

Aleksi Nummelin

Dissertation for the degree of Philosophiae Doctor (PhD)

Geophysical Institute
University of Bergen

August 2016

Freshening and warming
dear Arctic
it is the forcing
we saw it coming

Acknowledgements

The work leading to this dissertation would not have been possible without the help, support, and love of several individuals. I would like to thank my family for being supportive throughout the years, and especially I would like to thank Noora for always being there for me, supporting me, but also reminding me that there is life outside academia (who would have thought), and in general for being crazy enough to be with me.

I thank my supervisors Camille, Lars Henrik, and Bjørg. I really appreciated all the freedom I had to explore my own paths, but also your firm guidance when it was needed. Camille, I would like to thank you for showing the open attitude towards all the new science and not just the narrow field of one's own. I think many of the collaborations that were initiated during my PhD owe for that attitude. I would also like to thank you all for introducing me to the fascinating world of paleoclimates. Even though the thesis is rather modern I think the paleo-perspective is a great source of both inspiration and interesting scientific questions for the future.

On the more technical side, several people helped me out with the initial setup of NorESM1-M. Especially, Ingo, Mats, and Mehmet deserve my sincere gratitude. Ingo, the tracers never ended up being in any article (maybe one day), but those really helped my analysis. Mats and Mehmet, I hope my struggle with the heat budget analysis was helpful in terms of the model development.

Erwin, Lisbeth, Marius, Patrik, and Paul deserve a special thanks for reviewing and proofreading the dissertation.

I would also like to thank all the great people who together contribute to the academic environment at the Geophysical Institute and the Bjerknes Centre for Climate Research. I am especially grateful for the amazing PhD community in Bergen – you have made my whole time here in the rainy city such a fun experience. I would also like to thank the gang at SKD aquarium for all those fun days at work. Many people have contributed to different activities without which the whole PhD would have been a very different experience, you know who you are: thanks for all those fun nights with board games; thanks for introducing me to all those German card games and playing Munchkin even if it was not everyone's favorite; thanks for all the adventures: thanks for skiing (and all those car rides), hiking, sailing, and climbing with me; thanks for sharing those university huts as I never got lucky in the lottery; and finally, thanks for all those nights in hot tubs, saunas, dance floors, and other warm places!

In winter 2013-2014 I had the chance to visit McGill University in Montreal, and I would like to thank Bruno Tremblay and the whole sea ice group for making my time so much fun, even though the weather ended up being really cold.

I would also like to thank several people for discussing science with me, special thanks to our Friday discussion group. In addition, Erwin, Tor, Per, and Johan deserve

a special thanks for all those discussions around watermass transformations.

ResClim has supported my travels and brought together an amazing Norwegian wide community of young climate scientist. I am certain that this type of funding really pays off in the future. I am also happy that I had the chance to be part of a growing movement bringing together the Scandinavian wide community of young earth scientists.

Some people make great science, some people make great science possible, and some a bit of both. I would like to thank Kerim, and the rest of ice2ice folks, for trusting a bunch of PhD students and for providing generous funding for us to make the bootcamp idea true. For the people on those sofas that night: I think we started something great! Even though the work is still ongoing I also thank our bootcamp team (Mari, Søren, Eva, Henrik, Bjørg and Andreas) for putting together some really exciting science!

I also thank the Bjerknes Centre for Climate Research for providing funding for me and Erwin to invite Per in Bergen. This is a great opportunity to not only discuss the watermass transformations, but also to look in the bottom of this framework. I am really excited to see what comes out of our collaboration.

Finally, some rather unqualified words about life and philosophy. Even though science is about doing good science, it is also about working with people. I feel that more than finding the right people to work with, science, and life for that matter, is really about opening one's own mind to the people around you. With that, one quickly notices that there are always great people around to live, work, and make great science with.

Abstract

The Arctic Ocean remains one of the least known ocean regions due to its remote location, year-round sea ice cover, and harsh weather conditions. Today, knowledge of the Arctic atmosphere-sea ice-ocean system increases in parallel with the need to understand this changing environment under anthropogenic greenhouse warming. Indeed, the Arctic is an area where the effects of anthropogenic greenhouse warming are already visible and among the strongest on Earth; the atmosphere and the ocean are warming, the sea ice cover is diminishing, and the freshwater input to the ocean through river inflow, precipitation, and ice melt is increasing.

It is this rapidly changing, but poorly understood, Arctic climate system that motivates us to study its fate in a fresh and warm future. Our objective is to assess how the ocean circulation, the ocean heat content, and the ice cover respond to increasing freshwater input and overall greenhouse warming. We also ask whether changes in the ocean affect the atmosphere, i.e., is the atmospheric surface warming modified by the changing ocean? We choose to seek answers to these questions with a hierarchy of model simulations.

We focus on the North Atlantic-Arctic sector and examine changes in the ocean circulation and ocean heat content under greenhouse warming. We use idealized model simulations to assess changes in freshwater forcing, and global climate model simulations to examine the changing ocean heat budget. With this hierarchy of models we build a comprehensive understanding of the changing high latitude climate system and compile this dissertation around three main scientific findings.

First, we increase the Arctic river runoff in an idealized column model which represents the large scale average conditions of the Arctic ocean-sea ice-atmosphere system. A larger Arctic river runoff leads to a new equilibrium with a fresher surface and a warmer subsurface. Interestingly, even though the fresher surface leads to larger vertical density differences and suppresses vertical mixing, the vertical heat flux towards the surface remains close to constant. This is because stronger density and temperature differences balance the heat flux: even a relatively small amount of warm water carries a relatively large amount of heat. As a result changes in the sea ice thickness remain small.

Second, we extend our focus to larger scales and increase river runoff in a global ocean-sea ice model. Again, we find a fresher surface and a warmer subsurface Arctic Ocean as a response to increasing Arctic river runoff. The model also simulates a slightly weaker flow of water between the Arctic Ocean and its surrounding ocean basins. However, the heat exchanges between the central Arctic Ocean and the lower latitude oceans remain relatively constant. In a wider North Atlantic perspective, the subpolar North Atlantic shows an opposite response to the Arctic Ocean. The river runoff that enters the Arctic Ocean flows south along the coasts of Greenland and

through the Canadian Arctic Archipelago and mixes into the subpolar North Atlantic. The additional freshwater weakens the large scale horizontal and vertical density differences and the ocean flow that depends on these density differences. The weaker ocean circulation brings less warm waters to the subpolar North Atlantic and the ocean cools as a result.

Third, we find that, as the ocean heat content increases under greenhouse warming, the rate of the increase only weakly depends on the latitude in climate models. Only the Arctic Ocean, the northern part of the Southern Ocean, and the mid-latitude North Atlantic are warming slightly faster than the global average. We find that this stronger warming is associated with changes in the surface heat fluxes between the atmosphere and the ocean. In contrast, the subpolar North Atlantic is warming slightly slower than the global average because of the weaker ocean circulation that transports less warm waters towards the north.

In summary, under greenhouse warming the high latitude ocean freshens and warms. Freshening at northern high latitudes acts to weaken the vertical heat exchanges between surface and subsurface waters which warms the Arctic Ocean. However, freshening in the north also acts to slow down the ocean circulation in the subpolar North Atlantic which reduces the northward ocean heat transport and cools the ocean there. Greenhouse warming leads to ocean warming and most of the small differences in the rate of ocean warming from latitude to latitude can be explained by changes in surface heat fluxes.

List of papers

1. Nummelin A., C. Li, and L. H. Smedsrud (2015) Response of Arctic Ocean stratification to changing river runoff in a column model, *J. Geophys. Res. Oceans*, **120**, 2655–2675, doi:10.1002/2014JC010571.

2. Nummelin A., M. Ilicak, C. Li, and L. H. Smedsrud (2016), Consequences of future increased Arctic runoff on Arctic Ocean stratification, circulation, and sea ice cover, *J. Geophys. Res. Oceans*, **121**, 617–637, doi:10.1002/2015JC011156.

3. Nummelin A., C. Li, and P. Hezel, Connecting ocean heat transport changes from the mid-latitudes to the Arctic Ocean, *prepared for submission to J. Climate*.

Contents

Chapter 1

Introduction

Under greenhouse warming the Arctic Ocean freshens and warms. In the coupled climate system changes in the Arctic Ocean will affect other parts of the global ocean and the global climate system. Describing and quantifying changes in the Arctic Ocean and some aspects of the large scale feedbacks is the focus of this dissertation. The following provides background information for the results of this dissertation.

We start by describing Earth's energy balance both in a stable and in a changing climate, focusing on the Arctic region (section 1.1). We then describe the basic physical features of the Arctic Ocean (section 1.2), and briefly describe the observational and modelling perspective to Arctic oceanography, before moving on to a description of freshwater effects on ocean circulation (section 1.3). After presenting the objectives of this dissertation and motivating the approach (chapter 2) we give the main conclusions (chapter 3) with future perspectives (chapter 4). Finally, we present the main scientific results in chapter 5.

1.1 The Arctic in the Climate System

1.1.1 Stable Climate

From the perspective of Earth's energy balance, the extra-tropics, including the Arctic, are an area of net outgoing radiation at the top of the atmosphere which balances the net radiation surplus in the tropics (Figure 1.1a). The atmosphere and the ocean carry heat poleward, connecting the tropical areas of net heating to the polar areas of net cooling (Figure 1.1b). There is also considerable heat exchange between the ocean and the atmosphere. Interestingly, these ocean-atmosphere heat fluxes are not directly linked to the top of the atmosphere radiative balance. For example in the Northern Hemisphere the ocean loses heat to the atmosphere north of $\sim 28^{\circ}$N, while the top of the atmosphere balance turns negative almost 10° further north (note the dashed gray lines in Figure 1.1a). It is in this $\sim 10^{\circ}$ latitude band that the atmosphere gains heat from the ocean, only to transport it further north. On the other hand, the ocean warms at $\sim 50^{\circ}$S (due to net radiation surplus *Czaja and Marshall* (2015)) because the atmospheric heat transport accomodates the negative top of the atmosphere radiation balance.

In terms of the Arctic heat budget the atmosphere plays a major role and transports most of the heat to the Arctic. The ocean releases a major part of its heat already at the subtropical latitudes and carries only a relatively small amount of the tropical heat

to the Arctic Ocean (Figure 1.1b). The atmospheric heat transport takes place through both sensible and latent heat transport. The latent heat is released within the Arctic by condensation and freezing and the resulting precipitation falls directly into the ocean (or on sea ice), or flows to the ocean through rivers. The atmospheric heat and freshwater cycles are therefore intimately coupled, and form a strong boundary condition for ocean and sea ice conditions (section 1.2).

Despite the atmosphere's dominant role in the overall northward heat transport, ocean heat transport appears equally crucial for the Arctic sea ice cover. This is because the ocean always transports heat relative to the freezing/melting point of sea water/sea ice. The atmosphere is different, as it transports a large amount of heat relative to 0 K, but a much smaller amount of heat relative to the freezing/melting point of sea water/sea ice. Indeed, *Bitz et al.* (2005) demonstrated that the ocean heat transport convergence determines the location of the sea ice edge, and subsequent studies have shown a strong linkage between ocean heat transport and the winter sea ice edge (*Årthun et al.*, 2012; *Onarheim et al.*, 2014, 2015), and with the summer sea ice edge at sufficiently long timescales (*Zhang*, 2015). Such a linkage follows a simple argument: the annual mean sea ice edge (and the winter sea ice edge) is to first order found where the ocean freezes under the cold atmosphere. Therefore, a larger ocean or atmospheric heat transport will always lead to a warmer ocean surface at a given latitude and push the point where the ocean freezes northward.

1.1.2 Warming Climate

The ongoing increase in atmospheric greenhouse gas concentrations leads to enhanced absorption of surface outgoing longwave radiation and enhanced emittance of the absorbed radiation back to the surface. There is an imbalance at the top of the atmosphere – less heat is radiated out than received. The climate system then adjusts to accommodate this imbalance. In simple terms the oceanic and atmospheric heat content increase until the outgoing longwave radiation is large enough to account for the enhanced downward long wave radiation and remove the top of the atmosphere imbalance. In reality, the initial warming induces a number of feedback processes (*Soden and Held*, 2006) that affect surface warming and become more important in sustaining the top of the atmosphere imbalance than the initial effect of anthropogenic greenhouse gasses (*Donohoe et al.*, 2014). Due to uncertainties related to these feedback processes, the sensitivity of the Earth's surface temperature change for an initial greenhouse forcing is not well known (*Forster*, 2016). While the overall uncertainty of global warming is not the focus here, we discuss two promiment features of the Arctic warming that link to the different feedback mechanisms: Arctic amplification and the sea ice cover retreat.

Arctic Amplification

Even though greenhouse gasses are well mixed in the atmosphere, greenhouse warming is not homogeneous over the globe owing to the feedback mechanisms acting on the initial warming. The high latitudes undergo much stronger warming than the tropical latitudes. This amplification of the warming is strongest in the Northern Hemisphere where it is called Arctic amplification. Arctic amplification is visible in observations

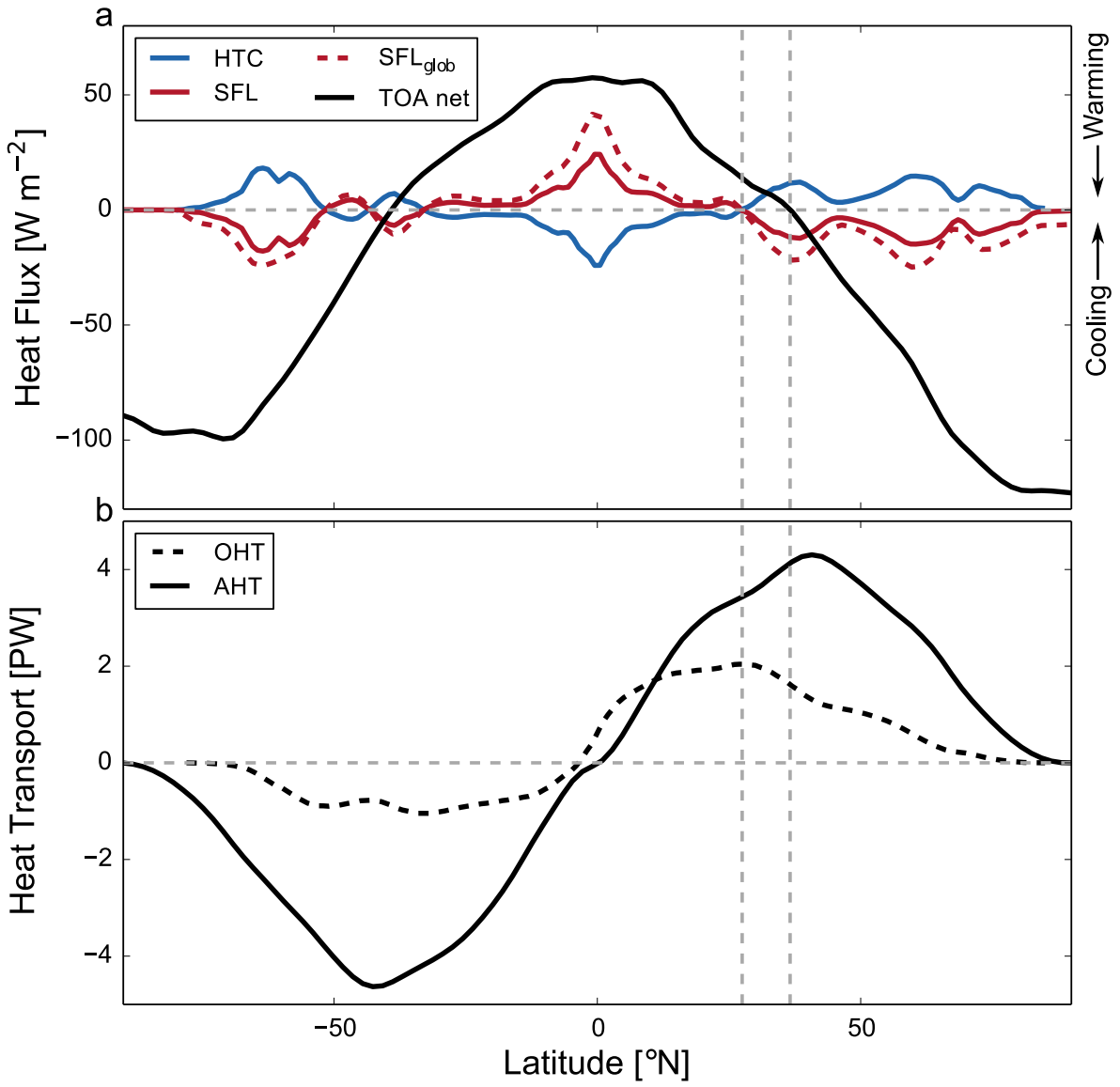

Figure 1.1: The global surface heat budget in the unforced control simulation of the Norwegian Earth System model. (a) shows the ocean heat transport convergence (HTC), the surface heat flux over the ocean (SFL), the global average surface heat flux (SFL$_{glob}$ i.e. the average surface flux over land and ocean surfaces), and the top of the atmosphere net radiation (TOA net) (b) shows the northward heat transport in the ocean (OHT) and in the atmosphere (AHT). Vertical dashed lines illustrate where the ocean turns to net source of heat in the Northern Hemisphere ($\sim$28°N) and where the Earth as a whole starts to lose heat ($\sim$37°N). Note that all variables are scaled by global surface area in each zonal band (i.e. also heat flux in the ocean surface is divided by global surface area). In panel (a) directions are defined positive down i.e. local surface flux (SFL) warms the ocean in the tropics, and cools the ocean in the extra-tropics. In a steady state ocean heat transport convergence mirrors the surface heat flux i.e. heat is transported from areas of net divergence in the tropics to areas of net convergence in the polar regions.

(*Serreze and Barry*, 2011), in paleoproxy records (*Miller et al.*, 2010), in earth system model simulations (*Mahlstein and Knutti*, 2011; *Pithan and Mauritsen*, 2014), as well as in many idealized models (*Alexeev et al.*, 2005; *Langen and Alexeev*, 2007). Arctic amplification is also seen in the ocean as a rapid heat content increase (paper III).

The main reasons for Arctic amplification in the atmosphere are meridional differences in lapse rate feedback, Planck feedback, and albedo feedback (*Laîné et al.*, 2016; *Pithan and Mauritsen*, 2014; *Winton*, 2006). Both lapse rate and Planck feedbacks act to cool the tropics much more effectively than the Arctic. Albedo feedback acts to warm the Arctic much more than the tropics.

The lapse rate feedback is different in the low and high latitudes because in the convective tropical atmosphere warming is the strongest at high altitudes (mainly due to condensing moisture) while in the stratified Arctic atmosphere warming is the strongest at surface. The high altitude warming in the tropics mainly increases the outgoing radiation, while the Arctic surface warming induces large downward longwave radiation towards the surface which acts to warm the surface. Therefore the net outgoing surface long wave radiation increases much more in the tropics than in the Arctic. Differences in the Planck feedback follow directly from the temperature dependence of the outgoing long wave radiation ($\propto T^4$) which strengthens more in warm than in cold temperatures.

The positive ice-albedo feedback over the high latitude oceans follows a change from light sea ice surface to dark ocean surface, which allows the surface (ocean) to absorb more shortwave radiation. No such effect is seen in the tropics where albedo changes are small compared to the Arctic. The ice-albedo feedback is seasonal in nature; in summer shortwave radiation warms the ice free ocean surface which can also lead to warming of the atmosphere above, but the largest effect takes place in winter as the stored heat is released to the atmosphere leading to a longer ice free season, a thinner ice cover, and therefore a warmer atmosphere. This seasonal aspect is often referred to as the delayed ice-albedo feedback.

In addition to these feedbacks, the enhanced hydrological cycle increases atmospheric latent heat transport to the Arctic which adds to Arctic amplification (*Laîné et al.*, 2016; *Pithan and Mauritsen*, 2014; *Yoshimori et al.*, 2014). Greenhouse warming generally weakens the northward ocean heat transport, which is why it acts against Arctic amplification at large scales (*Pithan and Mauritsen*, 2014). However, high latitude ocean heat transport contributes to the intermodel spread in Arctic amplification (*Mahlstein and Knutti* (2011), and paper III)

Gradual and Reversible Arctic Sea Ice Loss

The ongoing sea ice cover decline has stirred interest in the possibility of irreversible and abrupt sea ice loss that could lead to stronger global warming and Arctic amplification through the ice-albedo feedback (*Notz*, 2009). By irreversibility we refer to a situation in which a system has multiple stable states and exhibits hysteresis behaviour. In the case of sea ice one would expect that after a warm climate perturbation the sea ice cover would require a much larger cold climate perturbation to recover to its original state. However, the irreversible behaviour seems not to be the case in full climate models (*Armour et al.*, 2011; *Ridley et al.*, 2012; *Tietsche et al.*, 2011), although winter sea ice loss (recovery) has been shown to be faster (slower) than summer sea ice loss (*Armour et al.*, 2011; *Bathiany et al.*, 2016). In fact *Wagner and Eisenman* (2015)

suggest that poleward heat transport together with seasonality remove the bistabilities that have been found in idealized models (*Eisenman and Wettlaufer*, 2009). Furthermore, *Bathiany et al.* (2016) suggest that the abrupt loss of winter sea ice is not linked to any radiative feedback mechanism and does not support multiple stable states. In fact *Bathiany et al.* (2016) argue that the summer sea ice loss is gradual because of the heterogenous thickness distribution. Gradual melting moves ice from thicker to thinner classes, but any abrupt behaviour is hard to achieve. However, winter sea ice cover is based on freezing, and after the summer sea ice is lost the thickness distribution is relatively homogeneous. In this case the ice cover can be lost abruptly: sea ice cover grows rapidly when surface temperatures cool below freezing, but loss of sea ice area is rapid if one winter the surface does not reach the freezing point anymore. Finally, decadal scale events of rapid sea ice loss can still take place outside the multiple equilibria framework (*Drijfhout et al.*, 2015; *Holland et al.*, 2006). In light of these results greenhouse warming leads primarily to gradual and reversible sea ice loss.

1.1.3 Forced Change and Internal Variability

In this dissertation we focus on long term changes under greenhouse warming. These forced changes take place on top of the large internal variability across timescales. While our perspective is interesting for understanding how the climate system responds to a given forcing we note that robust observations of such a response require a long timeseries and/or a large forced signal compared to the internal variability. While parameters such as air temperature (*Collins et al.*, 2013) and ocean heat content (*Levitus et al.*, 2012) already show a detectable forced signal, for other parameters such as the Atlantic Meridional Overturning Circulation (AMOC), the observational timeseries is still too short and/or the forced signal is too weak to robustly detect the forced change from the relatively large background internal variability (*Böning et al.*, 2016; *Haine*, 2016; *Jackson et al.*, 2016; *Robson et al.*, 2016).

However, under strong future greenhouse forcing, changes due to forcing become comparable to (or larger than) the internal variability. In the modelling framework we can illustrate how this relationship between the forced signal and internal variability depends on the latitude, timescale, and parameter in question (Figure 1.2). For simplicity we define the forced signal to be the linear change over a given time period, and internal variability to be twice the standard deviation of the detrended timeseries (this method captures $\sim$95% of the range of internal variability, assuming the variability is normally distributed). The ratio between the two is the signal to noise ratio. A larger ratio implies a larger influence of the forcing on the overall change, e.g. when the ratio is larger than 1 the forced change over the time period is larger than most ($\sim$95%) of the internal variability within the time period. We note that a large ensemble would be needed to robustly infer the forced change and the internal variability (*Tandon and Kushner*, 2015), but because such ensemble is not available for Norwegian Earth System Model (NorESM1-M) we proceed with our idealized approach.

We focus on the sea surface temperature and the northward ocean heat transport and use results from a NorESM1-M simulation under the Representative Concentration Pathway 8.5 (RCP8.5) forcing (*Taylor et al.*, 2012). The simulation suggest that the forced change of a zonally averaged annual mean sea surface temperature timeseries starting at year 2000 will become larger than the internal variability in year 2030 in the

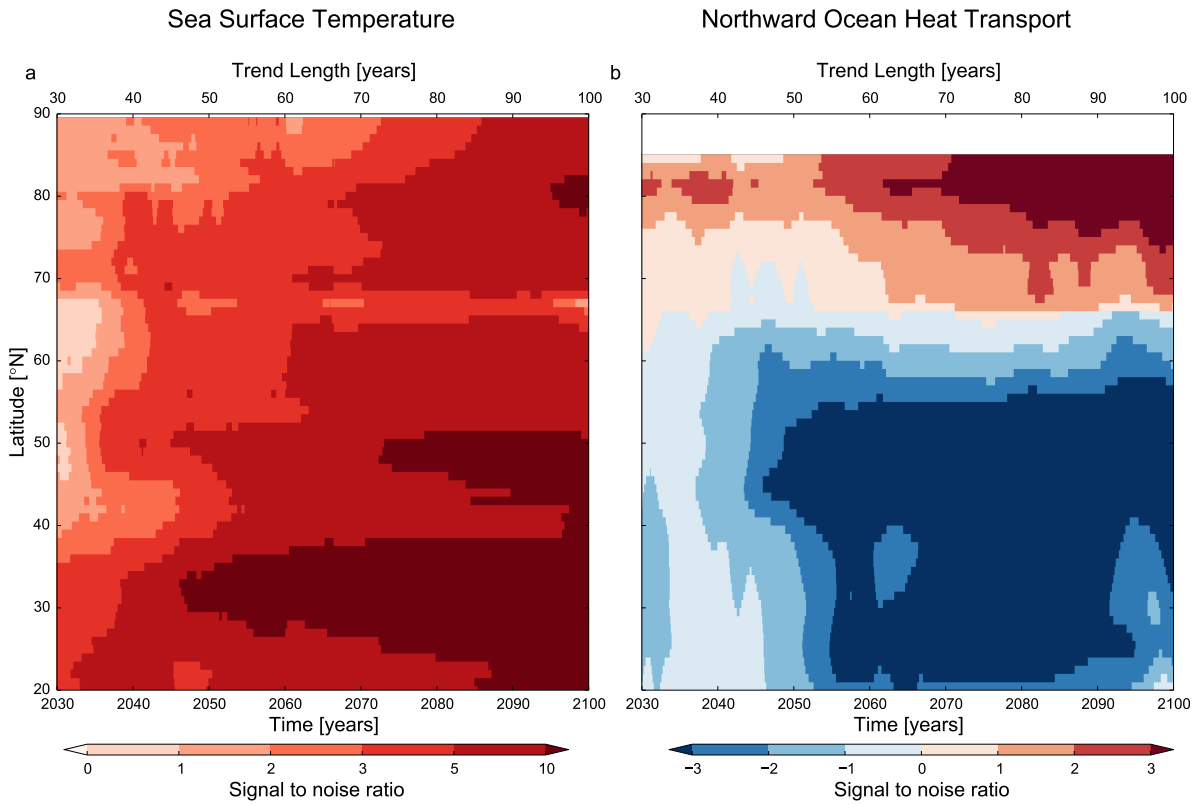

Figure 1.2: Signal to noise ratio, here defined as the ratio between forced change (change due to linear trend) and the internal variability (twice the standard deviation) for (a) the zonally averaged sea surface temperature and (b) the zonally integrated northward ocean heat transport in the Atlantic basin. Note that for both variables we low-pass filter (12 month filter) the monthly timeseries. The trend period starts from year 2000 and increases further in time, i.e. year 2030 corresponds to 30 year trend, year 2040 corresponds to 40 year trend and so forth. Similarly, the standard deviation is calculated over the trend period. Note that the timeseries is combined from the historical (2000–2005) and RCP8.5 simulation (2005 onwards).

Northern Hemisphere, except for a slight delay in the ∼45-70°N latitude band. Similar analysis of the northward ocean heat transport in the Atlantic basin suggests that a forced change already has a large effect on the heat transport to the Arctic in 2030, while it takes generally a decade longer for the forcing to have similar influence in the subtropical to subpolar region.

Haine (2016) suggested that in terms of the observational evidence of the AMOC, and the related heat transport, the internal variability still dominates and no anthropogenic signal can be detected. According to NorESM1-M, this might be the case for ocean heat transport at the location of the major measurements arrays (RAPID array at 26.5°N (*McCarthy et al.*, 2015) and OSNAP array around 60°N between Greenland and Scotland) for a few decades to come as the internal variability dominates until the 2040s, even under the strong RCP8.5 forcing. However, forced changes in the Arctic domain, the focus of this dissertation, are already important compared to the internal variability by the 2030s.

1.2 Arctic Oceanography

Geological boundary conditions are one of the main constraints for the physical behaviour of the Arctic Ocean. The Arctic Ocean basin is characterized by large shelf seas (∼54% of the area is shallower than 500 m when the Barents Sea is included) and two large deep basins, the Canada basin and the Eurasian basin which are divided by the Lomonosov ridge (Figure 1.3). The Eurasian basin is further divided into the Nansen and the Amundsen basins. The deepest connection to the world oceans is through the Fram Strait (2545 m depth), while the other connections, the Barents Sea, the Bering Strait, and the different straits through the Canadian Arctic Archipelago, are considerably shallower and, except for the Barents Sea, narrower than the Fram Strait. A large fraction of the deep basins lie below the Fram Strait sill depth which disconnects them from other world oceans. Inside the Arctic, the Lomonosov Ridge further limits the water exchange from the Canada Basin to the Eurasian Basin (*Björk et al.*, 2010; *Timmermans and Garrett*, 2006; *Timmermans et al.*, 2003).

The physical oceanography of the Arctic Ocean is characterized by strong vertical density stratification (Figure 1.4). Salinity dominates density at cold temperatures: cold and fresh waters lie on top of warm and saline waters. The fresh surface owes its existence to a large freshwater input (total of 0.3 Sv) by river runoff (0.13 Sv, ∼10% of the global runoff), net precipitation (0.07 Sv), Greenland meltwater (0.01 Sv), and inflow of relatively fresh Pacific water through Bering Strait (0.08 Sv) (*Haine et al.*, 2015). Roughly 25% of the freshwater input leaves the Arctic Ocean as sea ice (mainly through Fram Strait), while the rest flows out as liquid freshwater via the Canadian Arctic Archipelago and the East Greenland Current (*Haine et al.*, 2015). The relatively warm Atlantic inflow (approximately $0-1°C$, i.e. $2-3°C$ warmer than surface freezing point) characterizes the mid-depth Arctic Ocean. The Atlantic inflow forms a warm geostrophic boundary current at around 200-500 m depth that flows around the Arctic along the shelf break, and the main submarine ridges (*Rudels et al.*, 1996). A strong halocline separates the fresh and cold surface layer from the relatively warm and saline Atlantic Water at depth (Figure 1.4c). Specific to the Arctic Ocean, the cold surface temperatures extend to the lower part of the halocline. This feature has been called the "cold halocline" and it is formed by cold shelf water intrusions and local winter convection (*Rudels et al.*, 1996; *Steele and Boyd*, 1998). Both shelf water formation and the local convection are partly fuelled by the input of dense brine during sea ice formation (salt cannot be part of the growing ice crystals). It is noteworthy that the process of brine formation, and the input of brine plumes to the ocean, are both parameterized sub-grid scale processes in large scale climate models and therefore a potential source of error. The strong salinity stratification and the cold temperatures below the surface mixed layer in the halocline effectively decouple the surface layer from the warm Atlantic layer, as mixing through the upper salinity stratification only entrains cold water to the surface. On the Pacific side the halocline is characterized by seasonally changing inflow through Bering Strait: Pacific Summer Water forms a warm layer at around 50 meters depth, while the Pacific Winter Water contributes to the cold halocline below this depth (Figure 1.4c).

The fresh surface, the weak vertical ocean heat flux, and the strong surface cooling lead to formation of the Arctic sea ice cover (Figure 1.4a). The sea ice cover is an important part of the physical oceangraphy in the Arctic Ocean as it suppresses wind

driven mixing and restricts shortwave radiation driven warming of the upper ocean. Currently the Arctic sea ice extent and volume are declining mainly due to greenhouse warming (*Stroeve et al.*, 2011, 2012), although internal variability contributed 5-30% to the sea ice retreat between 1979-2010 (*Day et al.*, 2012). The decadal-to-multidecadal variability in the sea ice extent (*Miles et al.*, 2014; *Serreze et al.*, 2007) is connected to variability in ocean heat transport, which has proven to be useful predictor for the Arctic sea ice extent at long timescales (*Yeager et al.*, 2015; *Zhang*, 2015). On the other hand, internal variability in the Arctic sea ice export can affect the sea surface salinity, the deep water formation, and the large scale circulation of the North Atlantic (*Häkkinen* (1993); section 1.3.1).

In summary the upper ocean stratification in the Arctic is very stable and the warm intermediate layers induce only a weak heat flux towards the surface. Therefore the Arctic Ocean is perennially ice covered and it is only at the entrance of the Atlantic and the Pacific sector that the warm ocean is in contact with the surface and can directly affect the sea ice cover and the atmosphere above (*Onarheim et al.*, 2014; *Rudels*, 2016).

In addition to stratification, both the small and large scale dynamics of the Arctic Ocean are distinct from the other world oceans. Small scale vertical mixing in the Arctic is mainly restricted to tidal induced mixing over steep topography (*Rippeth et al.*, 2015), whereas in the interior vertical mixing is small compared to other world oceans (*Fer*, 2009) and dominated by double diffusion (*Rudels et al.*, 1999; *Sirevaag and Fer*, 2012), as the extensive ice cover restricts wind energy input. However, with the diminishing sea ice cover the small direct wind wave mixing (*Thomson and Rogers*, 2014; *Wang et al.*, 2016) and mixing due to the wind driven internal waves (*Dosser and Rainville*, 2015) both increase. Large scale ocean dynamics outside the Arctic are dominated by Sverdrup balance: vorticity input due to wind stress curl is balanced by friction at narrow western boundary currents. However, the Sverdrup balance is not applicable in the Arctic Ocean because there is no meridional boundary along which a boundary current could form. Instead, in the Arctic, the geostrophic eddy fluxes and friction balance the vorticity input due to wind stress curl (*Yang et al.*, 2016).

1.2.1 Arctic Observations

Until late 19th century the central Arctic Ocean remained one of the last uncharted waters of the world due to its remote location and extensive ice cover. At that time many thought that there would be permanently ice free portions inside the Arctic Ocean, mainly because of the large heat input through the Norwegian Atlantic Current (see review by *Rudels* (2015)). However, measurements by Nansen in the late 19th century revealed that the Atlantic Water layer was isolated from the surface ice cover by strong salinity stratification. In the subsequent decades there were few observations made of the Arctic Ocean and its ice cover, with notable exceptions being ice breaker expeditions and Soviet Russian polar camps (*Rudels*, 2015). At the beginning of the satellite period frequent observations of the ice extent started, but observations of the ocean below, and the ice thickness remained sparse. Other world oceans have seen a recent rapid expansion of autonomous ocean observing methods such as ARGO floats and gliders, but the subsurface Arctic Ocean is heavily undersampled because the sea ice cover restricts the usage of autonomous observing platforms other than the ice tethered

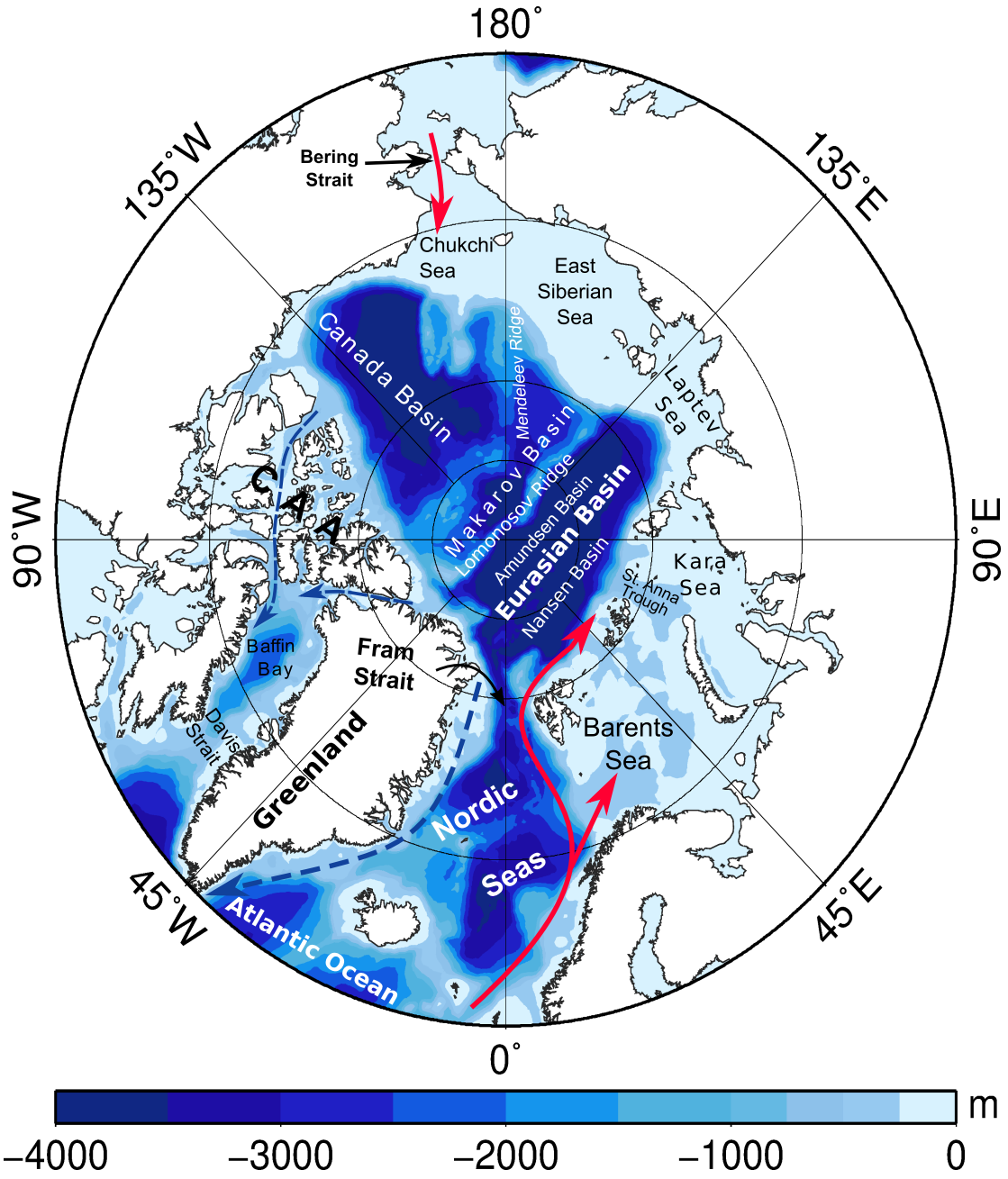

Figure 1.3: Bathymetry of the Arctic Ocean with the main surface currents and geographical features overlaid. Light colors denote shallow waters while dark colors denote deep waters; blue dashed arrows are the cold surface outflows, red solid arrows are the warm surface inflows. CAA stands for Canadian Arctic Archipelago.

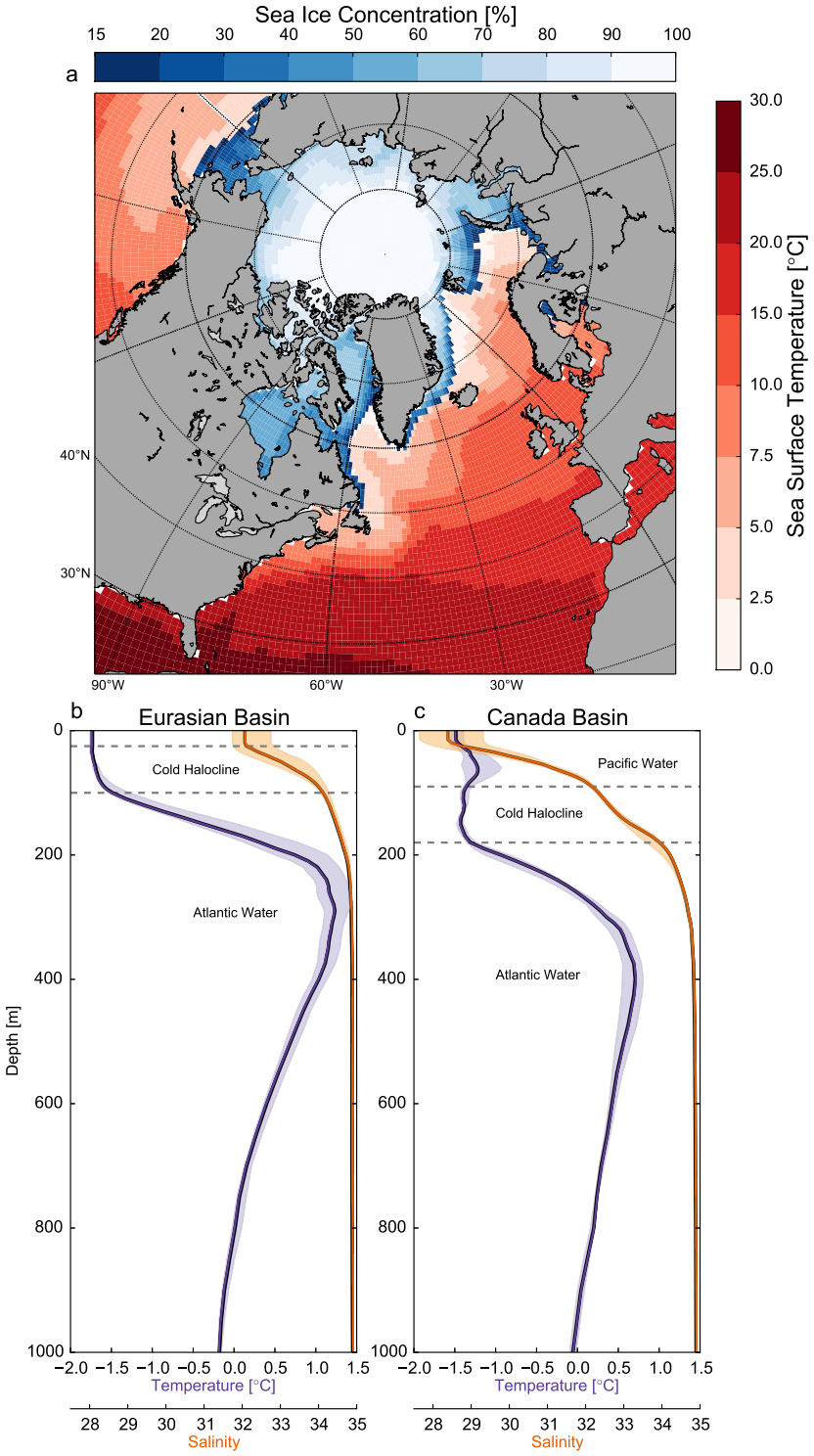

Figure 1.4: (a) The annual mean Sea Surface Temperature and Sea Ice Concentration for the period 2000-2010 in the North Atlantic-Arctic sector (using NOAA_OI_SST_V2 data *Reynolds et al.* (2002)) and climatological temperature and salinity profiles using MIMOC climatology (*Schmidtko et al.*, 2013) for (b) Eurasian and (c) Canada Basins. Shading shows the interquartile range of temperature and salinity profiles in the respective basins. NOAA_OI_SST_V2 data provided by the NOAA/OAR/ESRL PSD, Boulder, Colorado, USA, from their Web site at `http://www.esrl.noaa.gov/psd/`)

profilers (http://www.whoi.edu/website/itp/overview). Currently the global ocean has ∼3700 active Argo profilers which means on average ∼10 Argo floats per million square kilometers, while there is only ∼1 ice tethered profiler per million square kilometers in the Arctic Ocean.

Despite the sparse observations, during the past decades we have observed increasing temperatures both in the atmosphere (*Stroeve et al.*, 2011) and in the ocean (*Carmack et al.*, 2015). Satellite observations have revealed diminishing ice cover, especially in summer in the western Arctic (*Stroeve et al.*, 2011), but also in winter in the Eastern Arctic (*Onarheim et al.*, 2015). The diminishing ice cover has also led to observations of delayed ice-albedo feedback, where summer shortwave radiation penetrates below the shallow surface layer and creates a near surface temperature maximum (NSTM, *Jackson et al.* (2011)) which then limits the ice growth in the following (early) winter (*Timmermans*, 2015). Both observations (*Gallaher et al.*, 2016) and modelling results (*Ding et al.*, 2016) indicate that atmospheric shortwave radiation into the ocean is preferentially (∼3/4 *Gallaher et al.* (2016)) used to melt the ice and secondly (∼1/4 *Gallaher et al.* (2016)) used to warm the ocean (delayed ice-albedo feedback).

1.2.2 Challenges in Arctic Ocean Modelling

The Arctic has proven to be a difficult area to acquire observational data and it is also a challenging area for modelling of the atmosphere, the sea ice, and the ocean. We focus on the ocean, but note that the challenges for the atmospheric modelling come mainly from the representation of vertical humidity and temperature stratification, and from representation of mixed phase clouds, all of which affect the surface energy balance (*Vihma et al.*, 2014). In the following we review the main challenges for ocean modelling, which represent primary caveats of this model-based dissertation.

Perhaps the most fundamental challenge for ocean modelling in the Arctic comes from the small internal Rossby radius of deformation, which is proportional to the water depth and the strength of the vertical stratification (mean buoyancy frequency), and inversely proportonial to the Coriolis parameter (*Chelton et al.*, 1998). At this scale the rotational effects become as important as buoyancy effects for fluid motion. The Rossby radius limits the size of geostrophic (mesoscale) eddies and the horizontal extent of baroclinic ocean currents and fronts. Consequently, the internal Rossby radius is also the scale at which most of the ocean kinetic energy is found, as the geostrophic eddies are the main path via which potential energy is converted to kinetic energy (*Ferrari and Wunsch*, 2009). In the Arctic the Rossby radius of deformation is particularly small because the Coriolis parameter is strong, and at the shelves the shallow water depth and weak (winter) stratification further decrease the Rossby radius.

Because the internal Rossby radius is of such importance for the ocean circulation, ocean models would need to resolve these scales (a model would need to a have grid size which is less or equal to half of the internal Rossby radius) in order to properly resolve the ocean dynamics. The available computer resources have made it practically impossible to use an adequate resolution in the Arctic where the internal Rossby radius can be on order of ∼1-15km (*Nurser and Bacon*, 2014). With this limitation it is clear that most of today's climate models and even the regional ocean models depend on parameterizations to be able to resolve the mesoscale circulation. Dependence on parameterizations might be problematic because the ocean eddies seem to play an im-

portant role in the Atlantic inflow (*Hattermann et al.*, 2016; *von Appen et al.*, 2016) and in the interior Arctic Ocean (*Lique et al.*, 2015; *Spall*, 2013; *Yang et al.*, 2016) dynamics.

In addition to the small internal Rossby radius, numerical models often struggle to properly represent the vertical stratification, and therefore to adequately simulate vertical mixing and vertical fluxes of heat and salt in the Arctic Ocean. Recently *Ilicak et al.* (2016) showed that both the depth and temperature of the Atlantic layer, as well as the cold halocline, are poorly represented in ocean components of the current generation climate models. The authors link the Atlantic layer temperature biases to biases in the Fram Strait inflow temperatures and the Barents Sea heat loss. Cold-biased models had overly weak and cold inflow of Atlantic Water through the Fram Strait, and often produced too much cooling in the Barents Sea (vice versa for the warm-biased models). Note that in paper II we use a cold-biased model. The difficulties the models have in reproducing the cold halocline structure are likely to be linked to the watermass transformations in the shelf seas, and in the central basins (mainly the Nansen Basin). The observed cold halocline in the deep central basins is the result of winter convection and brine production, both on site and in the shelf seas, from where the brine enriched shelf water is advected to the central basins. Due to the coarse resolution, most of the models cannot represent coastal leads where the ice production and brine rejection are the strongest, possibly leading to too little shelf water formation and an anomalously warm halocline. In addition, the models often inject the brine from sea ice formation into the upper model layer(s). In nature the brine would convect as a plume to a level of neutral density, entraining some of the ambient water on its way. These two processes could lead to two very different watermass properties.

Altogether, these difficulties are clearly a challenge for an appropriate representation of the ocean base state. However, it is not as clear whether the shortcomings of the current models affect trends under strong climate forcing which is the focus in this dissertation. For example in papers II and III we show that most of the changes in the Arctic ocean heat budget take place because of changes in local surface fluxes or in the inflow temperatures that change with the forcing. Also, greenhouse warming primarily melts the summer sea ice from the top and pushes poleward the point where the winter sea ice forms, which is why deficiencies in the vertical ocean stratification inside the Arctic might be of lesser importance. Better representation of the Arctic Ocean would certainly be desirable for many applications, such as short term climate predictions, but the current generation of climate models seem adequate to simulate the main large scale processes related to greenhouse warming.

1.3 Freshwater and Ocean Circulation

A focal point of this dissertation is the influence of freshwater on the large scale ocean circulation and heat budget, and here we provide some background information, which papers I and II build upon.

Freshwater is a source of buoyancy and affects the ocean circulation by changing vertical and horizontal density gradients. In the Arctic, large freshwater input leads to strong vertical stratification that suppresses vertical heat fluxes, and enables sea ice to grow despite the relatively warm subsurface waters. In addition, freshwater acts to both

drive (*Lambert et al.*, 2016; *Rudels*, 2010; *Spall*, 2013; *Stigebrandt*, 1981) and hinder (*Lambert et al.*, 2016; *Rudels*, 2010) the volume exchanges between Arctic Ocean and the surrounding basins (see also section 5.2.1). At large scale, enhanced high latitude vertical density gradients hinder dense water formation, and slow down the global scale overturning circulation (*Stommel*, 1961; *Stouffer et al.*, 2006).

While the large scale ocean gyre circulation is set by the atmospheric winds (*Munk*, 1950; *Stommel*, 1948; *Sverdrup*, 1947), buoyancy forcing affects horizontal density gradients and therefore intensity of the gyre circulation. For example the cyclonic North Atlantic subpolar gyre is strengthened by buoyancy loss, in addition to winds. Additional freshwater (buoyancy input) reduces the density of the water column, reducing the horizontal density and sea surface height gradients, and leading to slowdown of the gyre circulation at long timescales (*Deshayes et al.*, 2014). Further, in terms of the subpolar gyre circulation freshwater might trigger a non-linear response: *Born and Levermann* (2010) demonstrated that a freshwater forcing can trigger a shift between a weak and a strong subpolar gyre equilibrium states (*Born and Stocker*, 2013; *Born et al.*, 2013).

The local ocean heat content change appears from a balance between the weakening of ocean heat transport and the strengthening of local stratification. The weakening overturning and gyre circulation reduce the northward ocean heat transport, which acts to cool the ocean. However, a large enough freshwater perturbation will effectively isolate the deep ocean from the atmosphere. In areas of net heat loss (extra-tropics) this implies increasing ocean heat content as the deep ocean layers are not ventilated, even though the surface ocean cools (*Mignot et al.*, 2007).

The overall response of ocean circulation and heat budget to a freshwater perturbation depends on the strength, location, and duration of the perturbation. Buoyancy dependence links the two large scale effects together: freshwater forcing in the convective areas slows down both the overturning and the gyre circulation. As such both effects act to reduce the ocean heat content in the subpolar North Atlantic.

1.3.1 Internal Freshwater Flux Variability at Northern High Latitudes

The results of this dissertation focus on the relatively slow (∼centennial scale) freshening of the North Atlantic-Arctic domain due to greenhouse warming. However, the regional freshwater budgets exhibit a large shorter term (∼ decadal) variability. The largest changes in sea surface salinities during the observational period have been called Great Salinity Anomalies (GSAs) (*Belkin*, 2004). These decadal scale events of low salinity surface waters have been observed across the northern North Atlantic in the 1970s, in the 1980s and in the 1990s. The anomalies are typically first identified in the Labrador Sea from where they propagate around the subpolar gyre and the Nordic Seas. The origin of these events is still somewhat debated, but several authors have suggested an Arctic origin, either sea ice and freshwater export through the Fram Strait (*Dickson et al.*, 1988; *Häkkinen*, 1993), or freshwater from anomalously large ice cover in Baffin Bay accompanied by freshwater export through Canadian Arctic Archipelago (*Belkin et al.*, 1998). Recently *Glessmer et al.* (2014) showed that the decadal scale variability in the Nordic Seas freshwater content is caused by anomalous salt advection from the North Atlantic. While their results suggest that sea ice or freshwater export through the Fram Strait is not causing the GSAs in the Nordic Seas, their results also do not reject

the possible increase of freshwater export through the Canadian Arctic Archipelago to the Labrador Sea and subsequent advection of this anomaly to the Nordic Seas. In support of the Arctic source of the GSAs, *Proshutinsky et al.* (2015) showed that the Arctic freshwater content, which follows the Arctic Oscillation (*Morison et al.*, 2012; *Proshutinsky et al.*, 2015), has increased since the 1990s possibly explaining the lack of GSAs since. Altogether it is fully possible that the source of the observed GSAs are different in different decades. The common feature seems to be the reduced convection and propagation of the salinity anomalies around the subpolar North Atlantic and the Nordic Seas with the mean circulation.

1.3.2 Forced Freshwater Flux Increase at Northern High Latitudes

Greenhouse warming can increase the freshwater flux to the high latitude oceans in two major ways, either via an enhanced hydrological cycle or via melting of ice (land ice, sea ice, and permafrost). Presently, melting of sea ice and the intensification of hydrological cycle still dominate the Northern Hemisphere freshwater flux increase (*Haine et al.*, 2015), although melting and increased dynamical loss of the Greenland ice sheet is expected to become a large additional freshwater source over the century (*Little et al.*, 2016; *van den Berk and Drijfhout*, 2014). The focus of this dissertation in terms of additional freshwater sources is on the strengthened hydrological cycle.

The mean hydrological cycle consists of poleward atmospheric moisture transports, which transports moisture from areas of net evaporation over the tropical oceans to areas of net precipitation at high latitudes, and the equatorward oceanic freshwater transport which closes the loop. Greenhouse warming intensifies the atmospheric freshwater cycle because warmer air can hold more moisture, which means that more water evaporates in the tropics and more precipitates in polar regions. Consequently the southward oceanic freshwater transport and the northward oceanic salt transport strengthen as well. The balance between these two opposing terms in the convective regions determines the large scale ocean response to the stronger hydrological cycle. Interestingly *Swingedouw et al.* (2007) showed that the southward freshwater advection due to the stronger high latitude precipitation dominates over the northward advection of more saline waters due to the stronger low latitude evaporation. In their modelling framework, intensification of the hydrological cycle in the North Atlantic leads to reduced convection which damps the overturning circulation.

Melting of ice (land ice, sea ice, and permafrost) alters the globally integrated freshwater budget, unlike the intensification of the hydrological cycle. The cryosphere is a slowly adjusting storage term in the global freshwater budget: it grows in cold climates and diminishes in warm climates. Melting of land based ice raises the sea level and decreases the global ocean salinity. In addition, melting of the land based ice can create large meltwater lakes that can induce large and abrupt freshwater flux events (*Margold et al.*, 2011; *Spielhagen et al.*, 2005).

Despite the differences in the sources of freshwater, the large scale ocean response in the North Atlantic sector is qualitatively similar whenever freshwater affects the North Atlantic convection sites (*Roche et al.*, 2010). To the first order it does not matter whether the freshwater is added to the Arctic ocean (*Peltier et al.*, 2006; *Rennermalm et al.*, 2006, 2007; *Tarasov and Peltier*, 2005), coast of Greenland (*Gerdes et al.*, 2006; *Yu et al.*, 2015), or directly to the convective regions in the Labrador Sea, the Irminger

Sea or the Nordic Seas (*Mignot et al.*, 2007; *Rennermalm et al.*, 2007; *Stouffer et al.*, 2006). The AMOC and the subpolar gyre will weaken, acting to cool the subpolar North Atlantic.

While the robustness of the responses in models gives us confidence in our understanding of freshwater effects on ocean circulation, translating this model based knowledge to the past freshwater events through proxies can be challenging. Similarity of the responses makes attribution rather difficult without a direct evidence of the freshwater forcing itself. For example, subpolar temperature, salinity, or sea ice proxies can mainly indicate whether an freshwater event took place, but other evidence (e.g. *Muschitiello et al.* (2015, 2016); *Swärd et al.* (2015)) would be required to locate the source of such an event.

Chapter 2

Objectives and Methods

Ongoing greenhouse warming (*Collins et al.*, 2013) changes the surface ocean forcing globally and especially at high latitudes where buoyancy forcing strongly affects the circulation. The warmer atmosphere, and the related increase in poleward moisture transport, act to increase the surface ocean buoyancy in the high latitudes.

Here our interest is mostly in the North Atlantic - Arctic sector, which shows the largest and perhaps most intriguing ocean circulation, ocean heat content, and sea ice cover response to greenhouse warming. In the Arctic Ocean, theoretical work suggests that the ocean circulation might strengthen with a larger freshwater input (*Lambert et al.*, 2016; *Rudels et al.*, 2012; *Stigebrandt*, 1981). Past observations and model simulations of future climate suggest that heat transport to the Arctic increases (*Koenigk and Brodeau*, 2013; *Spielhagen et al.*, 2011), and although some have postulated that this is because of a stronger ocean circulation (*Bitz et al.*, 2006), many have suggested that northward advection of the anthropogenic warming signal with the climatological ocean circulation causes the ocean heat transport increase (*Marshall et al.*, 2014, 2015). In contrast to the Arctic, in the subpolar North Atlantic both the atmospheric warming and the stronger freshwater forcing act to decrease surface densities and to weaken the ocean circulation. Consequently, less heat is transported to the subpolar region and the ocean heat content decreases (paper II).

Our objective is to achieve a more detailed picture of the Arctic response to freshwater and global warming, and to understand the Arctic response in the larger North Atlantic and global framework. We summarize the key objectives to the following questions

1. How do ocean circulation, ocean heat content, and sea ice cover in the Arctic respond to increasing Arctic freshwater forcing?

2. How does high latitude ocean heat transport respond to greenhouse warming, and do changes in ocean heat transport affect the atmosphere?

Due to the short and limited observational record (constructing heat and freshwater budgets from the observational records for long time periods is not possible) we choose to use a modelling approach. In paper I we use an idealized Arctic column model (*Björk*, 1989, 1992, 1997; *Smedsrud et al.*, 2008) to answer the first objective. The idealized nature of the model allows us to explore the uncertain parameter space and construct a model setup that closely reproduces the observed mean Arctic salinity and temperature stratification. For paper II (and for section 5.2.1) we widen this approach and

use the ocean–sea ice component of the Norwegian Earth System model (NorESM1-M, *Bentsen et al.* (2013)). While the small scale features are not resolved because the model itself is relatively coarse ($\sim 1^\circ$ horizontal resolution), simulations of the large scale features benefit from the use of a global setup which allows for global adjustment of the ocean circulation. The setup enables direct comparison with the fully coupled NorESM1-M setup used as part of the Coupled Modelling Intercomparison Project (CMIP5). This is useful since in paper III we turn to multimodel CMIP5 ensemble to study the high latitude ocean heat transport. Using this hierarchy of models allows us to assess the robustness of our findings.

Chapter 3

Summary

Paper I: *Response of Arctic Ocean stratification to changing river runoff in a column model*

In paper I we use a 1D column model of the Arctic Ocean in which we perturb the freshwater flux entering the Arctic Ocean through rivers. We show, that to first order, a larger freshwater flux leads to a new steady state with a fresher surface layer and a warmer Atlantic water layer at depth. From a heat budget perspective the new steady state emerges as a balance between an increasingly stable density stratification and an increasingly unstable temperature stratification. The vertical heat flux is relatively insensitive to changes in the freshwater flux, as we keep the heat flux convergence constant. Consequently, changes in the sea ice cover are relatively small, and can be explained to a large extent by changes in the freezing point temperature of the surface waters.

Paper II: *Consequences of future increased Arctic runoff on Arctic Ocean stratification, circulation, and sea ice cover*

In paper II we expand the 1D perspective of paper I to a 3D perspective using a coupled ocean-sea ice model. The 3D model avoids using the fixed lateral boundary conditions and the assumption of a constant ocean heat transport convergence that we used in the 1D model. Similar to paper I we perturb the freshwater flux entering the Arctic Ocean through rivers. We examine the ocean and sea ice response both in the Arctic and in the North Atlantic Ocean. Comparable to the 1D column model results in paper I, the 3D model adjusts to increased freshwater with a fresher surface and a warmer Atlantic layer. Interestingly, the ocean heat transport convergence, and the vertical heat flux, remain relatively constant in the Arctic Ocean. Changes in sea ice cover are therefore mostly related to changes in sea ice convergence and divergence. We find that the freshwater added to the Arctic flows south and is entrained into the convective regions in the North Atlantic, similar to many freshwater hosing studies. As a result the subpolar gyre slows down, cools, and freshens.

In section 5.2.1 we perform additional analysis of the same simulations focusing on changes in the volume transports between the Arctic Ocean and the surrounding oceans.

We use an estuarine and overturning circulation framework and show that exchanges between the Arctic Ocean and lower latitude oceans can be understood as a balance between the generally decreasing overturning circulation and intensifying estuarine circulation. Interestingly, we find that a small increase in the freshwater forcing leads to an increase in both the overturning and the estuarine components due to the salt advection feedback.

Paper III: *Connecting ocean heat transport changes from the mid-latitudes to the Arctic Ocean*

In paper III we examine changes in the Northern Hemisphere ocean heat budget and Arctic amplification under greenhouse warming in fully coupled climate models. The greenhouse warming leads not only to a radiative imbalance at the top of the atmosphere, but also alters atmosphere-ocean heat exchange and the heat carried poleward by the two media. Ocean heat content increases globally as the ocean receives more heat than it loses. However, in the Arctic Ocean, in the equatorward flank of Southern Ocean, and in the Northern mid-latitudes, the ocean heat content increases faster than the global average. The faster than average heat content increase in the Arctic Ocean and in the equatorward flanks of the Southern Ocean follows from advection of warmer waters from upstream regions of reduced ocean-to-atmosphere heat loss. In the mid-latitude Northern Hemisphere the Hadley cell expansion, and the related increase in the local surface shortwave radiation, drives the ocean heat content increase. Finally, the advection of warmer waters to the Arctic Ocean links to the intermodel differences in Arctic amplification. Climate models that have the largest increase in the ocean heat transport to the Arctic Ocean tend to have the largest Arctic amplification.

Main Conclusions

The results summarized above lead to the following overall conclusions:

- Vertical heat fluxes in the central Arctic Ocean are relatively stable for larger freshwater input (papers I and II) due to a balancing effect between salinity and temperature stratifications. A buoyant fresh surface layer acts to reduce vertical mixing, but a warm Atlantic layer acts to increase the vertical heat flux; the vertical heat flux remains relatively constant since a small volume of warm water carries a large amount of heat.

- Ocean heat content increase is relatively homogeneous in the zonal average under greenhouse warming (paper III). The positive anomalies in this relatively homogeneous field follow either from stronger radiative warming (mid-latitude North Atlantic), or reduced ocean-to-atmosphere surface heat loss which the climatological ocean circulation modifies (Arctic Ocean and Southern Ocean).

- The imprint of greenhouse forcing on the ocean heat transport is of the opposite sign in the Arctic Ocean compared to the North Atlantic (paper II and III). If the

greenhouse forcing moves along the RCP8.5 trajectory we expect a reduction in the Atlantic Meridional Overturning Circulation, and a related reduction in the mid-latitude northward ocean heat transport, but an increase in the ocean heat transport to the Arctic Ocean.

- To first order, the large scale ocean circulation response to an increase in the Arctic river runoff – slowdown of the Atlantic Meridional Overturning Circulation and the subpolar gyre – is similar to any positive freshwater perturbation in the North Atlantic-Arctic sector (Paper II).

Chapter 4

Future Perspectives

The results of this dissertation point toward a number of open questions and we list the most pressing ones below.

The results from paper II and section 5.2.1 illustrate a need for further understanding of watermass transformations inside the Arctic Ocean, and how they relate to the overall exchanges between the Arctic and the surrounding ocean basins. As expected, changes in the large scale sea surface height gradients control the net flow between the Arctic and the surrounding oceans while watermass transformations control the *total exchanges* (strength of the in and outflows). In the case of freshwater perturbations, it is obvious that the two should be connected as freshwater affects both sealevel and watermass transformations. However, we still lack a framework combining the two.

The Atlantic Meridional Overturning Circulation, the North Atlantic Subpolar Gyre, and the associated heat transport show a consistent decrease after a positive freshwater perturbation (paper II). While observational studies also support a linkage between North Atlantic convection sites and the lower limb of the Atlantic Meridional Overturning Circulation, it is not clear how the upper limb of this circulation, which carries the poleward ocean heat transport, connects from subtropical to subpolar latitudes (*Buckley and Marshall*, 2015; *Burkholder and Lozier*, 2011, 2014; *Foukal and Lozier*, 2016; *Lozier*, 2012; *Palter et al.*, 2008). Merging the perspectives of integrated measures such as the AMOC, or the meridional heat transport, with a Lagrangian based analysis is needed to increase our understanding of the mechanisms that connect the subtropical and subpolar surface circulation in the North Atlantic.

The results in paper III show that we still lack understanding of the reasons behind the model spread in the high latitude amplification of greenhouse warming. The results indicate that some part of the models simulate temperature amplification in the midlatitudes, while others simulate temperature amplification only at the high latitudes. It should be a future task to find out whether these differences follow from the models' base climatology, or from intermodel differences in the feedback mechanisms.

Finally, the results in this dissertation are largely based on idealized, and/or coarse resolution models where many of the important physical processes are parameterized. With these models we can robustly infer first order dynamics at large scales. However, high model resolution is important for several features of the climate system. For example, ocean heat transport to the Arctic Ocean (*Hattermann et al.*, 2016), mixing of heat and freshwater from the boundary currents to the convective regions of the subpolar North Atlantic (*Kawasaki and Hasumi*, 2014), surface heat and moisture fluxes

affecting winter time precipitation (*Ma et al.*, 2015), and near-decadal predictability in the North Atlantic Ocean (*Siqueira and Kirtman*, 2016) all depend on small scale ocean features. With a move towards higher resolution coupled models the research community can move towards robust assessments of these higher order problems and respond to the need for understanding the regional patterns of climate change and the interannual-to-decadal scale climate variability.

Chapter 5

Scientific results

Paper I

5.1 Response of Arctic Ocean stratification to changing river runoff in a column model

Nummelin A., C. Li, and L. H. Smedsrud (2015) Response of Arctic Ocean stratification to changing river runoff in a column model, *J. Geophys. Res. Oceans*, **120**, 2655–2675, doi:10.1002/2014JC010571.

AGU PUBLICATIONS

JGR

Journal of Geophysical Research: Oceans

RESEARCH ARTICLE
10.1002/2014JC010571

Key Points:
- Expected future increase in Arctic river runoff intensifies ocean stratification
- Stronger vertical stratification leads to warming below surface mixed layer
- Changes in heat flux to the base of the ice and in ice thickness are small

Supporting Information:
- Table S1
- Supporting Information S1

Correspondence to:
A. Nummelin,
aleksi.nummelin@uib.no

Citation:
Nummelin, A., C. Li, and L. H. Smedsrud (2015), Response of Arctic Ocean stratification to changing river runoff in a column model, *J. Geophys. Res. Oceans*, *120*, 2655–2675, doi:10.1002/2014JC010571.

Received 7 NOV 2014
Accepted 25 FEB 2015
Accepted article online 02 MAR 2015
Published online 7 APR 2015

Response of Arctic Ocean stratification to changing river runoff in a column model

Aleksi Nummelin[1,2], Camille Li[1,2], and Lars H. Smedsrud[1,2,3]

[1]Geophysical Institute, University of Bergen, Bergen, Norway, [2]Bjerknes Centre for Climate Research, Bergen, Norway, [3]University Centre in Svalbard, Longyearbyen, Norway

Abstract A one-dimensional model of the atmosphere-ice-ocean column is used to study the effects of changing river runoff to the Arctic Ocean. River runoff is the largest contributor of freshwater to the Arctic and is expected to increase as the hydrological cycle accelerates due to global warming. The column model simulates the stratification of the Arctic Ocean reasonably well, capturing important features such as the fresh surface layer, the salty cold halocline, and the temperature maximum within the Atlantic Water layer. The model is run for 500 years with prescribed boundary conditions to reach steady state solutions. Increasing river runoff is found to strengthen the stratification and to produce a fresher and shallower surface mixed layer with warming (up to ~1°C for a doubling of present-day runoff) in the Atlantic Water layer below. An important consequence is that the effect of the larger vertical temperature gradient is able to balance that of the stronger stratification and yield a close to constant vertical heat flux toward the surface. As a result, the sea ice response is small, showing only slight increase (up to ~15 cm for a doubling of present-day runoff) in annual mean ice thickness. Limitations of the study include the idealized nature of the column model and uncertainties in the background vertical mixing within the Arctic Ocean.

1. Introduction

The Arctic Ocean is distinguished from the rest of the world's oceans by unique oceanographic conditions. At the surface is a cold, fresh surface mixed layer while deep below is a layer of warmer, saltier Atlantic Water (AW). In between is a halocline, a relatively thin layer of increasing salinity with depth. The resulting stratification is essential for the presence of Arctic sea ice, with the halocline protecting the cold surface layer from the heat stored in the AW layer below. One of the critical factors maintaining this stratification is freshwater supplied by continental river runoff, which increases as the hydrological cycle accelerates due to global warming [*Rawlins et al*., 2010]. The increase in runoff is already measurable, with a reported 9.8% increase in the 30 year period between 1977 and 2007 [*Overeem and Syvitski*, 2010]. While the projections for future changes are somewhat uncertain, a runoff sensitivity of 0.007 Sv/°C is estimated from observations [*Peterson et al*., 2002] and the multimodel CMIP5 ensemble predicts an increase of approximately 0.03 Sv (30%) by 2100 for the RCP8.5 scenario (see supporting information Figure S1). Understanding the effects of changing river runoff on the stratification, heat fluxes, and sea ice cover in the Arctic Ocean is the main goal of this study. To this end, we perform and analyze a series of sensitivity experiments using a one-dimensional atmosphere-ice-ocean column model.

A special feature of the stratification in the Arctic Ocean is the cold upper part of the halocline, which has higher salinities than the surface layer but temperatures still close to the freezing point. The cold upper halocline derives from waters formed on shallow shelves and in the Arctic proper during sea ice formation [*Rudels et al*., 1996; *Steele and Boyd*, 1998; *Rudels et al*., 2004]. This cold halocline effectively reduces the heat flux to the surface mixed layer from below because any mixing penetrating the halocline only entrains cold (close to freezing point temperature) water [*Steele and Boyd*, 1998].

The net effect of increased runoff on this system is not easy to predict. One might expect increased runoff to strengthen the stratification by freshening the surface. On the other hand, a fresher surface layer sets up a larger density contrast between the Arctic Ocean and the Nordic Seas. This could increase the surface outflow from the Arctic, leading to stronger entrainment of the warm AW below [*Stigebrandt*, 1981]. A fresher surface would also modify shelf water formation, a water mass that feeds into the cold halocline. These

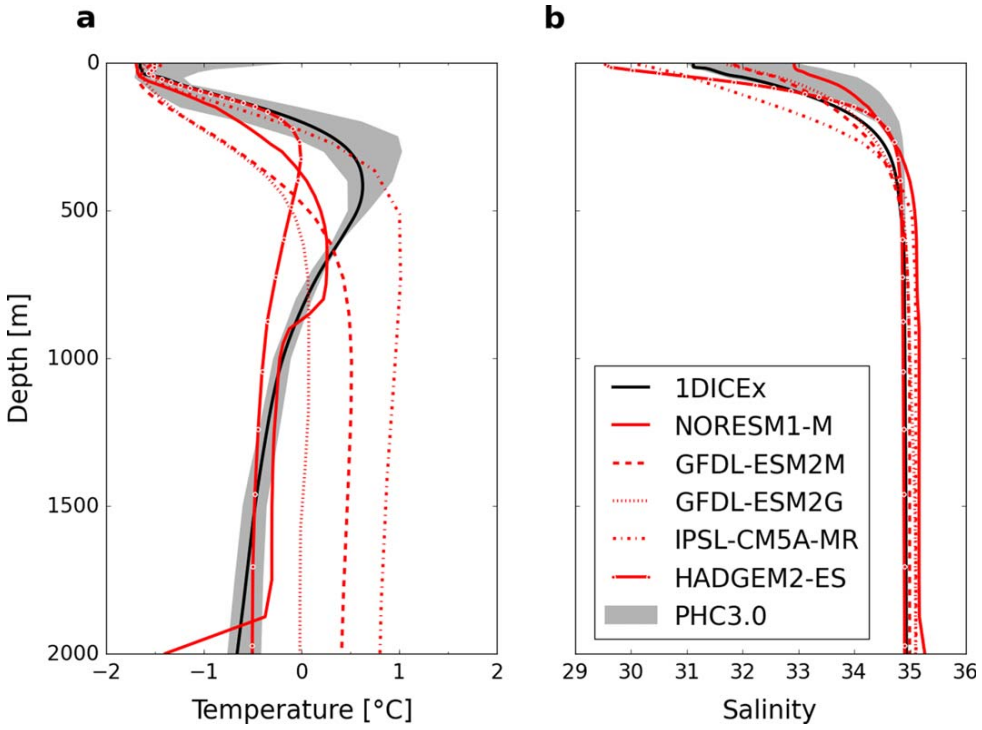

Figure 1. Observed and simulated (a) annual mean temperature and (b) salinity in the Arctic Ocean. Observed (PHC3.0 updated from *Steele et al.* [2001]) 25–75% quartile range is shown with gray shading. Results from the column model are shown in black. Selected climate model results for simulations of the 1970–2005 historical period are shown in red (Norwegian Earth System Model, NorESM [*Bentsen et al.*, 2013], ESM2M and ESM2G [*Dunne et al.*, 2012], HadGem2-ES [*Jones et al.*, 2011], and IPSL-CM5A-MR [*Mignot et al.*, 2013]), with profiles averaged over the Arctic Ocean (Barents Sea excluded).

various changes have different, and in some cases opposite, influences on the vertical heat flux toward the surface mixed layer and the base of the sea ice.

Climate models have trouble simulating the vertical structure of the upper Arctic Ocean (Figure 1), implying that they do not accurately represent some of the processes responsible for maintaining the stratification. Particularly difficult is capturing the strength of the halocline, as well as the depth and structure of the AW layer. The halocline and AW layer extend over a broader depth range in the models than in observations, are generally too weak and in most cases too deep (Figure 1). These features are crucial for a realistic response to perturbations in freshwater balance because they help set the vertical fluxes of heat among the ocean, ice, and atmosphere. This study uses an idealized one-dimensional coupled atmosphere-ice-ocean column model, motivated by the fact that the model is able to simulate these stratification features relatively well (Figure 1). The column model has a reduced set of variables and is computationally efficient, allowing us to perform many sensitivity experiments and to derive nearly steady state solutions. Furthermore, it is possible to separate forcings and responses and better interpret mechanisms that include complicated and contradicting feedbacks.

The original version of the column model used here was first presented by *Björk* [1989], and different versions have since been developed and used [e.g., *Björk and Söderkvist*, 2002; *Smedsrud et al.*, 2008; *Linders and Björk*, 2013]. The model simulates a horizontally averaged vertical atmosphere-ice-ocean column. Originally, the model domain extended from the top of the atmosphere to the core of the AW layer at 300 m depth, where temperature and salinity were fixed to mean AW properties. In this study, we extend the model by expanding the model domain down to 2000 m and including a parameterization to compensate the heat loss due to upwelling from the AW layer (i.e., a prescribed heat convergence via Atlantic inflow with given T/S properties). The extended model allows the AW layer to respond dynamically to changes in river runoff and plays an active role in determining the resulting stratification.

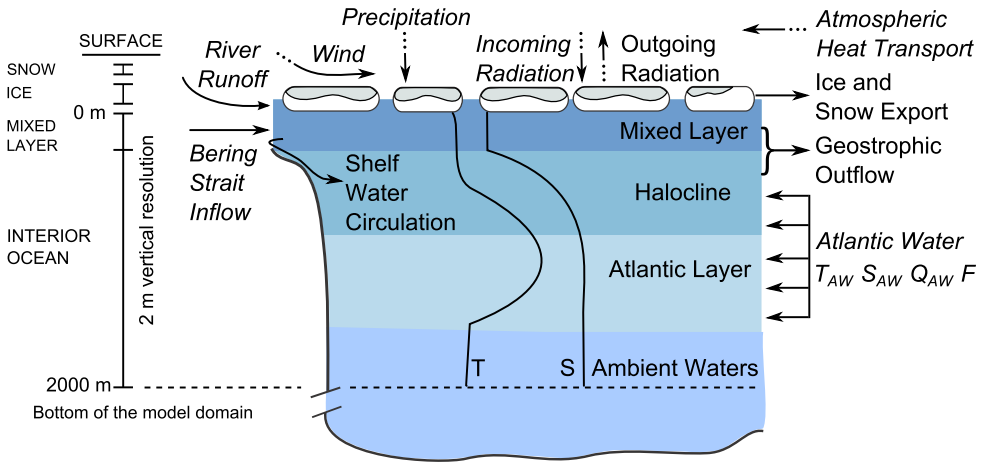

Figure 2. Sketch of the 1DICEx Arctic atmosphere-ice-ocean column model setup. The components of the model are indicated at the far left, and the cartoon shows the model forcings, simulated processes and resulting vertical stratification. See details and full list of abbreviations in the appendices.

The paper is structured as follows: we describe and evaluate the modified one-dimensional atmosphere-ice-ocean column model in section 2, present the results of the runoff experiments in section 3, and discuss the context and limitations of the study in section 4. Some conclusions on the effects of increased runoff on Arctic Ocean stratification and sea ice are presented in section 5. The model is described in more detail in Appendix A, a list of symbols is included in Appendix B, and the climatological forcing is given in Appendix C.

2. Extended 1DICE (1DICEx) Model

In this study, we use a version of the one-dimensional Arctic column model, 1DICE, which derives from the work of *Björk and Söderkvist* [2002] and *Björk* [1997, 1992, 1989]. Figure 2 shows a sketch of the setup used in this study. A more detailed description of the model including the extensions made in this study can be found in Appendix A.

The column model is set up to represent mean conditions in the Arctic Ocean following *Björk and Söderkvist* [2002]. The main forcings comprise climatological monthly mean values of atmospheric heat transport and downward shortwave radiation. The freshwater budget includes prescribed precipitation, river runoff, and transport from the Pacific Ocean through Bering Strait. There is an additional parameterized flow of brine-enriched water from the Arctic shelves to the deep Arctic basin. The surface outflow in the column is geostrophic and depends on the density gradient between the Arctic column and the Atlantic (the Atlantic is not explicitly included in 1DICEx, but prescribed AW properties are used). 1DICE includes a thermodynamic sea ice model with a ridging parameterization and up to 42 ice thickness classes. Sea ice export is driven by prescribed divergence based on measured values in the Fram Strait and the geostrophic surface outflow (Figure 2). The gray body atmospheric component of the model solves for atmospheric temperatures from prescribed atmospheric heat transport and solar radiation and calculated surface fluxes.

The present-day scenario uses a river runoff of 0.082 Sv [following *Björk and Söderkvist*, 2002], a value which is very close to the 0.088 Sv reported by *Lammers et al.* [2001] for the Arctic Ocean excluding the Barents Sea. The values for our runoff experiments are scaled from the climatology used by *Björk and Söderkvist* [2002], so we change the annual mean and monthly runoff, but preserve the seasonality of the forcing (see Appendix C for values of present-day scenario).

The main modification made for this study is the inclusion of an interactive AW layer in the column. This allows the temperature, salinity, and stratification of the column to adjust as we vary runoff. In the following sections, we discuss some of the assumptions related to the addition of the interactive AW layer and evaluate the performance of the extended 1DICEx model.

2.1. Interactive AW Layer

The bottom of the original model domain was set at 300 m. This bottom boundary was assumed to be the core of the AW layer, and temperature and salinity were fixed to constant "AW" values here. We have

extended the ocean column down to 2000 m to allow for an interactive AW layer, a modification that requires the addition of a heating term within the AW layer to compensate the surface heat loss and outflow. Physically, this can be seen as a parameterization for the heat and salt transported into the Arctic by the Atlantic inflow. Practically, it is implemented by requiring a fixed amount of AW heat transport at each time step and solving for the associated salt transport based on fixed AW *T/S* properties, which can largely be based on observations (see Appendix A and section 2.2).

In nature, variations in both volume transport and AW temperature can alter heat transport of the Atlantic inflow over a range of time scales. In the idealized approach used here, we set the temperature T_{AW} and salinity S_{AW} of the Atlantic inflow, as well as the heat supply H_{AW} needed to compensate the surface heat loss and outflow, to constants. The inflowing AW enters and adjusts with the column to form the AW layer. This approach allows us to isolate the mechanisms for Arctic Ocean changes related to variability in runoff from the mechanisms related to variability in properties of the inflowing AW. While this approach simplifies the analysis of the results, it carries certain implications.

First, in order to have heat transport from the Atlantic toward the Arctic, the heat content of the inflowing AW must be larger than the heat content in the Arctic column, i.e., $(\rho_{AW} T_{AW}) > (\rho T)$, where ρ_{AW} and T_{AW} are the (constant) density and temperature of the inflowing AW and ρ and T are the (prognostic) density and temperature of the column. In essence, the AW inflow needs to be warm enough to provide the required heat to the column. The salt transport into the column is a function of the heat transport and the AW inflow salinity (S_{AW}). S_{AW} cannot greatly exceed the salinity below the halocline, otherwise an unrealistic intermediate high salinity layer will form; it cannot be too low either, otherwise the halocline will be eroded.

Second, we must make certain decisions about the character of the AW inflow in the extended model. The inflow enters the column as a 500 m thick layer below the surface mixed layer ($Z_{AW} = 500$ m). The model physics then create the halocline and the AW layer in the interior ocean component (Figure 2). The halocline forms in the upper part of the interior ocean, and the AW layer is the location of the temperature maximum. Note that while Z_{AW} is constant, the AW inflow moves up and down following the annual cycle of the mixed layer depth. We set the vertical distribution of the AW heat transport to be a simple, barotropic boxcar (tests with a parabolic distribution produced similar results). While T_{AW} and S_{AW} are fairly well constrained by observations, there are less constraints on the vertical diffusion coefficient κ, which should be regarded mostly as a tuning parameter.

2.2. Evaluation and Sensitivity of the Extended Model

In this section, we describe how we tune the extended model to produce simulated T/S profiles as close as possible to available observations. We do this by running the model using a range of AW inflow properties (T_{AW}, S_{AW}, H_{AW}) and vertical mixing coefficients (κ), and identifying the combination of values that yield an ocean heat content that is closest to equilibrium. The resulting fluxes are then discussed at the end of the section.

The robustness of the model to the optimal values is shown in Figure 3, in which simulated T/S profiles are plotted as a function of T_{AW}, S_{AW}, and κ for $H_{AW} = 1$ TW. The T/S profiles are quite similar for the ranges $T_{AW} = [1.5, 4.0]^{\circ}$C, $S_{AW} = [34.8, 35.1]$, and $\kappa = [3.0–5.0] \times 10^{-6}$ m^2 s^{-1}. However, differences are apparent for some parameter combinations, mostly due to emerging convection. Closer inspection reveals that low T_{AW} and/or high S_{AW} leads to too much salt transport into the column and the formation of an intermediate salinity maximum around 500 m. It is only at values of T_{AW} and S_{AW} outside a realistic range that this salinity maximum appears in the model, although a there is some evidence of a subtle salinity maximum in some parts of the Arctic Ocean [*Rudels et al.*, 1994]. On the other hand, low S_{AW} results in a cooler AW layer because the smaller density gradient allows for more mixing toward the surface. The vertical diffusion coefficient κ has a larger effect on the simulated T/S profiles than the AW properties. Higher diffusion brings more heat up from the warm AW layer to the surface, but the choice of κ is also affected by the value of the compensating heat flux H_{AW} (not shown). Reasonable T/S profiles can only be attained over a narrow range of H_{AW}, otherwise the column warms up extensively, so this sets a practical limit on κ.

Given limited observations, especially for κ, we used the stability of the column's heat content to finalize the optimal T_{AW}, S_{AW}, and κ values. Figure 4 shows the change in heat content over the last 100 years of the 500 year runs as a function of T_{AW} and S_{AW} for three different values of κ. An optimal solution is simply a

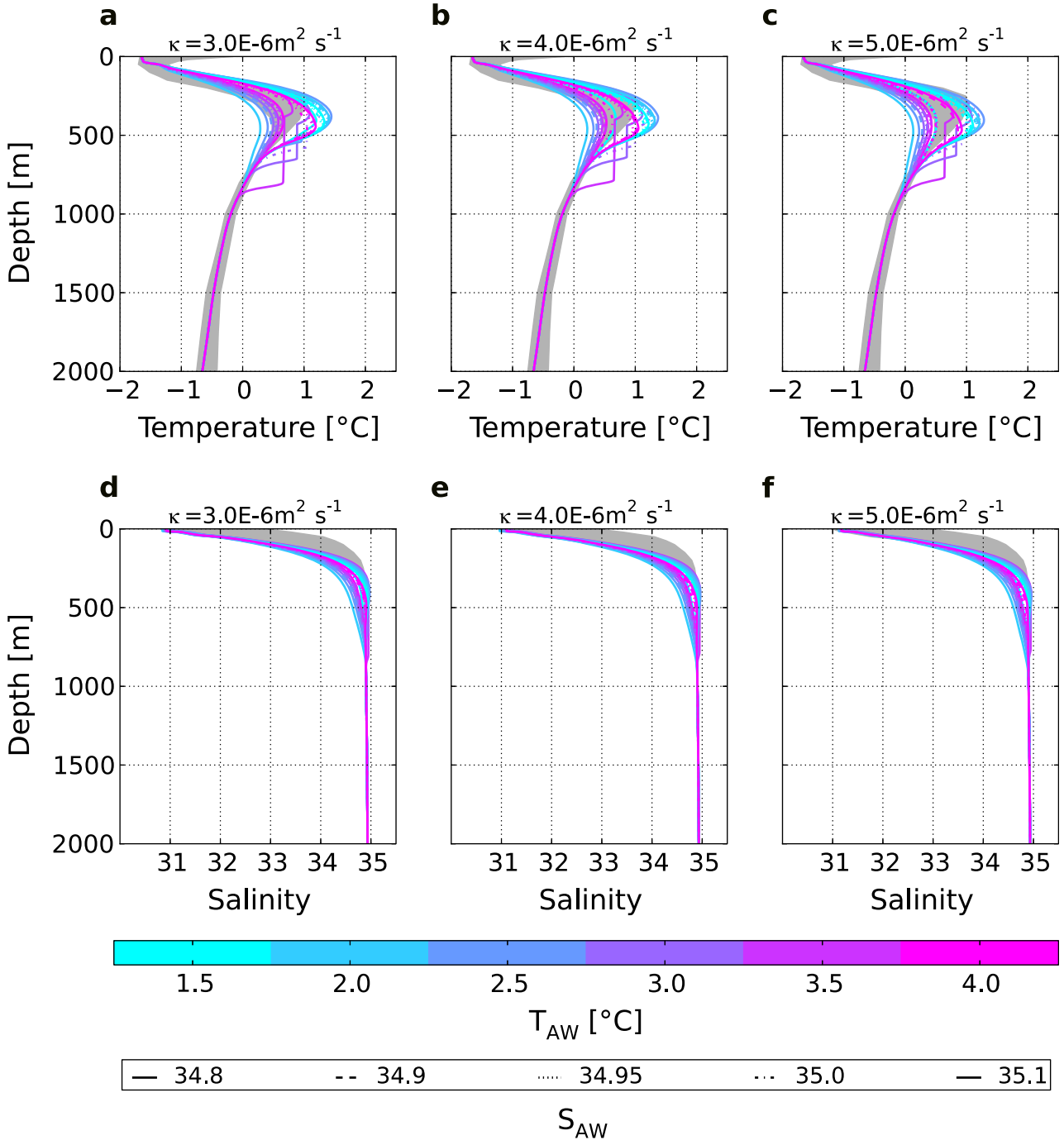

Figure 3. (top row) Simulated temperature (T) and (bottom row) salinity profiles (S) for three vertical diffusion coefficients (κ) and varying properties of inflowing Atlantic Water (T_{AW} indicated by different colors, S_{AW} indicated by different line types). Gray shading indicates the 25–75% quartile range calculated from observations (PHC3.0 updated from *Steele et al.* [2001]).

case where the change in the heat content $\frac{dE}{dt}$ is zero. It is possible to find such a solution by interpolating in T_{AW}-S_{AW}-κ space for the values where $\frac{dE}{dt}=0$. With the constraints provided by Figures 3 and 4, we arrive at values of $T_{AW}=3.5$°C and $S_{AW}=35.0$; a compensating heat flux of $H_{AW}=1$ TW by the AW inflow; and a vertical diffusion coefficient $\kappa=4.0\times10^{-6}$ m^2 s^{-1}. These values are comparable to the AW properties in the Fram Strait (PHC3.0 updated from *Steele et al.* [2001]), and κ values from the central Arctic Ocean [*Fer*, 2009].

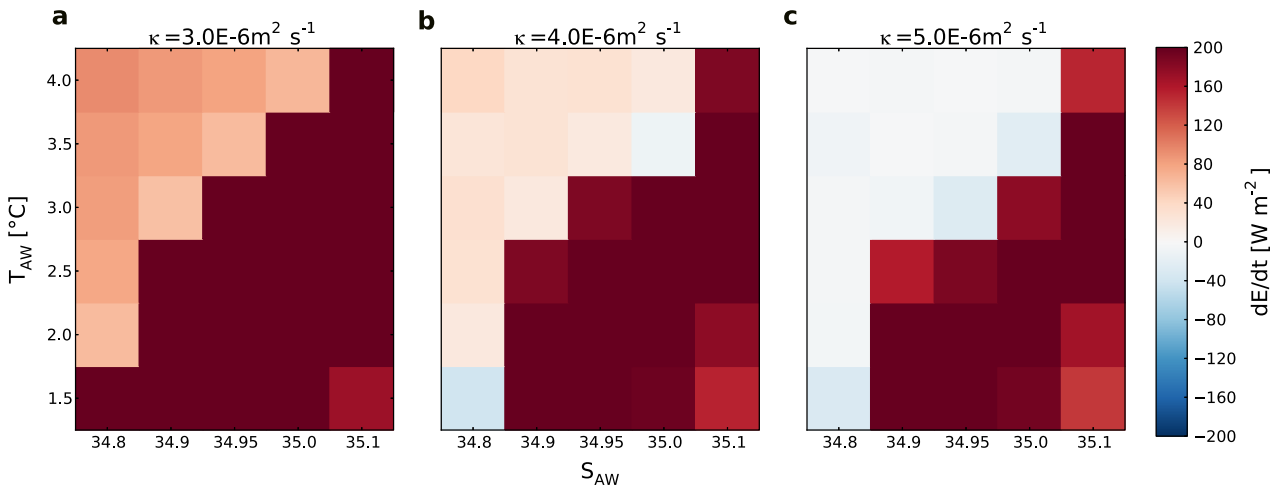

Figure 4. Simulated rate of change of internal energy $\left(\frac{dE}{dt}\right)$ over the last 100 years of each experiment for three vertical diffusion coefficients (κ) and varying properties of inflowing Atlantic Water (T_{AW}, S_{AW}).

As a consistency check, we examine the simulated volume and heat fluxes using the optimal values obtained above for the present-day runoff scenario. Details on how these fluxes are calculated appear in the introductory paragraph of this section and in Appendix A1. The main components of the freshwater budget in the present-day scenario are approximately 1.1 Sv of surface inflow (river runoff, Bering Strait inflow, and precipitation combined) balanced by approximately 1.2 Sv of geostrophic outflow in the upper part of the column. The outflow is of the same order of magnitude as observed (2–4 Sv) [*Marnela et al.*, 2013], although on the low side. The difference between the simulated and measured outflow could be due to several factors. First, we simulate a "steady state" Arctic Ocean. Observations covering a much shorter period should be expected to differ from such a long-term mean in any regard, but especially so for the Arctic today, which is undergoing rapid transition toward a warmer ocean and a thinner ice cover. Second, the simplified geostrophic outflow should not be expected to capture all aspects of reality, especially in complex regions like the Canadian Archipelago.

In addition to the main inflow and outflow terms, 1DICEx simulates 0.1 Sv of snow and ice export, which is a good match to the observed estimates of around 0.1 Sv [*Vinje*, 2001; *Spreen et al.*, 2009; *Schauer and Beszczynska-Möller*, 2009]. There is an additional 0.2 Sv of upwelling from the AW layer that balances the column volume fluxes. The associated $H_{AW} = 1$ TW heat supply converts to 0.13 W m^{-2} of heat flux toward the surface from below. This vertical heat flux also compares well with recent estimates of 0.1–0.2 W m^{-2} from the AW layer in the Canadian basin [*Lique et al.*, 2014].

2.3. Setup of River Runoff Experiments

In this study, we integrate 1DICEx over 500 years to obtain near-steady state solutions as a response to changing river runoff. The initial conditions for all runs are climatological conditions (PHC3.0 updated from *Steele et al.* [2001]), but river runoff is increased from just under one third (0.025 Sv) to just over 2 times (0.20 Sv) the present-day estimate of 0.082 Sv.

Figure 5 shows the adjustment of ocean temperature, salinity, and heat content for the various runoff scenarios over the 500 year simulation period. The mean temperature of the ocean column adjusts within the first few hundred years, although the highest and lowest runoff scenarios exhibit a small trend through the entire experiment. The column mean salinity equilibrates much more quickly, within a couple of decades, because it primarily reflects surface changes. With time, the heat content approaches steady state, and there is very little change over the last 200 years. Based on this analysis, we present results averaged over the last 100 years of each experiment, when most variables are close to steady state.

3. Results

To study the response of the Arctic Ocean to changes in river runoff, we run the 1DICEx column model with runoff values varying from 0.025 to 0.2 Sv. Reported present-day values are close to 0.1 Sv [*Peterson et al.*,

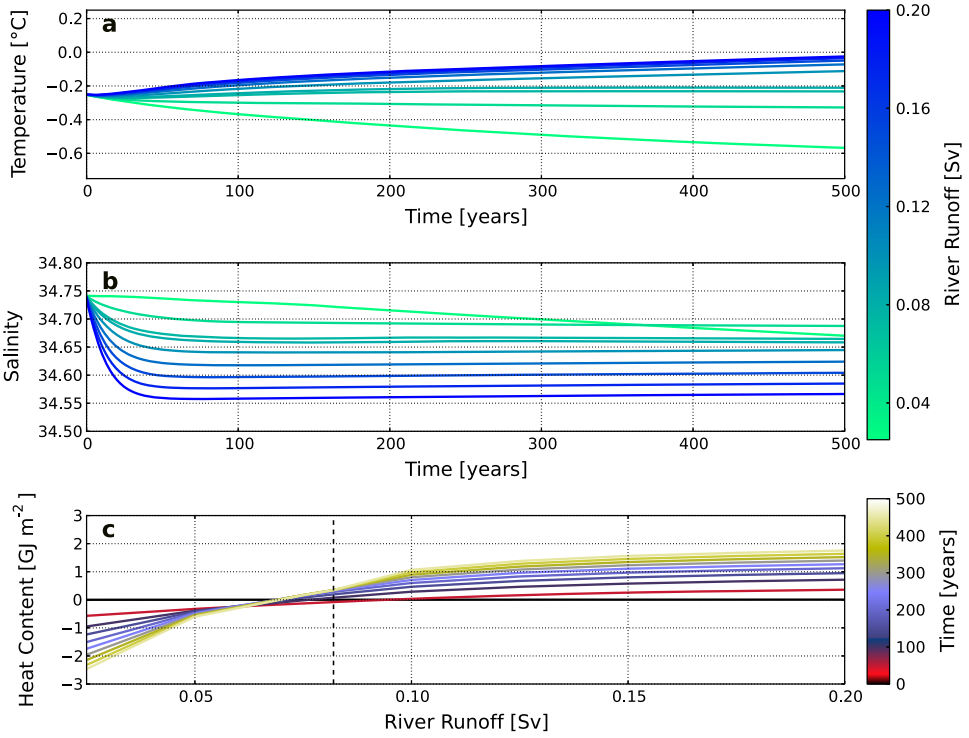

Figure 5. Transient response of 1DICEx model. Mass-weighted column-averaged (a) temperature and (b) salinity as a function of time (1 year running means); (c) column heat content anomaly referenced to initial conditions as a function of river runoff.

2002] for the pan-Arctic region and 0.088 Sv for the Arctic proper [*Lammers et al.*, 2001], which is the domain of interest here. A 9.8% increase is reported for the period between 1977 and 2007 [*Overeem and Syvitski*, 2010], while the projections for future runoff changes are rather uncertain, e.g., sensitivity of 0.007 Sv/°C from observations [*Peterson et al.*, 2002] and approximately 30% increase by 2100 in RCP8.5 for multi-model CMIP5 ensemble (supporting information Figure S1). The 0.025–0.2 Sv range of our experiments spans this uncertainty.

3.1. Ocean Response

The most obvious effect of increased river runoff is a freshening of the surface ML and the upper halocline (Figures 6a and 7). The annual mean surface salinity decreases from 31 for present-day runoff to below 26 for a doubling of runoff. The freshening effect penetrates to the upper halocline (around 80 m), below which the salinity response is small. As the surface freshens, the upper ocean becomes more stratified, resulting in a shallower winter ML (lower dashed gray line in Figure 6a). Because the summer ML is always quite shallow due to shortwave heating and ice melt, the seasonal cycle in mixed layer depth (MLD) weakens (distance between the dashed gray lines in Figure 6a). Experiments with less river runoff than present-day feature a saltier, deeper ML with a larger seasonal cycle in depth. The full seasonal cycle of the temperature and density structure is shown in supporting information Figures S2 and S3.

The temperature response to increasing runoff can be seen in Figure 6b, with general warming extending through most of the Arctic column. The warming is strongest between 200 and 600 m, in the AW layer, but there is also significant warming just below the ML above the cold halocline (see also Figure 7). The structure of the temperature response is the result of an intricate adjustment in stratification and mixing as the surface ML freshens and thins. We examine the details of this adjustment in the next section.

To first order, the heat budget of the ML is a balance between the surface fluxes and entrainment from below. The simulated surface fluxes (Figure 8b) include longwave and shortwave radiation and turbulent heat fluxes over open ocean and sea ice, and their net effect is to cool the ML. The shortwave component (solar radiation input, simulated as an exponentially decaying function with depth) penetrates to depths of

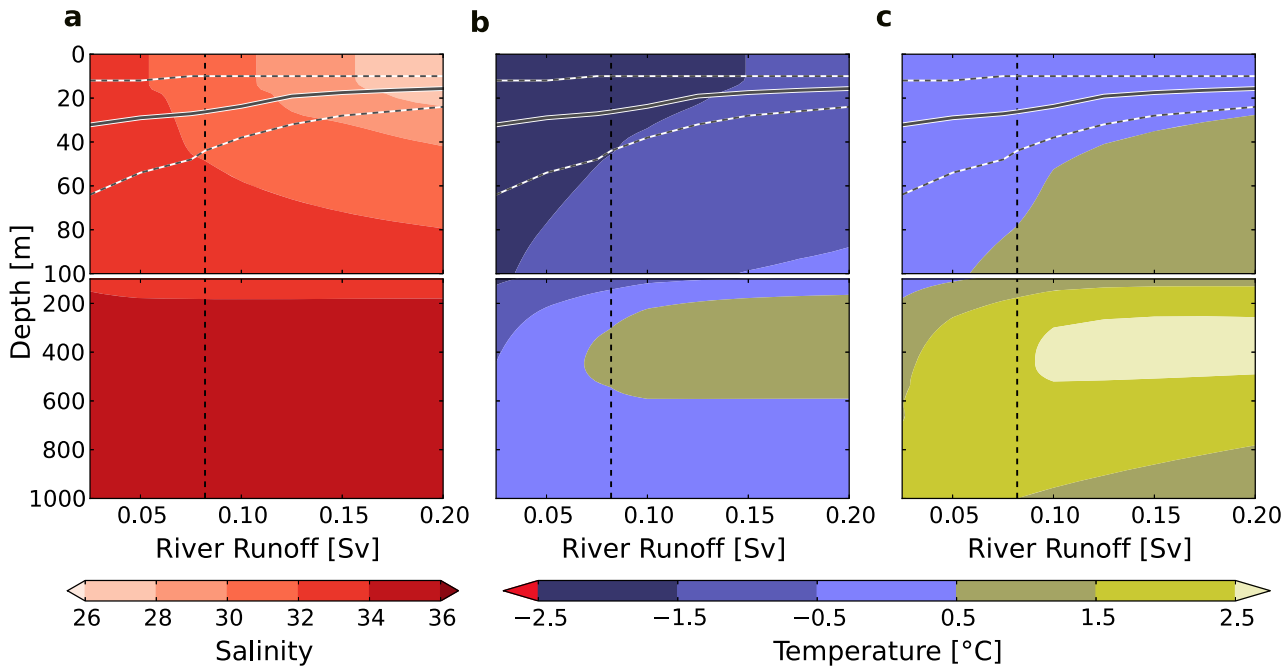

Figure 6. Simulated changes in (a) salinity (S), (b) temperature (T), and (c) temperature referenced to freezing point temperature (T_f) in response to increasing river runoff. The vertical black dashed line shows annual mean river runoff into the Arctic Ocean for the present day. The gray lines show the mixed layer depth (MLD; solid is annual mean, dashed are winter maximum and summer minimum).

60–70 m, so the influence of the surface fluxes also reaches these depths. The ML entrainment term (entrainment of water into the ML from below) consistently warms the ML (Figure 8c). At steady state, surface heat loss is compensated by entrainment of warmer waters through ML deepening. However, as increasing runoff causes the winter ML to shoal, a larger portion of the heat from shortwave radiation in summer is left in the water column in winter. This causes a warming of the upper halocline just below the winter ML, a feature similar to what is sometimes called the near-surface temperature maximum (NSTM) in observations [see also *Toole et al.*, 2010; *Jackson et al.*, 2011]. At lower runoffs, the winter ML forms deep enough that it reincorporates all the heat absorbed during summer.

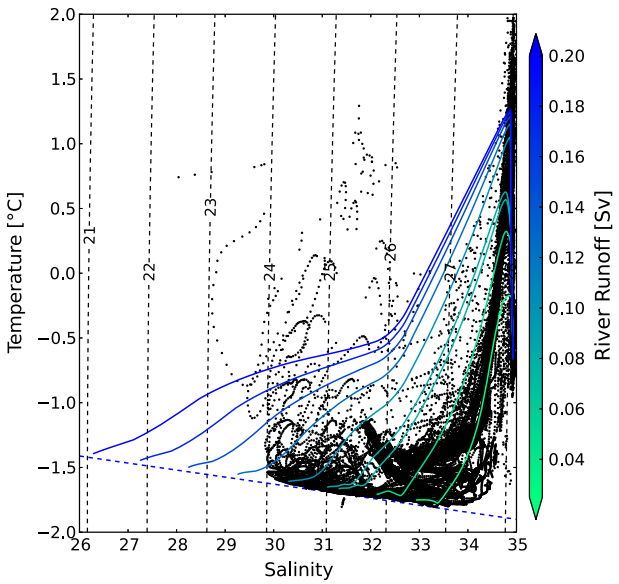

Figure 7. T-S diagram for the Arctic. The solid lines show the simulated steady state result for the runoff experiments, with colors indicating the runoff value. The black dots show observed climatological conditions (PHC3.0 updated from *Steele et al.* [2001]). The freezing point temperature is indicated by the dashed blue line.

The compensating heat flux in the AW layer warms nearly the entire column (Figure 8a). Recall that we fix the AW inflow properties in our experiments, so there is no change in T_{AW} and S_{AW} with time. The compensating heat flux balances the surface fluxes and maintains the warm subsurface waters for entrainment. The formulation of the interactive AW layer in 1DICEx carefully adjusts the implied AW volume flux to maintain this compensating heat flux. As runoff increases, the

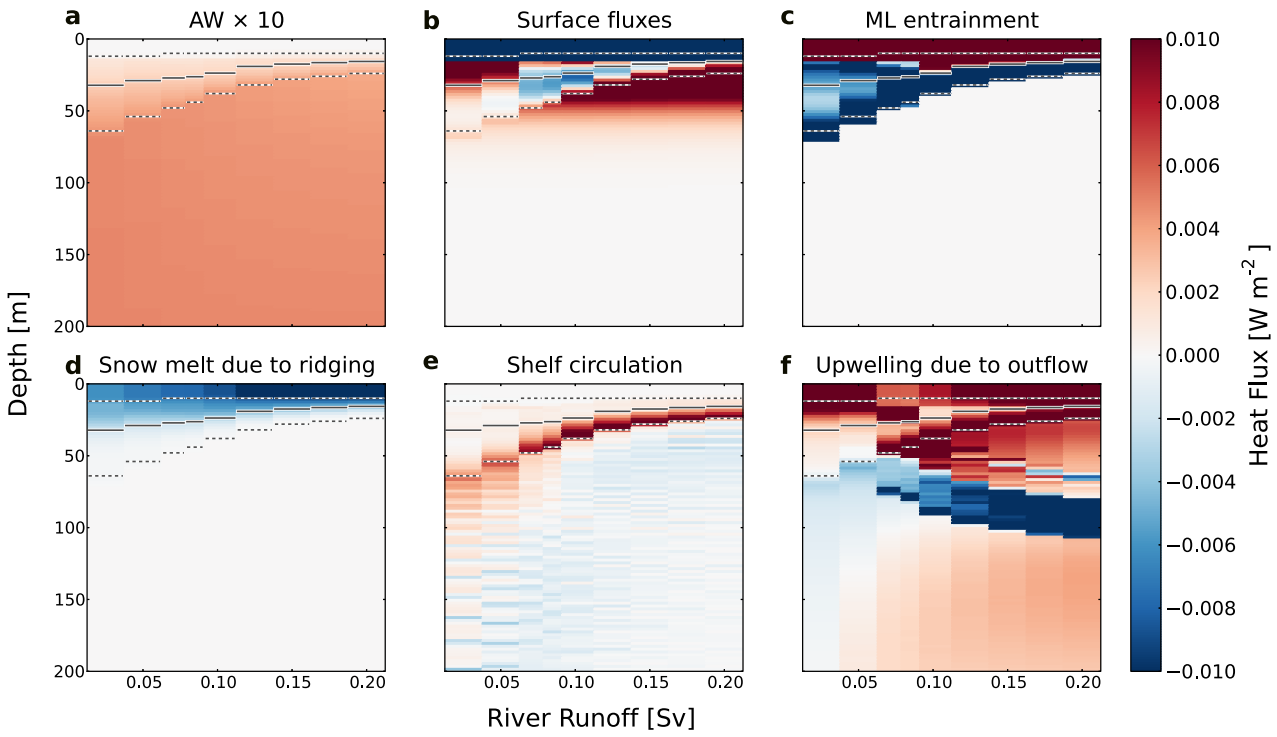

Figure 8. Contributions to heat flux convergence at each model level from: (a) compensating heat flux in the AW layer, (b) surface fluxes, (c) mixed layer entrainment, (d) snowmelt due to ridging, (e) shelf circulation, and (f) upwelling to replace geostrophic outflow. Note that the AW layer contribution is scaled by a factor of 10. The gray lines show the mixed layer depth (MLD; solid is annual mean, dashed are winter maximum and summer minimum).

stronger stratification inhibits entrainment, and more heat accumulates within the warming Atlantic layer (Figures 6b and 7). However, in equilibrium the warmer AW layer results in an increased vertical temperature gradient and vertical heat flux, balancing the compensating heat flux in AW layer. This mechanism is further discussed in the next section.

There are a number of additional terms that are important for closing the ocean heat budget. These also respond to changing runoff, but to a lesser degree. The snowmelt term (Figure 8d) comes from the sea ice ridging parameterization. When ridging occurs, the sea ice area fraction decreases, and the snow on the disappearing ice area is tipped into the ocean. The snowmelts in the ML, cooling it down. The shelf circulation term (Figure 8e) generally cools the waters below the ML and warms the lower part of the ML. Shelf water is created (parameterized) from ML water that enters the shelf area, cools to the freezing point, and becomes saltier due to brine rejection when sea ice forms. For mass continuity, the water leaving the ML and entering the shelf is replaced by warmer subsurface waters, a process that creates the warming signal seen at the base of the ML. The ML water modified on the shelf is injected into the halocline. Because this shelf water is at the freezing point, it has a cooling effect. Finally, upwelling due to geostrophic outflow from the column (Figure 8f) generally warms the upper water column because temperature increases with depth below the ML. However, because neither the temperature gradient nor the outflow are constant with depth, certain layers lose more heat upward than they receive from below, resulting in some localized cooling. It is worth noting that the geostrophic outflow increases as a function of the runoff leading to increased upwelling.

3.2. Sea Ice Response

Overall, the equilibrium changes in sea ice thickness with increasing runoff are small, on order of 15 cm (∼5%) at most (Figure 10). Increasing runoff leads to a decrease in surface salinity and increase in the vertical density gradient between the surface ML and the underlying AW layer. The stronger density gradient inhibits mixing of warm water to the surface (reduces vertical heat flux to the ML), which leads to warming of the column below the ML. At the same time, the subsurface warming increases the temperature gradient

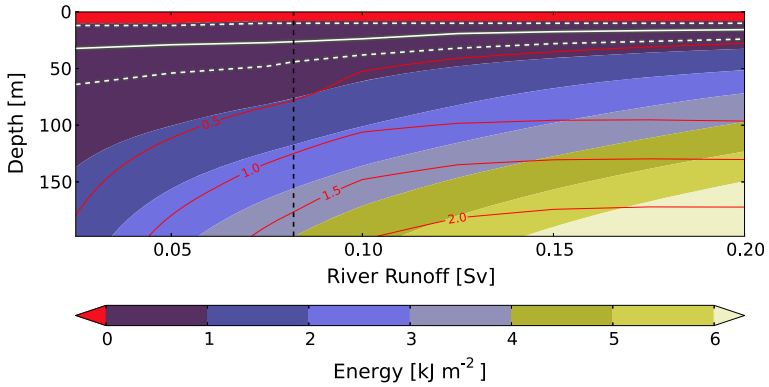

Figure 9. Energy required to mix away stratification as a function of river runoff. Color shading shows the energy (kJ m^{-2}) required to lift water from a given level to the surface mixed layer. Red contours show the temperature (°C) relative to the freezing point. The vertical black dashed line shows annual mean river runoff into the Arctic Ocean for the present day and the gray lines show the mixed layer depth (MLD; solid is annual mean, dashed are winter maximum and summer minimum).

between the ML and the underlying AW layer, making any mixing that does occur more effective (enhances vertical heat flux to the ML). The subsurface warming is a transient response that continues until the density and temperature gradients have adjusted to produce a vertical heat flux to the ML that is once again in equilibrium with the compensating heat flux below the ML.

One way to illustrate the net effect of the vertical temperature and density gradients is to calculate the mechanical energy needed to lift a parcel through the halocline to the ML. This represents the work done against gravity and is shown as a function of runoff in Figure 9. Just below the ML, the temperature contours follow remarkably well the energy contours. This implies that the energy needed to bring water of a certain temperature to the surface is largely independent of river runoff. Below 70–80 m and at runoffs above 0.1 Sv, the temperature contours become increasingly perpendicular to the energy contours. This suggests a more important role for runoff in the deep ocean, but note that mixing is parameterized with a constant diffusion coefficient in this part of the column.

While the balance of gradients accounts for why the steady state response of ice thickness to runoff is small, we must look to other factors to explain the subtle changes that do occur. In addition to the vertical heat flux from the ocean to the surface (or base of the ice), ice thickness also depends on the freezing point temperature T_f. Because freezing point temperature increases with the decreasing surface salinity, it is easier to form ice when there is more runoff, all other forcings remaining constant. A simple experiment shows that ice thickness can differ by a factor of two depending on whether constant or variable T_f is used (Figure 10). At runoff values larger than present day, about half (7 cm) of the ice thickening can be attributed to the effect of increasing T_f. SW radiation can also affect the column heat budget below the ML, as discussed in section 3.1. With present-day runoff, the heat from SW radiation that penetrates the ML is mixed back up during the next winter when the ML deepens. With more runoff, some of the SW heat remains trapped below the ML, further facilitating ice growth.

Increasing runoff alters the ice thickness distribution only slightly (not shown). The area of open water and the thinnest ice classes as well as that of the thickest ice classes appear to be largely unaffected. Most of the change in annual mean thickness (Figure 10a) comes from multiyear ice classes of 1–5 m thickness. This reflects the fact that ocean thermodynamical changes are most important for the nonridged multiyear ice classes while the thinnest and thickest ice classes are controlled by atmosphere and ice dynamics, respectively.

Finally, we note that our results include a slight imbalance in the ocean heat content that could be responsible for part of the ice thickness response to runoff. The column is not in complete equilibrium by the end of the 500 year simulations for the lower runoff scenarios (Figure 4). The immediate implication is that the assumptions of constant vertical heat flux discussed at the beginning of this section is not true for all scenarios, and varying ocean heat content could affect ice thickness as well.

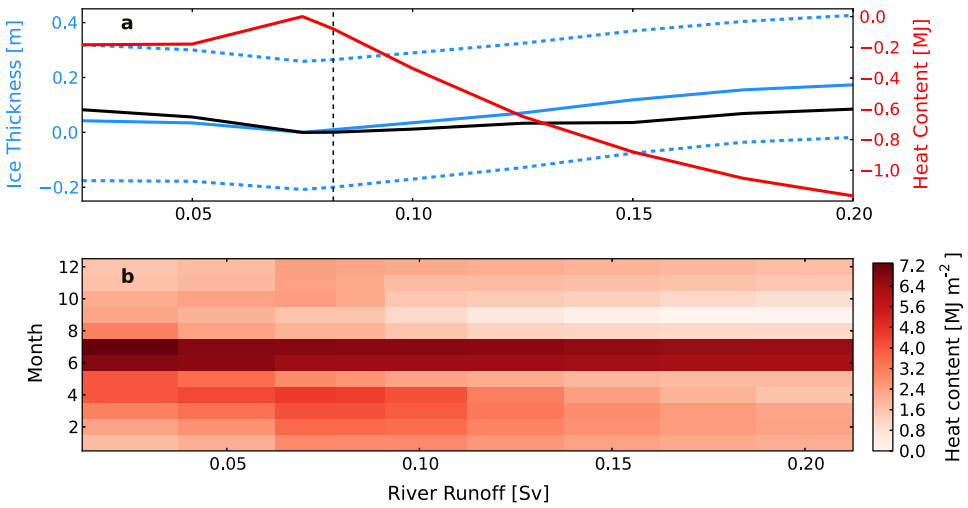

Figure 10. Simulated changes in sea ice thickness and mixed layer (ML) heat content in response to increasing river runoff. (a) The solid blue line is annual mean sea ice thickness calculated from the 42 model ice classes; the dashed blue lines are the seasonal maximum and minimum sea ice thickness; the solid black line is the same as solid blue line but for constant freezing point temperature. The red line is the annual mean ML heat content anomaly compared to case with 0.075 Sv runoff and when temperature is referenced to the surface freezing point. The vertical dashed black line shows annual mean river runoff into the Arctic Ocean for the present day. (b) Monthly climatology of ML heat content (relative to the freezing point temperature) as a function of river runoff.

4. Discussion

Our sensitivity study tests the response of an idealized Arctic Ocean to future increases in runoff, but some of the simulated results are consistent with observed changes in the Arctic under ongoing global warming. For example, warming of the AW layer has been observed, although the cause has been attributed to horizontal advection rather than changes in vertical stratification [*Schauer and Beszczynska-Möller*, 2009; *Grotefendt et al*., 1998]. Also storage of solar heating below the shallow ML has recently been documented in the Canadian basin [*Toole et al*., 2010; *Jackson et al*., 2011].

In addition, our results agree with previous analytical and simplified modeling studies. *Nilsson and Walin* [2010] found a shallower MLD and *Rudels* [2010] found increasing Arctic freshwater content as freshwater forcing increases. This is not surprising given that both studies are built on estuarine assumptions similar to ours, where the geostrophic outflow is balanced by vertical entrainment from the AW layer to the surface [*Stigebrandt*, 1981]. More recently, *Spall* [2013] developed an analytical model based on idealized, high resolution (eddy resolving) simulations of the Arctic Ocean. Here, the horizontal eddy transports from the boundary toward the interior are balanced by vertical entrainment in the interior, which is different from the estuarine model. Despite a different theoretical basis and conceptual model (see his Figure 11), the results are consistent with the ones presented here—that decreasing salinity at the boundary (as would be caused by increasing river runoff) leads to a thinner halocline and increased freshwater content in the Arctic domain.

While our study agrees rather well with other simplified modeling studies, the comparison to more complex model results is not as straightforward. For example, results from the 1DICEx model imply that a stronger density gradient across Fram Strait would lead to increased Fram Strait outflow by geostrophic arguments. However, *Arzel et al*. [2008] found a rapid decline in Fram Strait volume outflow in 20th and 21st century simulations performed with a coupled global climate model. They attributed decreased outflow to an atmospheric high pressure anomaly in the North Atlantic associated with surface freshening and sea ice expansion, a mechanism that is not represented in 1DICEx.

Assuming fixed North Atlantic temperature (T_{AW}) and salinity (S_{AW}) allows for a clean cause and effect study, but carries certain implications. Recall that the geostrophic surface outflow in 1DICEx is determined by the density difference between the North Atlantic (defined by T_{AW} and S_{AW}) and the Arctic column (prognostic). The assumption of fixed AW properties is reasonable for a system where freshwater outflow is small

compared to the volume of the surface layer in the North Atlantic. However, one might expect the AW properties—especially S_{AW}—to change as the Arctic comes to a long-term adjustment with increased runoff. Allowing the AW properties to vary would in some sense be more realistic, but it would also prevent us from identifying the isolated response to runoff.

In our perturbation experiments, all the forcings (including runoff) have a fixed seasonal cycle. In a warming climate, we might expect winter runoff to increase considerably but peak runoffs in late spring and summer to increase only a little if at all. Changes in ice growth and shelf water production would also be expected to be largest in winter, when these processes are most active. More runoff and a fresher surface could lead to shelf waters that are fresher and consequently less dense. While we have not accounted for these effects, they would likely affect any future change in the upper halocline of the Arctic Ocean.

One of the most poorly constrained parameters in our model is the vertical diffusion coefficient (κ). We chose κ along with T_{AW} and S_{AW} based on the available direct observations (section 2.2), and such that the set of values produced the best match to the observed T-S structure of the central Arctic Ocean. As with S_{AW}, it is likely that the value of κ varies with time. This variability could be driven by changes in the sea ice cover, which in turn alters the available fetch and size of waves produced during summer, the energy available for internal wave generation, and the associated mixing due to wave breaking. Given that the mean background level of vertical mixing in the Arctic Ocean is based on very few direct measurements [*Fer*, 2009; *Lique et al*., 2014] and is highly uncertain, a better observational basis is needed before we can reasonably introduce more complexity to how it is represented in the model.

Future work will focus on using more complex ocean and climate models to explore the regional expressions of the changes we have documented. NorESM future warming scenarios show similar Arctic responses to our 1DICEx study, with surface freshening, a sharpening of the halocline, and warming below the ML. In the NorESM scenarios, it is not only runoff that is changing, but preliminary runoff experiments with a stand-alone ocean-sea ice model also show similar results. Together, this range of modeling tools will help assess the regional variability and overall importance of the mechanisms presented here in a warming world.

5. Concluding Remarks

This study has investigated the response of a coupled atmosphere-ice-ocean column model of the Arctic Ocean to increasing river runoff. The column model reproduces the observed temperature and salinity structure of the central Arctic reasonably well. Increasing runoff freshens the surface and intensifies the stratification as expected, but also sharpens the halocline, and allows for larger heat content in the Atlantic Water layer with little change in the equilibrium vertical heat flux toward the surface. The equilibrium response of the 1DICEx column model to an increase in river runoff can be understood as follows.

1. Surface freshening leads to a stronger vertical density gradient, reduced mixing across the base of the ML, and a thinning of the ML. This tends to reduce the vertical heat flux toward the surface, thereby warming the AW layer.
2. A warmer AW layer leads to a stronger vertical temperature gradient across the halocline between the ML and the AW layer, which tends to enhance the vertical heat flux toward the surface.

The Arctic column reaches equilibrium when the vertical heat flux to the ML balances the compensating heat flux convergence in the AW layer. At equilibrium, changes in the net vertical heat flux in response to varying runoff are small.

1. Because the net vertical heat flux is not very sensitive to runoff, not much change is observed in either the heat supplied from the ocean to the base of the ice or the sea ice cover.
2. A modest increase in sea ice thickness (about 15 cm or 5%) is attributable to (1) an increase in the freezing point temperature of the ML as it freshens, and (2) an increase in the absorbed summer heat that is trapped below the ML and inaccessible to melt sea ice the following winter as the ML thins.

To better evaluate the effects of increased runoff (or any perturbation in stratification) to the Arctic in the future, tighter observational constraints on the large-scale vertical diffusion within the Arctic basin are needed.

Appendix A: Model Description

We review the most relevant parts of the model physics and describe the changes made for this study. The aim is to present the dynamical implications of the changes. For a complete description of the model development, the reader is referred to the studies by *Björk* [1989, 1992, 1997] and *Björk and Söderkvist* [2002]. See Appendix B for a table of the variable names and definitions and Appendix C for the climatological forcing used in this study.

A1. Ocean Component

The ocean model consists of a surface ML and the interior ocean. The bottom of the original model domain was set at 300 m, assumed to be the core of the Atlantic Water (AW) layer and also the level of no motion. We extend the bottom of the domain down to 2000 m and include a 500 m thick interactive AW layer that can respond to changes in river runoff.

In our extended model, the level of no motion is set to the depth of the temperature maximum in the column, which represents the core of the AW. This is an equivalent assumption to the original setup, where the level of no motion at the bottom of the domain (300 m) was also taken to represent the core of the AW and was set to a fixed AW temperature. To compensate the surface heat loss, we apply a constant heating term to the AW layer. This allows the temperature of the AW layer to adjust to runoff changes in the extended model. Note that the net heat transport into the column will not be constant because the overall balance is affected by adjustments in surface outflow, ice export (which represents heat transport into the column), and net surface radiation.

A1.1. Ocean Mixed Layer Dynamics

The ML dynamics are described in *Björk* [1989, 1997] and follow the pycnocline model developed by *Stigebrandt* [1985] [see also *Stigebrandt*, 1981], with conservation equations for ML thickness, temperature, and salinity.

The thickness of the ML, h, follows from the conservation of Arctic Ocean volume

$$\frac{dh}{dt} = (\mu Q_b + Q_f + \varepsilon Q_i + Q'_g)\frac{1}{A} + w_e \tag{A1}$$

where μQ_b is the Bering Strait inflow (forcing), Q_f is the river runoff (forcing), ε is the fraction of ice to water density, ϵQ_i is the water equivalent of the net change in ice volume, Q'_g is the geostrophic outflow, w_e is the entrainment velocity representing mixing through the bottom of the ML, and A is the area of the Arctic basin (excluding the Barents Sea). All transports are defined to be positive when adding volume to the Arctic. The parameter μ is zero if Bering Strait water is denser than water in the ML, otherwise (normally) it is one.

The entrainment velocity is defined as

$$w_e = \frac{2m_0 u_*^3/h_w - kB}{g'} = \frac{2m_0 u_*^3/h_w - kB}{g(\rho(h) - \rho_m)/\rho(h)} \tag{A2}$$

where m_0 is a constant relating the Richardson flux number R_f and the ice-ocean drag coefficient C_{di} ($m_0 = R_f/\sqrt{C_{di}}$), u^* is the friction velocity, h_w is the ML thickness excluding the ice thickness ($h_w = h - \varepsilon h i_i$), k is a factor controlling the energy available for mixing from the buoyancy flux B (0.05 when B is negative and 1 otherwise), g' is the reduced gravity, and ρ_m and $\rho(h)$ are the densities in and just below the ML, respectively.

The friction velocity, u^*, is a function of the ice velocity, Vi:

$$u_*^2 = C_{di} Vi^2 \tag{A3}$$

The ice velocity is parameterized as a function of 10 m wind, W_{10} (forcing):

$$Vi = a_0 W_{10} \tag{A4}$$

where a_0 is the ratio of wind speed to ice speed. *Linders and Björk* [2013] used the same model with an additional correction for W_{10} taking into account shorter term variability, but we do not adopt this correction.

The buoyancy flux B through the sea surface is defined as

$$B=g\left(\frac{\alpha Q_0}{c_{pw}\rho_w}-\beta(\varepsilon P_i S_m-Si+\varepsilon_s P_s S_m)+\frac{Q_f(\beta S_m+\alpha(T_m-T_r))}{A}+\frac{\mu Q_b(\beta(S_m-S_b)+\alpha(T_m-T_b))}{A}\right) \tag{A5}$$

where α is the thermal expansion coefficient, Q_0 is the net ice-ocean heat flux (mean over all ice classes, with positive values denoting a heat loss from the ocean), c_{pw} is the specific heat capacity of water, ρ_w is the density of water, β is the saline contraction coefficient, P_i is net ice growth, P_s is net snow accumulation, S_m is the salinity of the ML, Si is the salinity of the ice, T_r is the temperature of river water, and S_b and T_b are the specified salinity and temperature of the Bering Strait inflow. Positive values of B lead to positive w_e and deepening of the ML; if the Bering Strait water is denser than the model surface water then $\frac{Q_b(\beta(S_m-S_b)+\alpha(T_m-T_b))}{A}$ is zero. Negative values of B lead to negative w_e and thinning of the ML. For the thinning case, the thickness of the ML is set to the shorter of the Ekman (h_e) or Monin-Obukhov (h_m) lengths, defined as

$$h_e=\frac{Ku_*}{f} \tag{A6}$$

$$h_m=\frac{2m_0u_*}{B} \tag{A7}$$

where f is the Coriolis parameter and K is an empirical constant estimated to be 0.2 [*Björk*, 1989].

The ocean outflow Q'_g is parameterized assuming a geostrophically balanced coastal current following *Stigebrandt* [1981]. In this approach, the outflow at each level is the integral of the thermal wind equation from the bottom of the model domain to that level. The total outflow is the integral over the entire model domain multiplied by a scaling parameter λ, which depends on the number of outlets [*Björk*, 1989]. The outflow Q_T at each level i is

$$Q_T^i=\sum_{i=0}^{z}q^i\Delta z=\sum_{i=0}^{z}\left(-\frac{g}{\rho_{AW}f}\sum_{i=z}^{H_m}(\rho_{AW}-\rho^i)\Delta z\right)\Delta z \tag{A8}$$

where q^i is the geostrophic velocity at level i, ρ_{AW} is the AW density, and H_m is the level at which $\rho^i=\rho_{AW}$, i.e., the level of no motion. The total outflow from the basin is then given by

$$Q'_g=\lambda Q_T(i=h) \tag{A9}$$

In the model, the outflow is balanced by upwelling from the abyss, which means that the vertical velocity w_a at level i can be written as

$$w_a^i=\begin{cases}(\lambda Q_T^i+Q_f+\varepsilon Q_i)/A & i\le i_b\\ (\lambda Q_T^i+Q_f+\varepsilon Q_i+Q_b)/A & i>i_b\end{cases} \tag{A10}$$

where i_b is the level where Bering Strait inflow is inserted.

A1.2. Ocean Mixed Layer Salt and Heat Balance

The salt balance for the ML is

$$\frac{dS_m}{dt}=\frac{(\mu Q_b(S_b-S_m)-Q_fS_m)/A+\varepsilon P_i(S_m-Si)+w_e(S_h-S_m)}{h_w} \tag{A11}$$

where S_h is the salinity just below the ML.

The ML temperature is calculated based on prognostic equations. As explained by *Björk* [1997], for heat conservation, different equations must be used during melting and freezing. The equations are shown below and the reader is referred to *Björk* [1997] for more details. The ML temperature change ΔT_m in a time step Δt is defined as

$$\Delta T_m = \left(\frac{F_w \Delta t}{\rho_w c_{pw}} + (T_f - T_m)\Delta H_w\right) \frac{1}{h_w + \Delta h_w}, \text{for melting} \tag{A12}$$

$$\Delta T_m = \frac{F_w \Delta t}{\rho_w c_{pw}(h_w + \Delta h_w)}, \text{for freezing} \tag{A13}$$

where ΔH_w is the thickness of the layer of water that is formed by melting of ice or that freezes.

A1.3. Interior Ocean and the Extended Domain

The rate of change below the ML at each level *i* for salinity and temperature is

$$\frac{dS^i}{dt} = w_a^i \frac{\partial S^i}{\partial z} + \kappa \frac{\partial^2 S^i}{\partial z^2} + \mu_2 F^i (S_{AW} - S^i) \tag{A14}$$

$$\frac{dT^i}{dt} = w_a^i \frac{\partial T^i}{\partial z} + \kappa \frac{\partial^2 T^i}{\partial z^2} + \mu_2 F^i (T_{AW} - T^i) \tag{A15}$$

The first terms in each equation $\left(w_a^i \frac{\partial S^i}{\partial z} \text{ and } w_a^i \frac{\partial T^i}{\partial z}\right)$ represent changes due to dynamical upwelling, and the second terms $\left(\kappa \frac{\partial^2 S^i}{\partial z^2} \text{ and } \kappa \frac{\partial^2 T^i}{\partial z^2}\right)$ represent changes due to background mixing set by the diffusion coefficient κ (see also the discussion in *Björk* [1989] about the numerical diffusion). For this study, κ is set to be 10% smaller below the Atlantic layer than in the rest of the column as very little mixing is assumed to occur in the deep ocean. The third terms ($\mu_2 F^i (S_{AW} - S^i)$ and $\mu_2 F^i (T_{AW} - T^i)$) represent the heat and salt supply to the AW layer required to compensate the surface forcing and outflow. (Physically, they represent the heat and salt supply by the AW inflow to the column.) μ_2 is a step function, defined to be 1 for the AW layer (a 500 m thick layer below the base of the ML) and 0 elsewhere; F^i is a time-varying parameter that depends on the heat content difference between the AW and the column (see below); and S_{AW} and T_{AW} are the prescribed AW temperature and salinity. These terms are not found in the original model, where the AW layer was set to constant temperature and salinity.

The AW inflow must compensate the surface forcing and outflow, and the prescribed value of AW heat transport is chosen to satisfy this. The main idea behind the formulation of the third terms in equations (14) and (15) is to bring in enough AW to meet the heat transport requirement. At each time step, a fraction Δh of each model level within the AW layer of the column is replaced by AW. This fraction is determined by dividing the prescribed AW heat transport in a time step (ΔQ_{AW}^i) by the difference in heat content between the AW and model level (ΔQ^i). The exact value of ΔQ_{AW}^i depends on how the total AW heat transport is partitioned among the various levels of the AW layer. At each vertical level *i* within the AW layer, we have

$$\Delta h_{AW}^i = \frac{\Delta Q_{AW}^i}{\Delta Q^i} \tag{A16}$$

We divide the equation by the time step Δt and expand the ΔQ^i term to arrive at the expression for F^i

$$F^i = \frac{\Delta h_{AW}^i}{\Delta t} = \frac{\Delta Q_{AW}^i / \Delta t}{Z_{AW} A c_{pw} (\rho_{AW} T_{AW} - \rho^i T^i)} \tag{A17}$$

where $H_{AW} = Q_{AW}^i / \Delta t$ is the AW heat transport in W m^{-2} (forcing), Z_{AW} is 500 m (thickness of the layer where parameterization is applied), c_{pw} is the specific heat of water (constant 4000 kg m^{-3} is assumed). ρ_{AW} and ρ^i are the AW and column densities, respectively.

Since Δh^i is physically a fraction of the layer thickness, we can calculate the total volume input Ψ associated with the AW heat input as

$$\Psi = \frac{A \cdot \Delta z}{\Delta t} \cdot \sum_i \Delta h^i \tag{A18}$$

where *i* goes from $Z/\Delta z$ levels below the ML to the bottom of the ML.

It is interesting to note that the formulation of the new terms $F^i (S_{AW} - S^i)$ and $F^i (T_{AW} - T^i)$ is numerically equivalent to nudging temperature and salinity toward AW values with a relaxation parameter F^i, although the physical reasoning is quite different. These terms have to do with the thermal component of the circulation, the part of the AW transport that is required for heat balance.

A1.4. Shelf Water Circulation

Ice growth on the shallow shelves is important for the formation of the Arctic halocline. 1DICEx includes this phenomenon through a parameterization in which ML water is assumed to flow to the shelf, where it mixes with brine created during the formation of sea ice. The resulting "shelf water" is close to freezing point temperature and is more saline than the original ML water. This cold, salty water mass is inserted into the column below the ML at the appropriate density. The most important equations are described below; more details can be found in *Björk* [1989, 1997].

The strength of the shelf water input into the column is a linear decreasing function of the salinity (S)

$$q_s = q_0 \frac{S_2 - S}{S_2 - S_m} \tag{A19}$$

where S_2 is the maximum salinity allowed for shelf water; S_m is the ML salinity and also the minimum salinity allowed for shelf water ($S_m \leq S \leq S_2$); and q_0 is the volume flux when $S = S_m$. The total volume flux Q_s and the total salt flux Θ from the shelf into the column are integrals over the salinity range:

$$Q_S = \int_{S_m}^{S_2} q_s dS = q_0 \frac{S_2 - S_m}{2} \tag{A20}$$

$$\Theta = \int_{S_m}^{S_2} q_s S dS = \frac{1}{6} q_0 (S_2 - S_m)(S_2 + 2S_m) \tag{A21}$$

For salt conservation, the inflow of salt from the shelf into the column Θ must be balanced by the outflow of salt from the ML to the shelf as well as ice formation. We can write

$$\Theta = Q_S S_m + \varepsilon Q_i (S_m - S_i) \tag{A22}$$

where $Q_i = p_s wiA$ is the ice volume export from the column, p_s denotes the fraction of total ice formation that contributes to shelf water production, wi is the ice growth velocity $\left(\frac{dhi}{dt}\right)$, and Si is the salinity of ice. By substituting (20) and (21) into (22), solving for q_0 and inserting this expression back into (20), we arrive at an expression for the total volume flux from the shelves as a function of ice formation (note that this flux only exists when ice is growing)

$$Q_S = \begin{cases} 3\varepsilon Q_i \dfrac{S_m - S_i}{S_2 - S_m} & Q_i > 0 \\ 0 & Q_i \leq 0 \end{cases} \tag{A23}$$

A2. Sea Ice Component

The sea ice component was described by [*Björk*, 1992, 1997]. We are using the same setup, and so give only a short review for reference. For clarity, we use the same notation as [*Björk*, 1992].

The basis of the ice model is a limited number of ice classes (C), each with an associated ice thickness (hi), snow thickness (hs), area (a), and internal temperature (Ti). For a given ice class i we can write

$$C_i = (a_i, hi_i, hs_i, Ti_i) \tag{A24}$$

where $i = 0, n$, and C_0 is the open water fraction and C_n the thickest ice. By definition, the sum of the fractional areas over all ice categories equals unity

$$\sum_{i=0}^{n} a_i = 1 \tag{A25}$$

The cumulative ice thickness distribution, $G(hi_i)$, is given by

$$G(hi_i) = \sum_{j=0}^{i} a_j \tag{A26}$$

The spatial mean ice thickness, $\langle hi \rangle$, is defined as

$$\langle hi \rangle = \sum_{i=0}^{n} hi_i \cdot a_i \tag{A27}$$

The quantities (a_i, hi_i, hs_i, Ti_i) of each ice class evolve over time. Dynamical processes affect a_i as they can create new ice classes by ridging and ice export. In addition, existing ice classes are merged if their thicknesses become similar enough. The thermodynamic part of the ice model affects hi_i, hs_i, and Ti_i through ice growth and melt within each ice class, which might also result in merging of ice classes. For computational efficiency, the number of ice classes is limited to 42, which is sufficient to simulate the Arctic ice thickness distribution. In the following, we review the formulation of the dynamic and thermodynamic ice processes in the model.

A2.1. Sea Ice Dynamics

The model dynamics include ridging and ice export, both of which affect the evolution of the fractional area (a_i) per ice class (i)

$$\frac{da_i}{dt} = E_i + R_i \tag{A28}$$

where Ei_i is the rate of change due to ice export out of the domain and R_i is the rate of change due to ridging for each ice class. Ice export is assumed to occur for all ice classes (excluding open water) and is parameterized as a function of area fraction of ice exported per unit time (ei_i). Export decreases the area fraction of all the ice classes and creates open water area fraction at the same rate. We can write

$$Ei_i = \begin{cases} ei_i & i=0 \\ -\dfrac{ei_i \cdot a_i}{1-a_0} & i=1,n \end{cases} \tag{A29}$$

where $i = 0$ denotes open water. If no open water is present, the model will always create a new $i = 0$ class at that time step.

The rate of deformation in each ice class due to ridging R_i is given by

$$R_i = \begin{cases} r_i & i=0 \\ -(r_i M a_i)/((M-1)G_j) & i=1,j \\ 0 & i=j+1,n \\ (r_i a_{i-n})/((M-1)G_j) & i=n+1,n+j \end{cases} \tag{A30}$$

where r_i is the ridging area fraction change per unit time; M is the factor by which the ridging process thickens the ice. Note that the model differentiates between the deformed (ridged) and undeformed ice classes, creating new, ridged ice classes C_{n+1} to C_{n+j}. A cumulative fraction $G*$ determines the cutoff thickness (class $i = j$) above which ice is not ridged (in other words, the thinnest $G*$ fraction is active in the ridging process). After ridging, the model merges the new ridged ice classes with existing ice classes if their thicknesses are close enough. Snow thickness remains constant after ridging and the excess snow is given to the ML, where it is assumed to melt and alter the ML temperature and salinity.

The merging procedure is rather straightforward for the a_i, hi, and hs variables as they are simply area-weighted averages of the merging ice classes. Heat conservation requires a somewhat complicated calculation of the internal ice temperature [*Björk*, 1992]. During the summer melting season, the thinnest ice classes can also melt completely, in which case their area fraction merges with the open water class.

A2.2. Sea Ice Thermodynamics

The thermodynamic model is a simple, 1-level model where the ice has one internal temperature. Snow on top of the ice acts as an insulating layer. The model also includes internal phase changes and the effect of brine pockets inside the ice. The heat balance at the ice/snow surface is described in section A3 and the heat balance at the ocean/ice interface is described in section A1.

A3. Atmospheric Component

The atmosphere used in this model is a so-called "gray atmosphere," which is transparent to solar radiation [*Björk and Söderkvist*, 2002; *Thorndike and Colony*, 1982]. Because our study concentrates on the ice and

ocean components of the model, we review the atmospheric component briefly and refer the reader to *Björk and Söderkvist* [2002] for details. The vertical coordinate of the model atmosphere is the optical height, a length measure of absorbance in the longwave spectrum. The total optical depth is the optical height at the top of the atmosphere. A balance can be found between the upward and downward thermal radiation and the atmospheric heat transport at each optical height. The main interest in terms of the paper is the coupling at the surface where the upward conductive heat flux through the ice and snow is balanced by the net radiative and turbulent heat fluxes at the surface. The surface heat balance is thus given by

$$C_c(T_s - Ti) = (1-\alpha_s)F_{sw} + F_{DN}(0) - (A_{SB} + B_{SB}T_s) + C_T(T_a(0) - T_s) \tag{A31}$$

where $C_c(T_s - Ti)$ is the conductive heat flux from the ice/snow to the surface, C_c is a coefficient depending on the conductivity and thickness of the ice and snow layers, T_s is the surface temperature, Ti is the internal ice temperature, α_s is the surface albedo, F_{sw} is the incoming shortwave radiation (forcing), $F_D N(0)$ is the downward longwave radiation at the lowest atmospheric level, $A_{SB} + B_{SB}T_s$ is the Stefan-Boltzmann law linearized around the freezing point, and the $C_T(T_a(0) - T_s)$ term represents the turbulent heat flux from the surface.

Because there are multiple ice categories with different ice thicknesses, snow thicknesses and internal temperatures, the above heat balance must be satisfied for each category. The surface temperature for each ice class i is written:

$$T_s^i = \frac{(1-\alpha^i)F_{sw} - A_{SB} + C_c^i T^i + F_{DN}(0) + C_T T_a(0)}{B_{SB} + C_T + C_C^i} \tag{A32}$$

The atmosphere feels the area-averaged surface temperature over all the ice classes.

Appendix B: List of Symbols

The list of symbols and their definitions are given in Table B1.

Table B1. List of Symbols and Their Definitions[a]

Symbol	Definition	Variable Type	Value if Constant
α	Thermal expansion coefficient	Prognostic	
α_s	Surface albedo	Prognostic	
A	Area of the Arctic Ocean	Constant	0.7×10^{13} m^2
A_{SB}	Constant in the linearized Stefan-Boltzmann law	Constant	320 W m^{-2}
a	Ice category area fraction (0–1)	Prognostic	
a_0	Wind-ice speed ration	Constant	0.01
β	Haline contraction coefficient	Prognostic	
B	The buoyancy flux through the sea surface	Prognostic	
B_{SB}	Coefficient in the linearized Stefan-Boltzmann law	Constant	4.6 W m^{-2}
C_{di}	Ice-ocean drag coefficient	Constant	5.5×10^{-3}
C	Ice category		
C_c	Ice conductivity coefficient	Constant	2.034 W m K^{-1}
c_p	Specific heat of sea water	Constant	4.0 kJ kg K^{-1}
c_{pw}	Specific heat of water	Constant	4.18 kJ kg K^{-1}
C_T	Turbulent heat exchange coefficient at the surface	Constant	1.75×10^{-3}
ϵ	Ratio between the ice and water density	Constant	0.9
Ei	Rate of ice area fraction change due to ice export	Prognostic	
ei	Ice export in unit time	Prognostic	
f	Coriolis parameter	Constant	1.43×10^{-4} s^{-1}
F^i	Ocean relaxation parameter	Prognostic	
F_{DN}	Atmospheric downward longwave radiation	Forcing	
F_{SW}	Surface shortwave radiation	Prognostic	
g'	Reduced gravity	Prognostic	
g	Gravitational acceleration coefficient	Constant	9.81 m s^{-2}
G	Cumulative thickness distribution	Prognostic	
G_*	Ridging cutoff value for cumulative ice area fraction	Constant	7%
Δh^i	Fraction of the ocean level	Prognostic	
ΔH_w	Thickness of melted or frozen ice as water	Prognostic	
H_{AW}	Atlantic heat transport	Constant	1 TW
$\langle H \rangle$	Area-weighted mean ice thickness	Prognostic	
h	Ocean mixed layer thickness	Prognostic	
h_e	Ekman length scale	Prognostic	
hi	Ice thickness	Prognostic	

Table B1. (continued)

Symbol	Definition	Variable Type	Value if Constant
h_m	Monin-Obukhov length scale	Prognostic	
hs	Snow thickness	Prognostic	
h_w	Ocean mixed layer thickness excluding ice thickness	Prognostic	
κ	Internal mixing coefficient in the ocean	Constant	4.0 m^2 s^{-1}
λ	Scaling parameter for ocean outflows	Constant	0.7
μ	Bering Strait outflow flag	Constant	1 or 0
μ_2	AW inflow flag	Constant	1 or 0
M	Ridge thickness multiplier	Constant	6
m_0	$R_f/\sqrt{C_{di}}$	Constant	0.674
P_i	Net ice growth/melt	Prognostic	
P_s	Net snow accumulation/melt	Prognostic	
q	Geostrophic velocity at each level	Prognostic	
q_s	Volume flux toward the shelf	Prognostic	
q_0	Volume flux toward the shelf when the $S = S_m$	Prognostic	
ΔQ_{AW}	Atlantic heat transport in a time steps	Constant	
Q_0	Net ice-ocean heat flux	Prognostic	
Q_b	Bering Strait volume inflow	Forcing	
Q_f	River runoff	Forcing	
Q_i	Ice volume export	Prognostic	
Q'_g	Geostrophic outflow	Prognostic	
Q_S	Total volume flux due to shelf water production	Prognostic	
Q_T	Thermal wind transport	Prognostic	
ρ	Density of the ocean column	Prognostic	
ρ_{AW}	Density of the Atlantic inflow	Constant	1027.8 kg m^{-3}
ρi	Density of ice	Constant	900 kg m^{-3}
ρ_w	Density of water	Constant	1000 kg m^{-3}
R_f	Flux Rickhardson number	Constant	0.05
R	Rate of ice area fraction change due to ridging	Prognostic	
S	Salinity of the ocean column	Prognostic	
S_b	Bering Strait inflow salinity	Forcing	
S_{AW}	Salinity of the Atlantic inflow	Constant	35 g kg^{-1}
S_m	Mixed layer salinity	Prognostic	
Si	Salinity of the ice	Constant	5 g kg^{-1}
S_2	Maximum salinity of the shelf water	Constant	34.8 g kg^{-1}
S_h	Salinity just below the mixed layer	Prognostic	
T	Temperature of the ocean column	Prognostic	
T_a	Atmospheric temperature	Prognostic	
T_{AW}	Temperature of the Atlantic inflow	Constant	3.5°C
T_b	Bering Strait inflow temperature	Forcing	
T_f	Freezing point temperature	Prognostic	
Ti	(Internal) ice temperature	Prognostic	
T_m	Mixed layer temperature	Prognostic	
T_r	River water temperature	Constant	0°C
T_s	Surface temperature	Prognostic	
Θ	Total salt flux due to shelf water production	Prognostic	
u^*	Ocean friction velocity	Prognostic	
Vi	Ice velocity	Prognostic	
Z	Extent of the Atlantic heat transport	Constant	500 m
w_a	Upwelling velocity in the ocean column	Prognostic	
w_e	Entrainment velocity to the mixed layer	Prognostic	
wi	Ice growth velocity	Prognostic	
W_{10}	10 m wind velocity	Forcing	
Ψ	Total volume input by the AW parameterization	Prognostic	

[a]Variable types as follows: constant for model parameters, forcing for constants with seasonal cycle, prognostic for all model variables that are computed for new every time step.

Appendix C: Model Forcing

The climatological forcing used in this study is given in Table C1. Note that the river runoff is scaled from the climatological values so that the annual mean runoff is increased by the desired amount.

Table C1. Climatological Forcing Following *Björk and Söderkvist* [2002]

Variable	January	February	March	April	May	June	July	August	September	October	November	December
Surface SW radiation (W m^{-2})	0.0	5.1	32.9	142.4	256.8	302.0	232.6	132.9	47.6	9.6	0.0	0.0
Atm. heat transport (W m^{-2})	127.0	109.8	119.7	106.2	72.6	78.4	87.8	88.4	93.5	108.1	121.4	122.7

Table C1. (continued)

Variable	January	February	March	April	May	June	July	August	September	October	November	December
Optical thickness	2.3	2.3	2.3	2.3	4.5	5.3	5.3	5.3	5.3	4.5	3.1	2.3
Relative humidity	0.85	0.85	0.88	0.88	0.89	0.93	0.93	0.94	0.88	0.85	0.85	0.85
Snow albedo	0.85	0.84	0.83	0.81	0.82	0.78	0.64	0.69	0.84	0.85	0.85	0.85
Snow accumulation (mm d^{-1})	0.83	0.83	0.83	0.83	5.00	0.00	0.00	0.00	12.87	12.87	0.83	0.83
10 m wind velocity (m s^{-1})	5.6	5.7	5.3	5.1	5.0	5.2	5.2	5.4	6.2	6.2	5.8	5.5
Wind velocity std (m s^{-1})	3.3	3.3	3.0	3.0	2.7	2.9	3.1	3.2	3.8	3.5	3.5	3.2
Ice/wind velocity ratio (%)	1	1	1	1	1	2	2	2	1	1	1	1
Wind stress (N m^{-2})	5	5	5	5	5	5	5	5	5	5	5	5
River runoff (Sv)	0.026	0.021	0.022	0.023	0.106	0.294	0.164	0.117	0.094	0.063	0.031	0.026
Bering Strait inflow (Sv)	1.02	0.95	0.34	0.78	1.13	1.26	1.47	1.07	0.66	0.87	0.90	0.34
Bering Strait inflow S	32.2	32.6	32.7	32.6	32.3	32.2	32.4	32.1	32.0	31.6	31.5	31.7
Bering Strait inflow T (°C)	−1.7	−1.8	−1.8	−1.8	−1.2	0.8	3.8	4.3	4.2	3.1	−1.2	−1.7

Acknowledgments

This work was supported by the Bjerknes Centre project DYNAWARM. C.L. acknowledges the support of the Centre for Climate Dynamics (SKD) at the Bjerknes Centre. Thanks to Mehmet Ilicak, Doug Martinson, Bob Newton, Peter Schlosser, Bruno Tremblay, and Ingrid Onarheim for stimulating discussions and helpful suggestions on the manuscript. We also thank the three anonymous reviewers for their constructive comments on the manuscript. All the data, the model setup, and the analyzing scripts used in this study are available through the corresponding author by email at aleksi.nummelin@gfi.uib.no.

References

Arzel, O., T. Fichefet, H. Goosse, and J.-L. Dufresne (2008), Causes and impacts of changes in the Arctic freshwater budget during the twentieth and twenty-first centuries in an AOGCM, *Clim. Dyn.*, *30*(1), 37–58, doi:10.1007/s00382-007-0258-5.

Bentsen, M., et al. (2013), The Norwegian Earth System Model, NorESM1-M. Part 1: Description and basic evaluation of the physical climate, *Geosci. Model Dev.*, *6*(3), 687–720, doi:10.5194/gmd-6-687-2013.

Björk, G. (1989), A one-dimensional time-dependent model for the vertical stratification of the upper Arctic Ocean, *J. Phys. Oceanogr.*, *19*, 52–67, doi:10.1175/1520-0485(1989)019<0052:AODTDM>2.0.CO;2.

Björk, G. (1992), On the response of the equilibrium thickness distribution of sea ice to ice export, mechanical deformation, and thermal forcing with application to the Arctic Ocean, *J. Geophys. Res.*, *97*(C7), 11,287–11,298, doi:10.1029/92JC00814.

Björk, G. (1997), The relation between ice deformation, oceanic heat flux, and the ice thickness distribution in the Arctic Ocean, *J. Geophys. Res.*, *102*(C8), 18,681–18,698, doi:10.1029/97JC00789.

Björk, G., and J. Söderkvist (2002), Dependence of the Arctic Ocean ice thickness distribution on the poleward energy flux in the atmosphere, *J. Geophys. Res.*, *107*(C10), 3173, doi:10.1029/2000JC000723.

Dunne, J. P., et al. (2012), GFDLs ESM2 global coupled climate-carbon earth system models. Part I: Physical formulation and baseline simulation characteristics, *J. Clim.*, *25*(19), 6646–6665, doi:10.1175/JCLI-D-11-00560.1.

Fer, I. (2009), Weak vertical diffusion allows maintenance of cold halocline in the central Arctic, *Atmos. Oceanic Sci. Lett.*, *2*(3), 148–152.

Grotefendt, K., K. Logemann, D. Quadfasel, and S. Ronski (1998), Is the Arctic Ocean warming?, *J. Geophys. Res.*, *103*(C12), 27,679–27,687, doi:10.1029/98JC02097.

Jackson, J. M., S. E. Allen, F. A. McLaughlin, R. A. Woodgate, and E. C. Carmack (2011), Changes to the near-surface waters in the Canada Basin, Arctic Ocean from 1993–2009: A basin in transition, *J. Geophys. Res.*, *116*, C10008, doi:10.1029/2011JC007069.

Jones, C. D., et al. (2011), The HadGEM2-ES implementation of CMIP5 centennial simulations, *Geosci. Model Dev.*, *4*(3), 543–570, doi:10.5194/gmd-4-543-2011.

Lammers, R. B., A. I. Shiklomanov, C. J. Vörösmarty, B. M. Fekete, and B. J. Peterson (2001), Assessment of contemporary Arctic river runoff based on observational discharge records, *J. Geophys. Res.*, *106*(D4), 3321–3334, doi:10.1029/2000JD900444.

Linders, J., and G. Björk (2013), The melt-freeze cycle of the Arctic Ocean ice cover and its dependence on ocean stratification, *J. Geophys. Res. Oceans*, *118*, 5963–5976, doi:10.1002/jgrc.20409.

Lique, C., J. D. Guthrie, M. Steele, A. Proshutinsky, J. H. Morison, and R. Krishfield (2014), Diffusive vertical heat flux in the Canada Basin of the Arctic Ocean inferred from moored instruments, *J. Geophys. Res. Oceans*, *119*, 496–508, doi:10.1002/2013JC009346.

Marnela, M., B. Rudels, M.-N. Houssais, A. Beszczynska-Möller, and P. B. Eriksson (2013), Recirculation in the Fram Strait and transports of water in and north of the Fram Strait derived from CTD data, *Ocean Sci.*, *9*(3), 499–519, doi:10.5194/os-9-499-2013.

Mignot, J., D. Swingedouw, J. Deshayes, O. Marti, C. Talandier, R. Séférian, M. Lengaigne, and G. Madec (2013), On the evolution of the oceanic component of the IPSL climate models from CMIP3 to CMIP5: A mean state comparison, *Ocean Modell.*, *72*, 167–184, doi:10.1016/j.ocemod.2013.09.001.

Nilsson, J., and G. Walin (2010), Salinity-dominated thermohaline circulation in sill basins: Can two stable equilibria exist?, *Tellus, Ser. A*, *62*(2), 123–133, doi:10.1111/j.1600-0870.2009.00428.x.

Overeem, I., and J. P. M. Syvitski (2010), Shifting discharge peaks in Arctic rivers, 1977–2007, *Geogr. Ann., Ser. A*, *92*(2), 285–296, doi:10.1111/j.1468-0459.2010.00395.x.

Peterson, B. J., R. M. Holmes, J. W. McClelland, C. J. Vörösmarty, R. B. Lammers, A. I. Shiklomanov, I. A. Shiklomanov, and S. Rahmstorf (2002), Increasing river discharge to the Arctic Ocean, *Science*, *298*(5601), 2171–2173, doi:10.1126/science.1077445.

Rawlins, M. A., et al. (2010), Analysis of the Arctic system for freshwater cycle intensification: Observations and expectations, *J. Clim.*, *23*(21), 5715–5737, doi:10.1175/2010JCLI3421.1.

Rudels, B. (2010), Constraints on exchanges in the Arctic Mediterranean-do they exist and can they be of use?, *Tellus, Ser. A*, *62*(2), 109–122, doi:10.1111/j.1600-0870.2009.00425.x.

Rudels, B., E. P. Jones, L. G. Anderson, and G. Kattner (1994), On the intermediate depth waters of the Arctic Ocean, in *The Polar Oceans and Their Role in Shaping the Global Environment*, edited by O. M. Johannessen, R. D. Muench, and J. E. Overland, AGU, Washington, D. C., doi:10.1029/GM085p0033.

Rudels, B., L. G. Anderson, and E. P. Jones (1996), Formation and evolution of the surface mixed layer and halocline of the Arctic Ocean, *J. Geophys. Res.*, *101*(C4), 8807–8821, doi:10.1029/96JC00143.

Rudels, B., E. P. Jones, U. Schauer, and P. B. Eriksson (2004), Atlantic sources of the Arctic Ocean surface and halocline waters, *Polar Res.*, *23*(2), 181–208, doi:10.1111/j.1751-8369.2004.tb00007.x.

Schauer, U., and A. Beszczynska-Möller (2009), Problems with estimation and interpretation of oceanic heat transport conceptual remarks for the case of Fram Strait in the Arctic Ocean, *Ocean Sci.*, *5*(4), 487–494, doi:10.5194/os-5-487-2009.

Smedsrud, L. H., A. Sorteberg, and K. Kloster (2008), Recent and future changes of the Arctic sea-ice cover, *Geophys. Res. Lett.*, *35*, L20503, doi:10.1029/2008GL034813.

Spall, M. A. (2013), On the circulation of Atlantic Water in the Arctic Ocean, *J. Phys. Oceanogr.*, *43*(11), 2352–2371, doi:10.1175/JPO-D-13-079.1.

Spreen, G., S. Kern, D. Stammer, and E. Hansen (2009), Fram Strait sea ice volume export estimated between 2003 and 2008 from satellite data, *Geophys. Res. Lett.*, *36*, L19502, doi:10.1029/2009GL039591.

Steele, M., and T. J. Boyd (1998), Retreat of the cold halocline layer in the Arctic Ocean, *J. Geophys. Res.*, *103*(C5), 10,419–10,435, doi:10.1029/98JC00580.

Steele, M., R. Morley, and W. Ermold (2001), PHC: A global ocean hydrography with a high-quality Arctic Ocean, *J. Clim.*, *14*(9), 2079–2087, doi:10.1175/1520-0442(2001)014<2079:PAGOHW>2.0.CO;2.

Stigebrandt, A. (1981), A model for the thickness and salinity of the upper layer in the Arctic Ocean and the relationship between the ice thickness and some external parameters, *J. Phys. Oceanogr.*, *11*(10), 1407–1422, doi:10.1175/1520-0485(1981)011<1407:AMFTTA>2.0.CO;2.

Stigebrandt, A. (1985), A model for the seasonal pycnocline in rotating systems with application to the Baltic proper, *J. Phys. Oceanogr.*, *15*, 1392–1404, doi:10.1175/1520-0485(1985)015<1392:AMFTSP>2.0.CO;2.

Thorndike, A. S., and R. Colony (1982), Sea ice motion in response to geostrophic winds, *J. Geophys. Res.*, *87*(C8), 5845–5852, doi:10.1029/JC087iC08p05845.

Toole, J. M., M.-L. Timmermans, D. K. Perovich, R. A. Krishfield, A. Proshutinsky, and J. A. Richter-Menge (2010), Influences of the ocean surface mixed layer and thermohaline stratification on Arctic Sea ice in the central Canada Basin, *J. Geophys. Res.*, *115*, C10018, doi:10.1029/2009JC005660.

Vinje, T. (2001), Fram Strait ice fluxes and atmospheric circulation: 1950–2000, *J. Clim.*, *14*, 3508–3517, doi:10.1175/1520-0442(2001)014<3508:FSIFAA>2.0.CO;2.

Supporting Information for "Response of Arctic Ocean stratification to changing river runoff in a column model"

Aleksi Nummelin,[12] Camille Li,[12] Lars H. Smedsrud,[123]

Contents of this file

1. Figures S1 to S3

Introduction This file includes 3 Figures supporting the main conclusions of this study.

Corresponding author: A. Nummelin, Department of Geophysics, University of Bergen, Allégaten 70, N-5007 Bergen, Norway (aleksi.nummelin@gfi.uib.no)

[1]Geophysical Institute, University of Bergen and Bjerknes Centre for Climate Research, Bergen, Norway

[2]Bjerknes Centre for Climate Research, Bergen, Norway

[3]University Centre in Svalbard (UNIS)

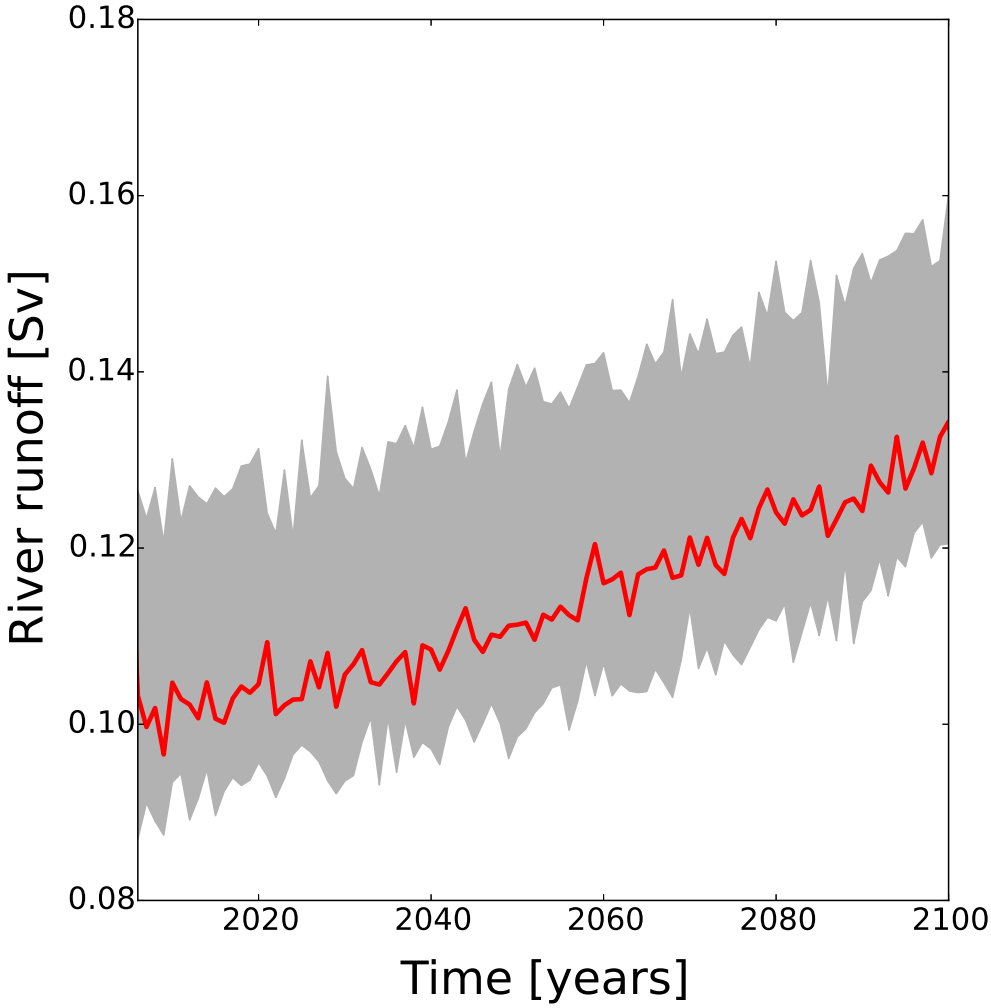

Figure S1. River runoff to the Arctic ocean in CMIP5 (RCP8.5) models. The red line is the multimodel median and the grey shading shows the interquartile range (25%–75%). The following models were used to calculate the median and the interquartile range: ACCESS1–0, ACCESS1–3, CCSM4, CNRM–CM5, GFDL–ESM2G, GFDL–ESM2M, HadGEM2–CC, HadGEM2–ES, IPSL–CM5A–LR, IPSL–CM5A–MR, IPSL–CM5B–LR, MIROC–ESM, MIROC–ESM–CHEM, MIROC5, MRI–CGCM3, MRI–ESM1, NorESM1–M, NorESM1–ME. For some models, more than one ensemble member was used; in total, the figure consists of 39 individual ensemble members.

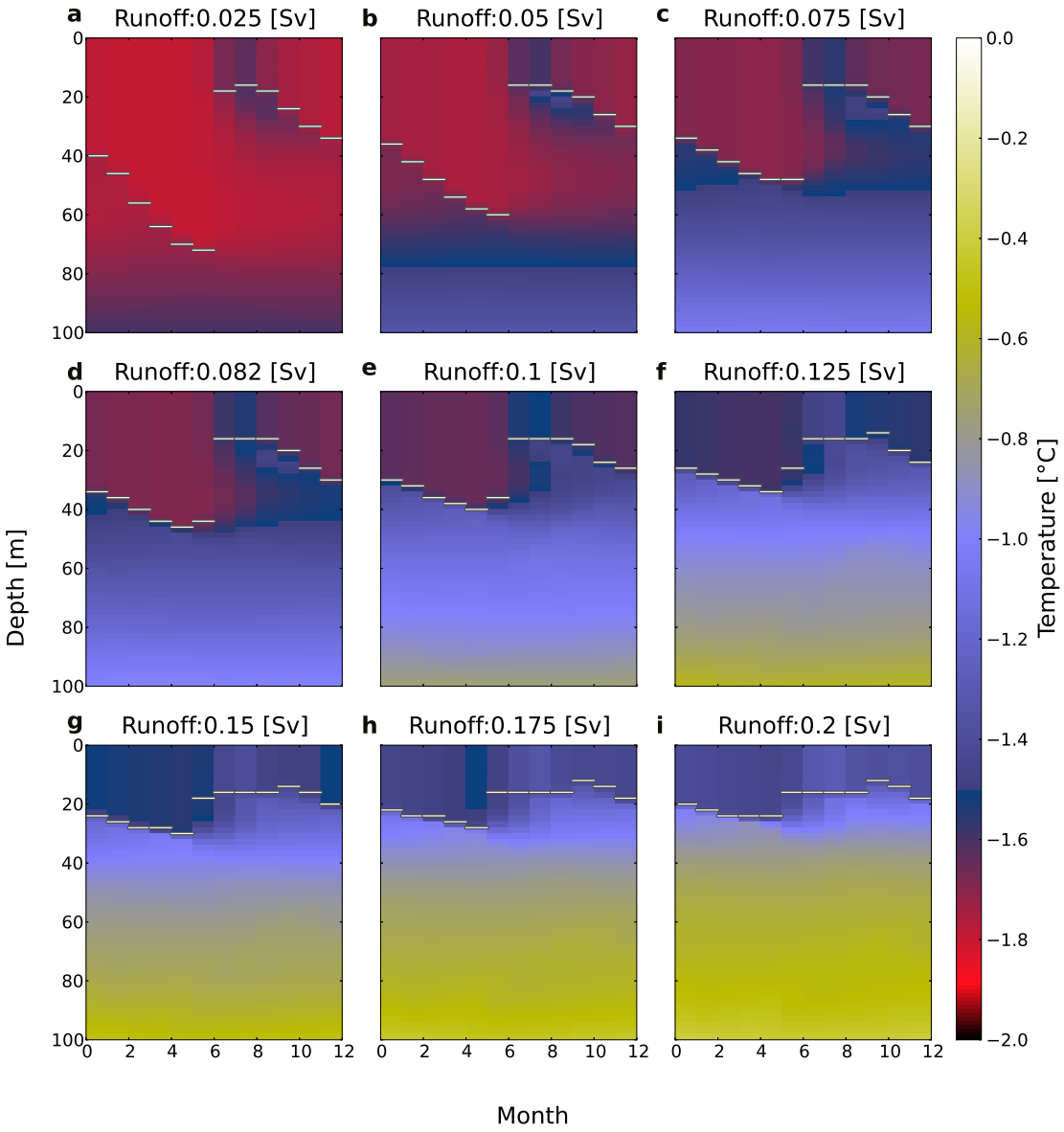

Figure S2. Seasonal temperature stratification. Mixed Layer Depth (MLD) is shown by the white–grey line. MLD is calculated using density criteria i.e. MLD is the depth where density exceeds surface density by 0.1 kg m^{-3}.

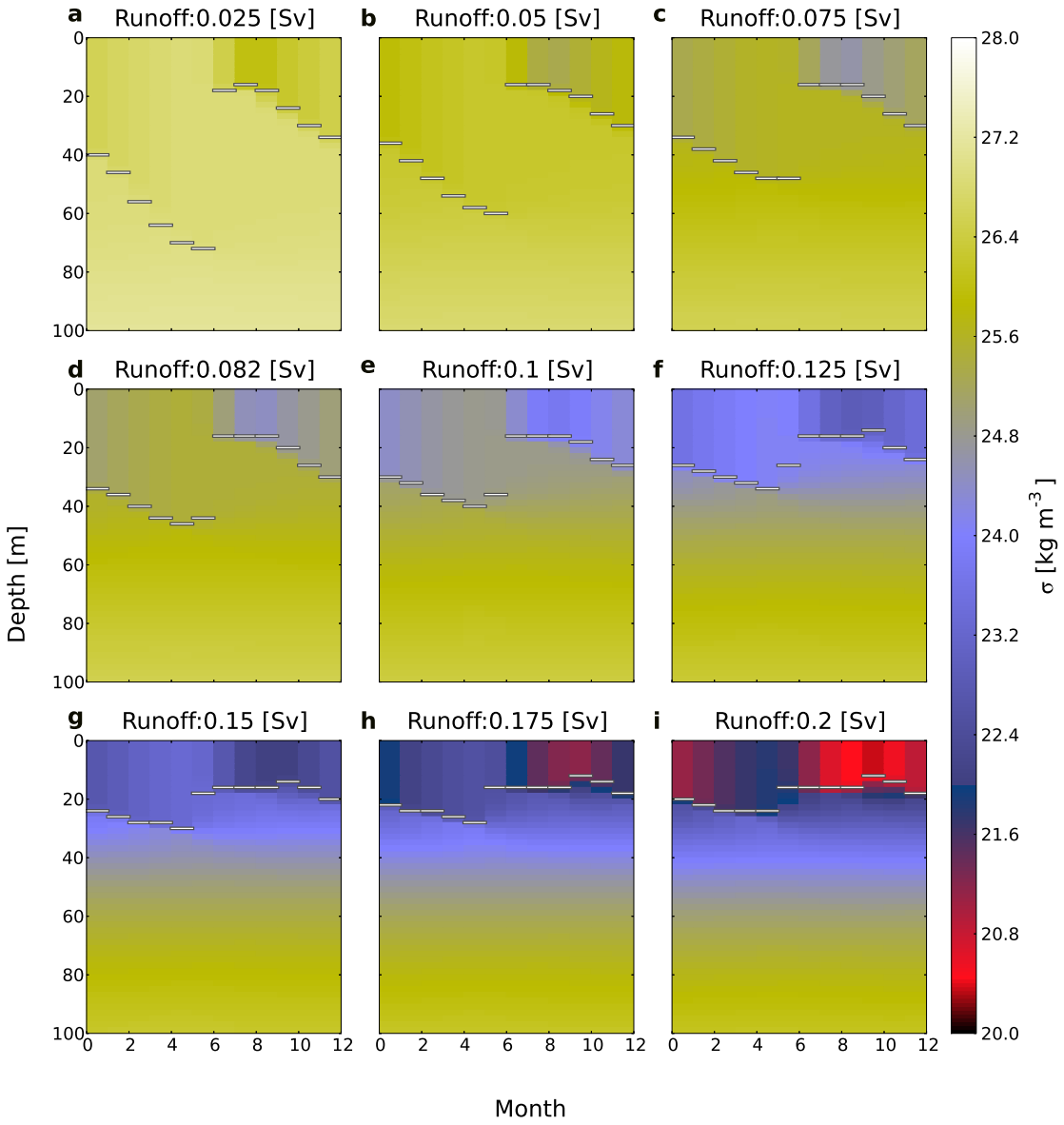

Figure S3. Seasonal density anomaly (σ) stratification. Mixed Layer Depth (MLD) is shown by the white–grey line. MLD is calculated using density criteria, i.e., MLD is the depth where density exceeds surface density by 0.1 kg m^{-3}.

Paper II

5.2 Consequences of future increased Arctic runoff on Arctic Ocean stratification, circulation, and sea ice cover

Nummelin, A., M. Ilicak, C. Li, and L. H. Smedsrud (2016), Consequences of future increased Arctic runoff on Arctic Ocean stratification, circulation, and sea ice cover, *J. Geophys. Res. Oceans*, **121**, 617–637, doi:10.1002/2015JC011156.

AGU PUBLICATIONS

JGR

Journal of Geophysical Research: Oceans

RESEARCH ARTICLE
10.1002/2015JC011156

Special Section:
Forum for Arctic Modeling and Observing Synthesis (FAMOS): Results and Synthesis of Coordinated Experiments

Consequences of future increased Arctic runoff on Arctic Ocean stratification, circulation, and sea ice cover

Aleksi Nummelin[1,2], Mehmet Ilicak[2,3], Camille Li[1,2], and Lars H. Smedsrud[1,2,4]

[1]Geophysical Institute, University of Bergen, Bergen, Norway, [2]Bjerknes Centre for Climate Research, Bergen, Norway, [3]Uni Research Climate, Bergen, Norway, [4]Department of Arctic Geophysics, University Centre in Svalbard (UNIS), Longearbyen, Norway

Key Points:
- Larger river runoff leads to stronger Arctic Ocean stratification and warmer subsurface
- Arctic Atlantic Water circulation strengthens while net exchange with surrounding oceans decreases
- Volume outflow and ice export through the Fram Strait increase with the runoff

Supporting Information:
- Supporting Information S1
- Figure S1
- Figure S2
- Figure S3
- Table S1

Correspondence to:
A. Nummelin,
aleksi.nummelin@uib.no

Citation:
Nummelin, A., M. Ilicak, C. Li, and L. H. Smedsrud (2016), Consequences of future increased Arctic runoff on Arctic Ocean stratification, circulation, and sea ice cover, *J. Geophys. Res. Oceans*, *121*, 617–637, doi:10.1002/2015JC011156.

Received 30 JUL 2015
Accepted 15 DEC 2015
Accepted article online 18 DEC 2015
Published online 21 JAN 2016

Abstract The Arctic Ocean has important freshwater sources including river runoff, low evaporation, and exchange with the Pacific Ocean. In the future, we expect even larger freshwater input as the global hydrological cycle accelerates, increasing high-latitude precipitation, and river runoff. Previous modeling studies show some robust responses to high-latitude freshwater perturbations, including a strengthening of Arctic stratification and a weakening of the large-scale ocean circulation; some idealized modeling studies also document a stronger cyclonic circulation within the Arctic Ocean itself. With the broad range of scales and processes involved, the overall effect of increasing runoff requires an understanding of both the local processes and the broader linkages between the Arctic and surrounding oceans. Here we adopt a more comprehensive modeling approach by increasing river runoff to the Arctic Ocean in a coupled ice-ocean general circulation model, and show contrasting responses in the polar and subpolar regions. Within the Arctic, the stratification strengthens, the halocline and Atlantic Water layer warm, and the cyclonic circulation spins up, in agreement with previous work. In the subpolar North Atlantic, the model simulates a colder and fresher water column with weaker barotropic circulation. In contrast to the estuarine circulation theory, the volume exchange between the Arctic Ocean and the surrounding oceans does not increase with increasing runoff. While these results are robust in our model, we require experiments with other model systems and more complete observational syntheses to better constrain the sensitivity of the climate system to high-latitude freshwater perturbations.

1. Introduction

As the hydrological cycle accelerates in a warming climate, we expect increasing precipitation at high latitudes and increasing runoff to the Arctic Ocean. Observations show a 7% increase in Eurasian runoff from 1936 to 1999 [*Peterson et al*., 2002] that may well already have influenced Arctic Ocean circulation and stratification, and therefore also the sea ice cover. By the end of the century, climate model projections show a 30% increase in Arctic runoff (Figure 1) with an indication of an increase in both the freshwater storage in the Arctic Ocean and freshwater export to the North Atlantic [*Lehner et al*., 2012].

The Arctic Ocean (Figure 2) is strongly stratified, largely ice covered, and receives anomalously large freshwater input per unit area compared to the other world oceans [*Rudels*, 2015; *Rawlins et al*., 2010]. The Arctic Ocean stratification is characterized by a cold and fresh surface, a relatively warm and salty Atlantic Water layer at depth, and an intermediate layer of cold but gradually saltier water often termed the cold halocline [*Rudels et al*., 1996; *Steele and Boyd*, 1998; *Rudels et al*., 2004]. The fresh surface waters are derived from river runoff, positive net precipitation, relatively fresh Pacific inflow, and seasonal ice melt. The surface circulation is dominated by the transpolar drift crossing the Arctic Basin from the East Siberian and Laptev Seas to the Fram Strait, and the anticyclonic Beaufort Gyre in the Canada Basin. The cold halocline, derived from brine-enriched shelf waters and local winter convection, is most evident in the Canada Basin and largely absent in the Nansen Basin [*Rudels et al*., 1996; *Rudels*, 2015]. The warm Pacific inflow enters the upper halocline through Bering Strait, affecting the stratification mainly in the Canada Basin. Atlantic Water (AW) enters the Arctic Ocean in two branches, one through the Fram Strait and the other through the Barents Sea. The AW advects cyclonically around the basin creating an AW layer at depth through most of the Arctic Ocean [*Rudels*, 2015; *Jones*, 2001].

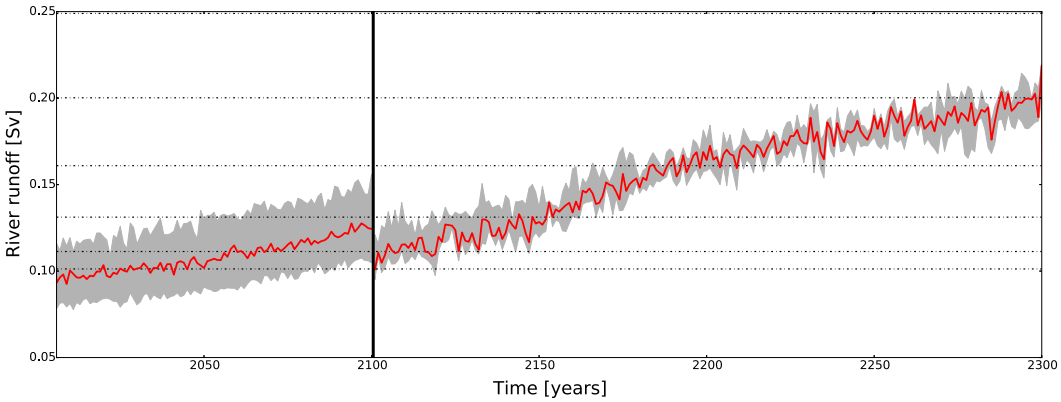

Figure 1. Expected annual mean runoff to the Arctic Ocean based on CMIP5 models using Representative Concentration Pathway (RCP) 8.5 (see supporting information Table S1 for models included in the ensemble). The red line shows the ensemble median, and the gray shading shows the interquartile range. The black dotted lines show the runoff values used in the idealized perturbation experiments (see Figure 3). The vertical line at year 2100 separates the period 2005–2100 with a large multimodel ensemble (19 models and total of 49 members) from the period 2100–2300 with a small ensemble (4 models and total of 6 members).

The variability in the pathways of Eurasian river runoff is largely governed by the Arctic Oscillation (AO), the leading mode of the atmospheric variability in the extratropical Northern Hemisphere. The AO influences the transpolar drift and the intensity of Ekman convergence to the Beaufort Gyre [*Morison et al*., 2012], both of which affect where freshwater tends to accumulate in the Arctic Basin. The bulk of the river runoff enters the vast Eurasian shelves and is transported mainly into the Canada Basin for a high AO index, but toward Fram Strait by the transpolar drift for a low AO index [*Morison et al*., 2012; *Alkire et al*., 2015]. Observations also suggest a linkage between the AO and the North American (mainly Mackenzie River) runoff pathways [*Yamamoto-Kawai et al*., 2009; *Fichot et al*., 2013]: there has been a shift from a rather direct outflow via the CAA in early 2000s to a northward pathway into the Beaufort Gyre around 2006 coinciding with a change to a strongly positive AO.

On the large scale, models respond to high-latitude freshwater perturbations with a slowdown of the oceanic circulation. In numerous hosing experiments, large amounts of freshwater are released over a 50°N–70°N latitude band in the subpolar North Atlantic Ocean. Such a freshwater perturbation reduces convection in the North Atlantic, slows down the surface circulation and Atlantic Meridional Overturning Circulation (AMOC), and reduces the northward ocean heat transport [*Manabe and Stouffer*, 1995; *Stouffer et al*., 2006; *Stocker et al*., 2007], as well as leading to a subsurface warming in the North Atlantic and Arctic Oceans [*Mignot et al*., 2007]. Similar results are achieved using more realistic perturbations with both Greenland meltwater [*Gerdes et al*., 2006; *Swingedouw et al*., 2014] and Arctic river runoff [*Rennermalm et al*., 2006, 2007]. In fact the large-scale ocean and climate response is found to be similar to that described above whenever the freshwater forcing originates upstream of the North Atlantic convection sites [*Roche et al*., 2010] while a qualitatively different response is found if the forcing is applied downstream of the convection sites [*Mignot et al*., 2007].

The local effects of Arctic river runoff have been studied in more detail using both observations and a variety of models. Idealized regional modeling work links surface freshening to stronger currents inside the Arctic Ocean [*Spall*, 2013], and high-resolution modeling work finds that increasing runoff induces stronger currents close to river mouths [*Whitefield et al*., 2015]. Runoff also affects the sea ice cover and dense water production in the shelf seas as well as the large-scale hydrography inside the Arctic Basin. More river runoff has been linked to more summer melt, but also to earlier freezing in both observations [*Bauch et al*., 2013; *Nghiem et al*., 2014] and modeling studies [*Whitefield et al*., 2015]. Observations also indicate that less river water on the shelf can increase local bottom water production [*Dmitrenko et al*., 2010]. Finally, *Nummelin et al*. [2015] showed that the density and temperature stratification of the Arctic Ocean are tightly linked: under stronger freshwater forcing, the large-scale hydrography approaches a steady state with a warmer subsurface, but stronger density stratification that together balance the vertical heat flux.

The overall effect of increasing runoff on the climate system requires a combined understanding of the local Arctic processes and those linking the Arctic to the surrounding oceans. While the large-scale response of the climate system to high-latitude freshwater perturbation in the Atlantic is rather well documented, the

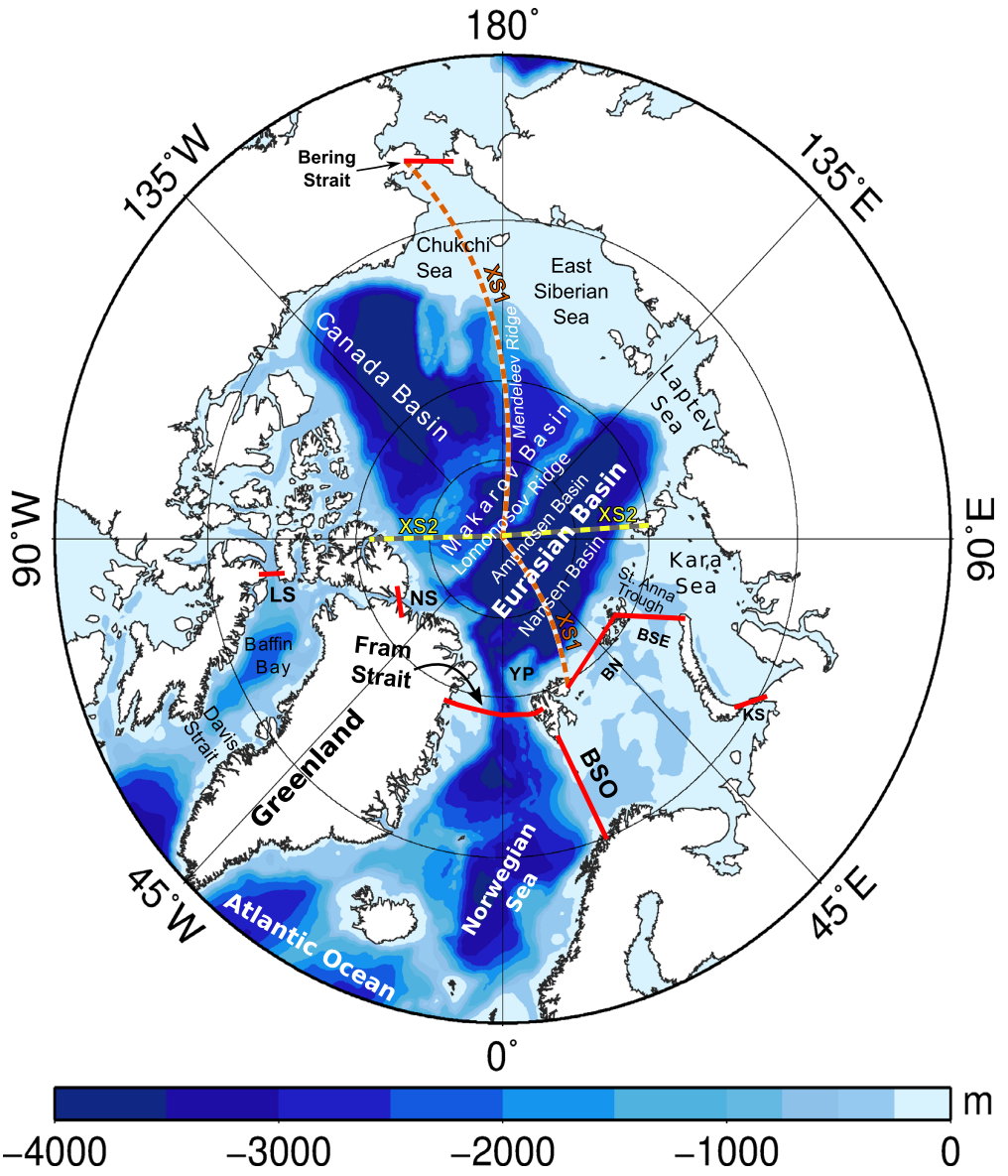

Figure 2. Arctic Ocean bathymetry. Main basins and connecting gateways are labeled. Abbreviations are: BSO, Barents Sea Opening; BN, Barents North; BSE, Barents Sea Exit; KS, Kara Strait; LS, Lancaster Sound; NS, Nares Strait. Labels XS1 and XS2 correspond to the cross sections shown in Figures 8 and 9.

regional response of circulation and hydrography in the Arctic Ocean has not been previously studied outside idealized settings. The conditions in the Arctic are strongly influenced by lower latitudes and vice versa, creating important oceanic connections that are as yet unexplored.

In this study, we use a coupled ocean-sea ice general circulation model to show two distinct responses to increasing Arctic runoff: (a) a spin-up of the circulation and warming in the Arctic Mediterranean, and (b) a slowdown and cooling south of the Greenland-Scotland ridge in the North Atlantic. Inside the Arctic Ocean, neither the dynamic nor thermodynamic response can be understood simply by a reduction in AMOC. For the North Atlantic, our results are largely consistent with previous freshwater hosing studies [*Stouffer et al.*, 2006; *Stocker et al.*, 2007; *Mignot et al.*, 2007; *Roche et al.*, 2010].

The paper is structured as follows: we describe the modeling strategy along with the control simulation in section 2; analyze the Arctic and large-scale oceanic responses to increasing runoff in section 3;

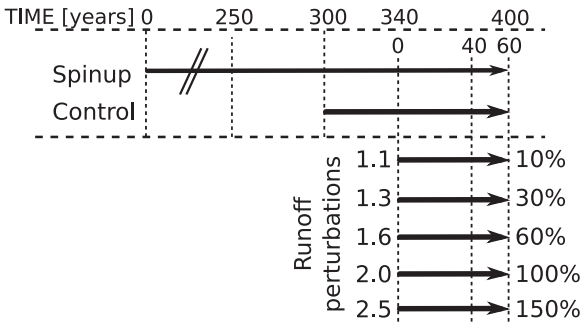

Figure 3. Design of spin-up and perturbation experiments. The labels 1.1–2.5 (10%–150%) indicate the factor (percentage) of runoff increase relative to the control run.

discuss our results in the context of earlier work in section 4; and present concluding remarks in section 5.

2. Model and Methods

2.1. Experimental Setup

In this study, we use the coupled ocean-sea ice component of the Norwegian Earth System Model (NorESM) [*Bentsen et al.*, 2013]. We use the bipolar grid with 1° nominal resolution previously used in the Coupled Model Intercomparison Project Phase 5 (CMIP5) for both ocean and sea ice components. The ocean component is based on Miami Isopycnic Coordinate Ocean Model (MICOM) [*Bleck and Smith*, 1990; *Bleck et al.*, 1992] with 51 isopycnic vertical levels and 2 levels with freely evolving density at the surface mixed layer. The ocean model has an Arakawa C discretization in the horizontal and uses leapfrog time stepping. The ocean model formulation is mass conserving (non-Boussinesq), but for simplicity, the transports are shown in units of volume transport (1 Sv = 1E6 m^3 s^{-1}) and the conversion is done simply by dividing the mass transport by a factor of 1E9 kg m^3 s^{-1}/Sv. The sea ice model is the version of the Los Alamos sea ice model (CICE4) [*Gent et al.*, 2011; *Holland et al.*, 2012] used in NorESM and the Community Climate System Model version 4 (CCSM4). The model is forced with the Coordinated Ocean-ice Reference Experiments (CORE) Normal Year Forcing (NYF), which is based on the 1958–2000 period [*Large and Yeager*, 2004], i.e., the atmospheric forcing is a repeating climatological year. Outgoing surface fluxes are calculated with bulk formulas, and incoming radiation is affected by changes in surface albedo (sea ice cover). River runoff is treated as a virtual salinity flux. A more detailed model description can be found in sections 2.3 and 2.4 of *Bentsen et al.* [2013].

The model is spun-up for 340 years in a two-stage process (Figure 3). The model starts from rest and is run first for 300 years with sea surface salinity (SSS) restored toward CORE climatological SSS. Due to lack of atmospheric feedbacks, the restoring term is necessary to keep model salinities from drifting too far from observations. The variable restoring term is forced to stay below $\pm$3.52E-3 m s^{-1} and for this first period, the restoring time scale is 6 days. To avoid generating large variability via the SSS restoring, we calculate a restoring climatology from years 250 to 300 and apply the climatological restoring together with a greatly reduced variable restoring (restoring time scale of 60 days, 10% of the variable restoring used for spin-up). This makes for a close to constant SSS restoring term so that the differences between the runs are not primarily due to the SSS restoring. Using the new SSS restoring, we run the model for another 40 years (until 340 years). We scale the magnitude of the restoring term down to zero at the river mouths by multiplying it with a mask (Figure 4a) that leaves the Arctic SSS largely free to evolve as we change the runoff.

At 340 years, we start the runoff experiments. We increase the runoff in the Arctic while using control runoff values elsewhere (Figure 4b). We ran five different perturbation experiments (Figure 3) with runoff increases of 10%, 30%, 60%, 100%, and 150% compared to the control simulation, which has close to 0.1 Sv freshwater runoff entering the Arctic Ocean via rivers. Note that we do not increase melting from Greenland. The runoff perturbations are applied for 60 years (from year 340 to 400) and unless otherwise specified results are shown for the last 20 years of the simulation (Figure 3). Significance is also calculated over the last 20 years using a Welch test. The freshwater content is calculated relative to a reference salinity of 34.8. During the 20 year analysis period, the Arctic Ocean hydrography and circulation have largely equilibrated, but the deep ocean is still adjusting. For example, the maximum AMOC in most of the perturbation experiments shows a downward trend (approximately 1.5 Sv/decade for the 2.0 experiment).

Runoff seasonality is of minor importance for the time and spatial scales in this study and is not taken into account. River water resides on the shelves for several years [*Schlosser et al.*, 1994; *Bauch et al.*, 2013]. The runoff-induced annual cycle in salinity is very small away from river mouths and is therefore not of first-order importance for the large-scale ocean response. Furthermore, in the future, the runoff is expected to be more equally distributed throughout the year. In a warmer climate, reduced snow cover leads to reduced

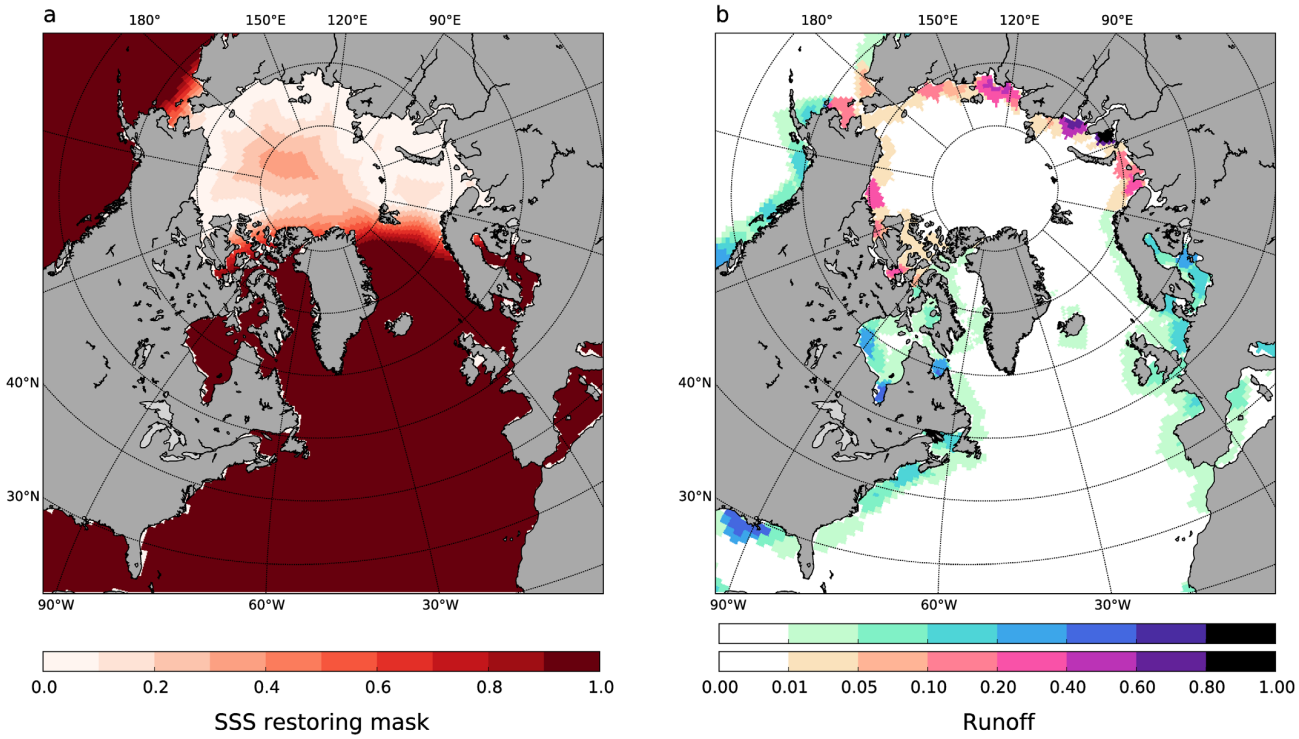

Figure 4. (a) Sea surface salinity restoring mask and (b) runoff forcing field. In Figure 4b, warm colors denote areas where the runoff increase is applied, and cool colors denote areas where runoff is kept at control levels. The intensity of the color denotes the strength of the runoff in both cases. Runoff values are normalized by the maximum value inside the Arctic Basin.

spring peak discharge while increases in winter (liquid) precipitation and snow melt lead to more winter runoff [*Rennermalm et al.*, 2010; *Overeem and Syvitski*, 2010]. We note that for shelf processes near the river mouths, the changing seasonality might bear some importance [*Bauch et al.*, 2013; *Whitefield et al.*, 2015], but these processes cannot be captured accurately in ocean models with 1° horizontal resolution and are thus beyond the scope of this work.

The main atmospheric feature of potential importance for the Arctic runoff distribution is the AO. The AO is a pattern of atmospheric variability commonly defined as the first Empirical Orthogonal Function (EOF) of monthly sea level pressure anomalies north of 20°N. *Morison et al.* [2012] argued that a positive AO pattern can lead to accumulation of Eurasian runoff in the Beaufort Gyre while a negative AO pattern drives the Eurasian runoff directly toward Fram Strait. We apply CORE NYF atmospheric forcing based on the 1958–2000 climatology, a period during which the mean AO was close to neutral (−0.12 using monthly data from http://www.cpc.ncep.noaa.gov/products/precip/CWlink/daily_ao_index/monthly.ao.index.b50.current.ascii). The implications of this are discussed in section 4.3.

For most of the analysis and graphics, we use the software packages matplotlib [*Droettboom et al.*, 2015; *Hunter*, 2007] and Physical Analysis of Gridded Ocean data (PAGO; available at http://www.whoi.edu/science/PO/pago/index.html [*Deshayes et al.*, 2014]).

2.2. Control Simulation

The simulated sea surface temperature (SST) and sea surface salinity (SSS) are in qualitative agreement with observations at large scales. Figure 5 shows simulated annual mean patterns compared to the World Ocean Atlas (WOA) 2013 [*Locarnini et al.*, 2013; *Zweng et al.*, 2013] in the Atlantic-Arctic sector. The main discrepancies relevant for this study are found in the Gulf Stream region and in the Arctic Ocean. The Arctic shelf regions are generally too cold and saline when compared to the observations (Figure 5b). This could be because the model mixed layer parameterization produces an overly cold, deep, and consequently saline mixed layer. In addition, sparse, summer-biased observations and large interannual variability in these

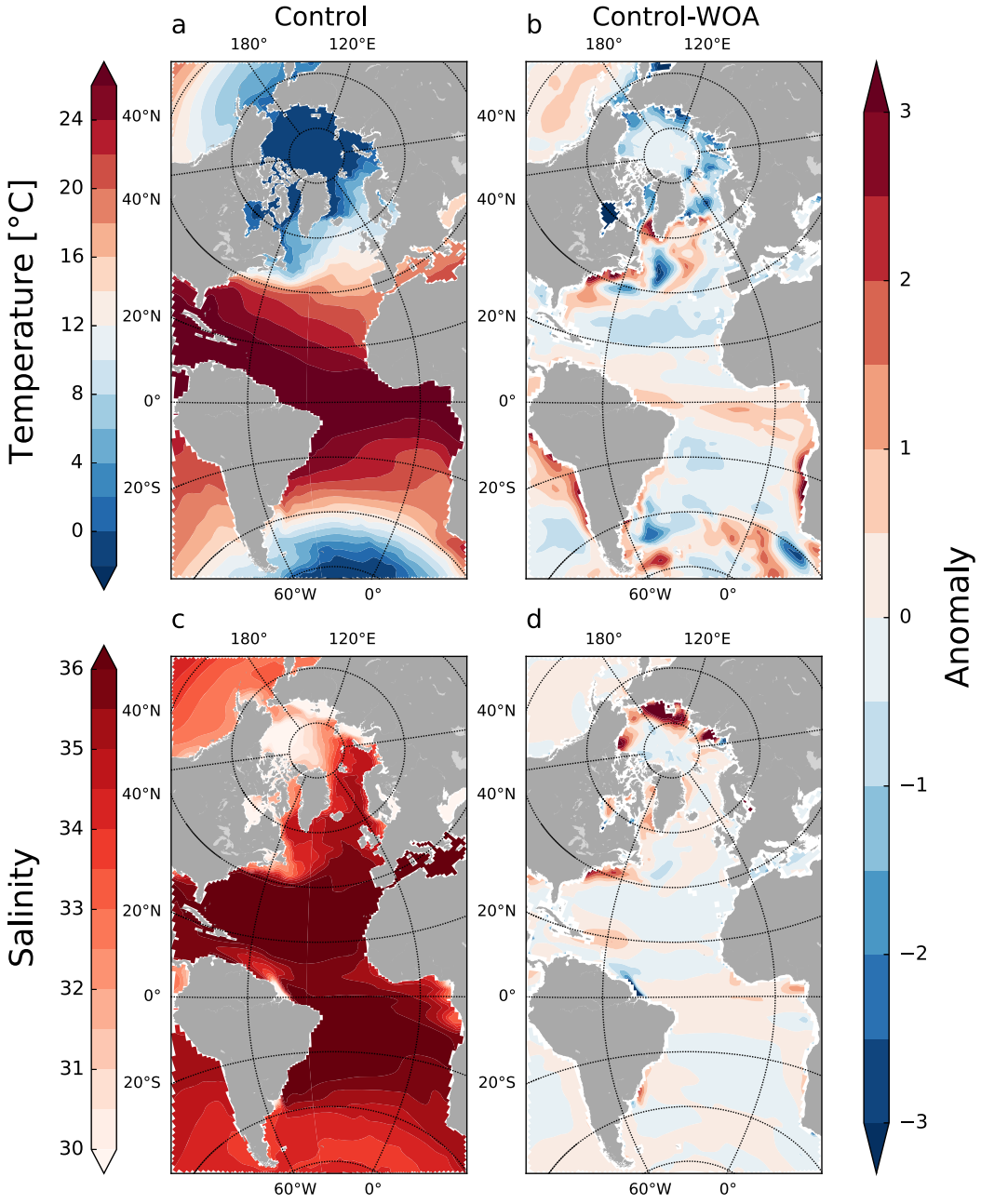

Figure 5. (a, c) Annual mean surface temperature and salinity in the control simulation, and (b, d) the anomalies between the control simulation and WOA13 climatology [*Locarnini et al.*, 2013; *Zweng et al.*, 2013]. The largest temperature and salinity biases in the Arctic shelf regions are −4.4°C and 7.9 psu, respectively.

regions make direct data-model comparison difficult. In fact, comparison with other observational data sets (MIMOC [*Schmidtko et al.*, 2013] and PHC3.0 updated from *Steele et al.* [2001]) shows discrepancies of opposite sign in some shelf regions (supporting information Figures S1 and S2). The Gulf Stream is too far south, resulting in substantial SST differences compared with the WOA in the North Atlantic. The east coast of North America is too warm, likely because the horizontal resolution there is too low to correctly resolve the spreading of cold waters from the north along the coast with the Nova Scotia Current, and because the lateral mixing with the warm offshore waters might be overly large in the model.

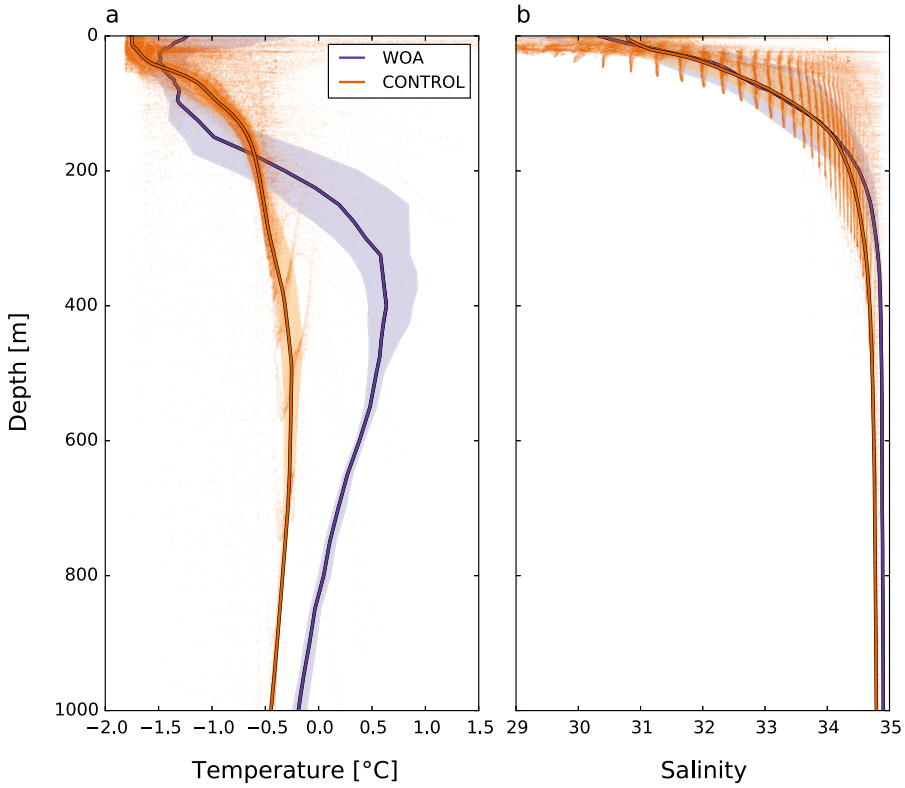

Figure 6. Vertical profiles of annual median (a) temperature and (b) salinity averaged over the Arctic Ocean (excluding the Barents Sea) for the control simulation and the WOA13 climatology [*Locarnini et al*., 2013; *Zweng et al*., 2013]. Shading shows the interquartile range while the dots show the individual grid cell values.

The simulated vertical stratification in the Arctic suffers from issues that are well known among coarse resolution models. Figure 6 shows simulated and observed vertical mean profiles of temperature and salinity for the Arctic Basin. The main biases are an overly cold surface, an overly warm halocline (Upper Polar Deep Water) and an AW layer that is too cold and fresh. The deficiencies in the vertical structure are common to many models with similar resolution and they are linked to too much vertical mixing in the Arctic Ocean [*Komuro*, 2014; *Pemberton et al*., 2015] and poor treatment of the brine released from sea ice formation [*Nguyen et al*., 2009].

The net volume exchanges in the Arctic gateways are close to observations (Table 1). The simulated net transport to the Arctic Ocean through the Barents Sea Opening (BSO; 2.45 Sv) is similar to the observed estimate (2.3 Sv), while the net transport through Fram Strait (−1.39 Sv) is smaller than observations indicate (−2.0 Sv). Note that the slightly negative (out of the Arctic) net transport through Fram Strait is the sum of much larger inflow and outflow terms that are not as well simulated. The simulated AW inflow through the Fram Strait and BSO combined is only 7.8 ± 0.1 Sv, of which the Fram Strait alone contributes 3.9 ± 0.1 Sv. The most recent observational estimate for the Fram Strait inflow is 6.6 ± 0.4 Sv [*Beszczynska-Möller et al*., 2012]. It is likely that the small Fram Strait inflow contributes to the discrepancies in the vertical profiles, especially the cold bias in the AW layer. The Bering Strait inflow (0.8 Sv) and CAA outflow (2.0 Sv) compare well with observations. However, the two main CAA gateways, Nares Strait and Lancaster Sound, have close to equal contributions to the outflow from observations [*Melling et al*., 2008], while the simulated Nares Strait contribution is 3 times larger than that of Lancaster Sound. The surface circulation and AW circulation in the Eurasian Basin (supporting information Figure S3b) in the control simulation are in qualitative agreement with observations, but the weak anticyclonic AW layer circulation in the Canada Basin (supporting information Figure S3) is likely a result of a long-term adjustment to relatively strong Beaufort Gyre (similar to response to strong Beaufort Gyre in *Karcher et al*. [2007]).

Table 1. Net Volume and Heat Transports in Arctic Gateways[a]

Source	Fram Strait	BSO	Bering Strait	CAA	Davis Strait
		Volume Transport (Sv)			
NorESM	−1.39±0.04	2.45 ± 0.02	0.94 ± 0.00	−2.0±0.02	−2.0±0.02
Woodgate et al. [2005]			0.8		
Melling et al. [2008]	−2.0	1.8	0.8	1–2	3
Smedsrud et al. [2013]		2.3			
Schauer et al. [2008]	−2.0				
		Heat Transport (TW)			
NorESM	26.49 ± 0.75	57.32 ± 0.43	5.15 ± 0.06	7.75 ± 0.07	
Schauer et al. [2008]	26−50				

[a]NorESM values are mean transports over the last 20 years of the control simulation ± standard deviation. All other values are observational estimates.

3. Results

The main Arctic Ocean responses to increased runoff are a fresher surface, a warmer halocline, and a warmer AW layer. These responses are visible in Figure 7 showing the median temperature and salinity profiles over the deep Arctic Basin. The increased runoff leads to stronger stratification, which in turn sharpens the temperature gradient across the halocline. Deeper down, the AW layer becomes warmer and rises in the water column. These first-order results are consistent with previous idealized modeling efforts [*Nummelin et al*., 2015; *Nilsson and Walin*, 2010].

In this section, we examine the response to increasing runoff in terms of the changes in the local stratification (section 3.1), the local circulation (section 3.2), the inflows and outflows to the Arctic Ocean (section 3.3), and the large-scale ocean circulation (section 3.4). We focus on the 2.0 runoff experiment, i.e., a doubling of present-day runoff that is projected to occur by the end of the 23rd century (Figure 1), because the responses shown are largely linear to runoff amount.

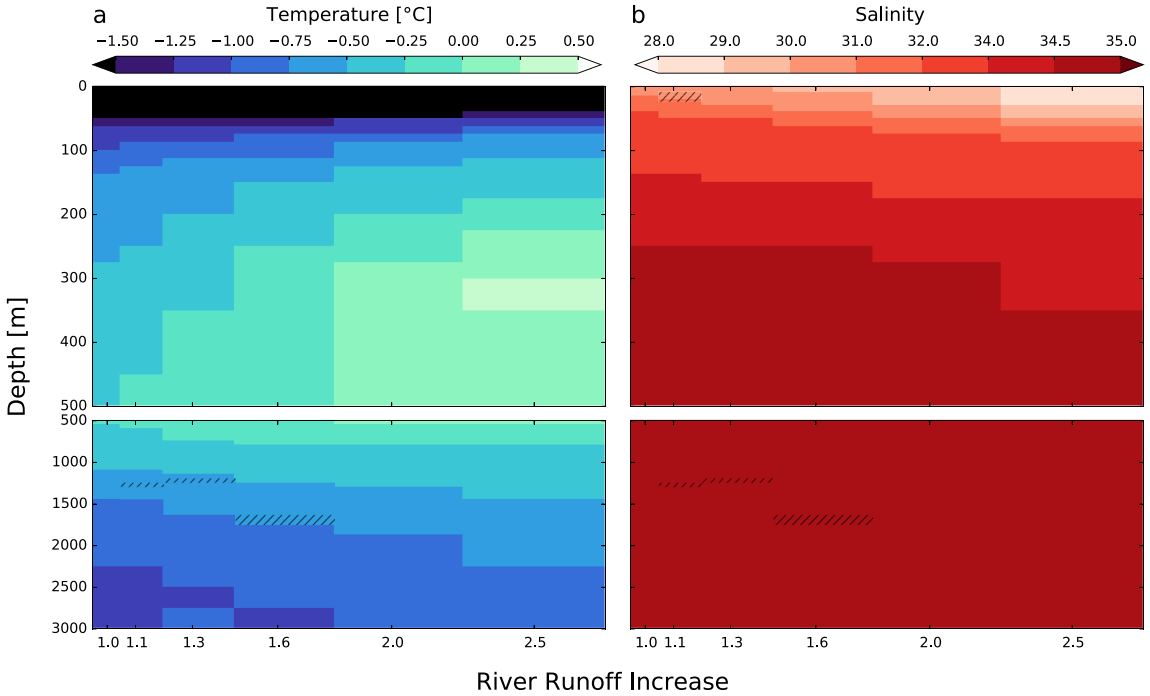

Figure 7. Vertical profiles of annual median (a) temperature and (b) salinity as a function of runoff averaged over the Arctic Ocean (excluding the Barents Sea). Hatching indicates values that are not significantly different from the control simulation at the 95% confidence level.

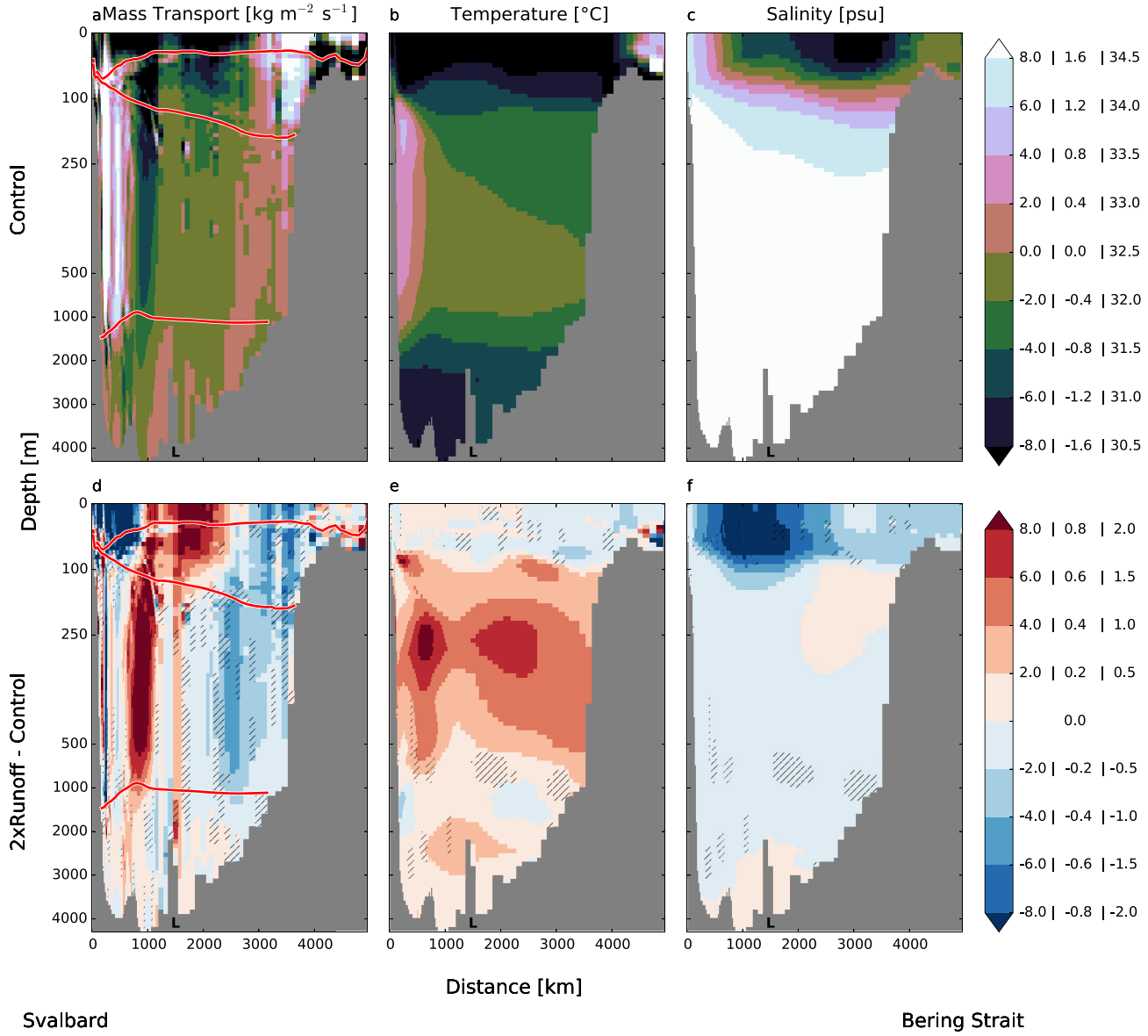

Figure 8. Cross-section XS1 through the Arctic from (left) Svalbard toward (right) Bering Strait showing (left) transport (positive values indicate flow toward Eurasia, and negative values indicate flow toward North America), (middle) temperature, and (right) salinity. The L in each plot indicates the location of the Lomonosov ridge. Figures 8a–8c show vertical profiles from the control simulation, and Figures 8d–8f show anomalies in the 2.0 runoff experiment (2.0 × runoff – control). Note that the transport anomalies are not absolute so a negative anomaly can indicate either stronger flow toward Eurasia or weaker flow toward North America. The color bar labels apply to the plot in the respective column (i.e., the left set of labels are for the mass transport, etc.). Hatching indicates values that are not significantly different from the control simulation at the 95% confidence level. The red lines in Figures 8a and 8d show boundaries of the surface mixed layer (model layers 1–2, approximately 0–50 m) and AW layer (model layers 33–45, approximately 100–1000 m) used in Figure 12. The cross-section XS1 is indicated on the map in Figure 2.

3.1. Changes in Arctic Hydrography

The hydrographic response to increased river runoff is a surface freshening and subsurface warming through the entire Arctic Ocean. In the Eurasian Basin north of Svalbard (Figures 8b and 8e), the warm anomaly is evident throughout the AW layer and peaks at around 1°C. In the Canada Basin, the anomaly continues to extend from Siberia to the CAA along the cyclonic flow path (Figures 8b, 8e, 9b, and 9e).

There is another, shallower warm core in the halocline (at about 100 m depth) throughout most of the Arctic Ocean (Figures 8–10c, and 10d). The warmer halocline is a result of changes on the shelves. In the control

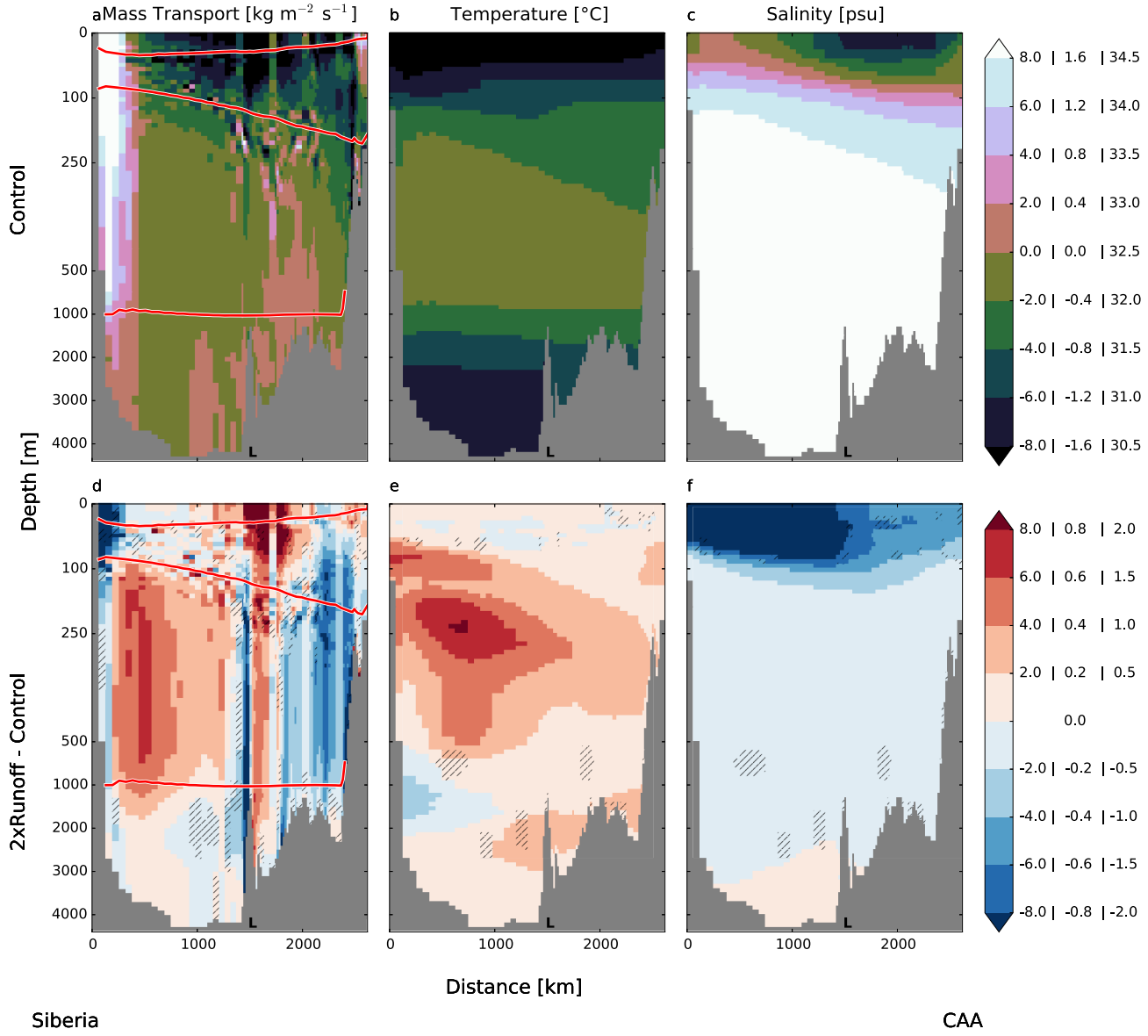

Figure 9. Same as Figure 8 but for cross-section XS2 through the Arctic from (left) Siberia to (right) the CAA.

simulation, the lowest temperatures in the central Arctic halocline are found off the Barents Sea and the Siberian shelves, indicating a flow of cold dense waters from the shelves toward the interior Arctic Ocean (Figure 10c). When the runoff is doubled, the coldest regions off and on the shelves become warmer (Figure 10d), indicating reduced cooling over the shelf regions due to stronger stratification. The cold anomaly off the Chukchi Shelf is related to reduced heat transport through Bering Strait and redistribution of fresher (and lighter), but still cold, shelf waters higher in the water column (see also the temperature and salinity signals in Figure 8).

Like the warmer halocline, the warmer AW layer also arises from processes internal to the Arctic Ocean. In the control simulation, the AW layer flows through the Fram Strait as a relatively warm current, but cools quickly as it flows along the northern slope of the Barents Shelf (Figure 10e). The cooling is a direct consequence of mixing with cold shelf waters, and heat loss to ice melt and the atmosphere. In the 2.0 runoff experiment, the AW layer is generally colder as it enters the Arctic Ocean (through the eastern Nordic Seas), but it is not cooled

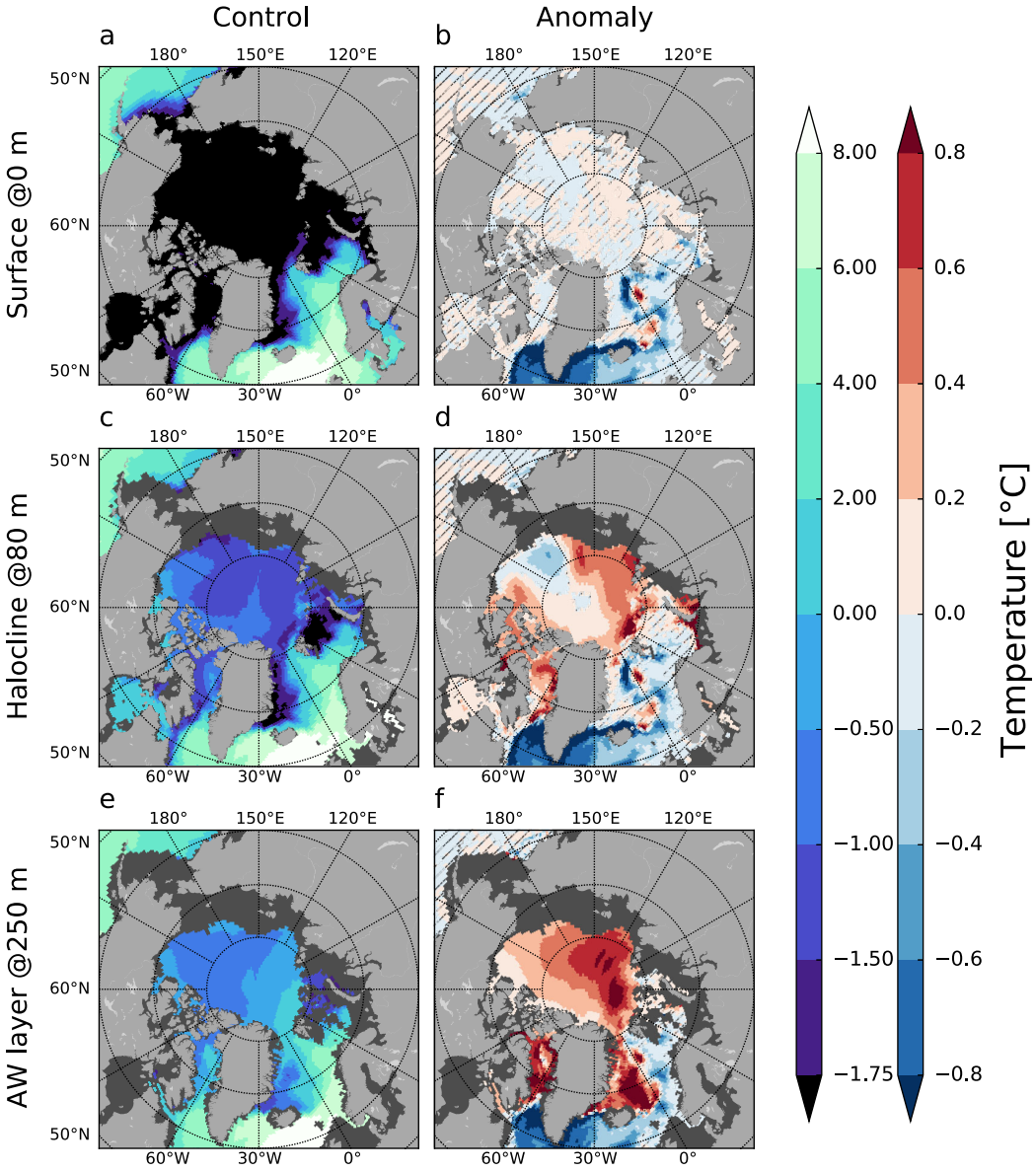

Figure 10. Winter (January to March) temperatures in the control simulation and anomalies in the 2.0 runoff experiment (2.0 runoff-control) at the (a, b) surface, (c, d) halocline (at 80 m depth), and (e, f) AW layer (at 250 m depth). Hatching indicates values that are not significantly different from the control simulation at the 95% confidence level. The left colorbar is for the control simulation and the right colorbar is for the anomalies.

as effectively as in the control simulation due to stronger stratification and warmer shelf waters (Figure 10f, see also section 3.4). Consequently, a warm anomaly develops further inside the Arctic Ocean.

Sea ice thickness changes are generally modest owing to competing effects in the perturbation experiments. The sea ice response is consistent throughout the year, and shows little seasonal difference within each region (Figure 11). There are thickness decreases in select places in the Eurasian Basin, and general increases in the Canada Basin, with the largest increases occurring close to the shelf break at Chukchi and East Siberian Seas, a region with a strong ice thickness gradient. For the Canada Basin, weaker Beaufort Gyre (see section 3.2) allows for a longer residence time of ice, increasing both the thickness and age of the ice in the Canada Basin, while for the Eurasian Basin, larger ice export through Fram Strait (approximately 9.5% or 5.5E3 m^3 s^{-1} increase in the 2.0 perturbation experiment) tends to thin ice. The stronger

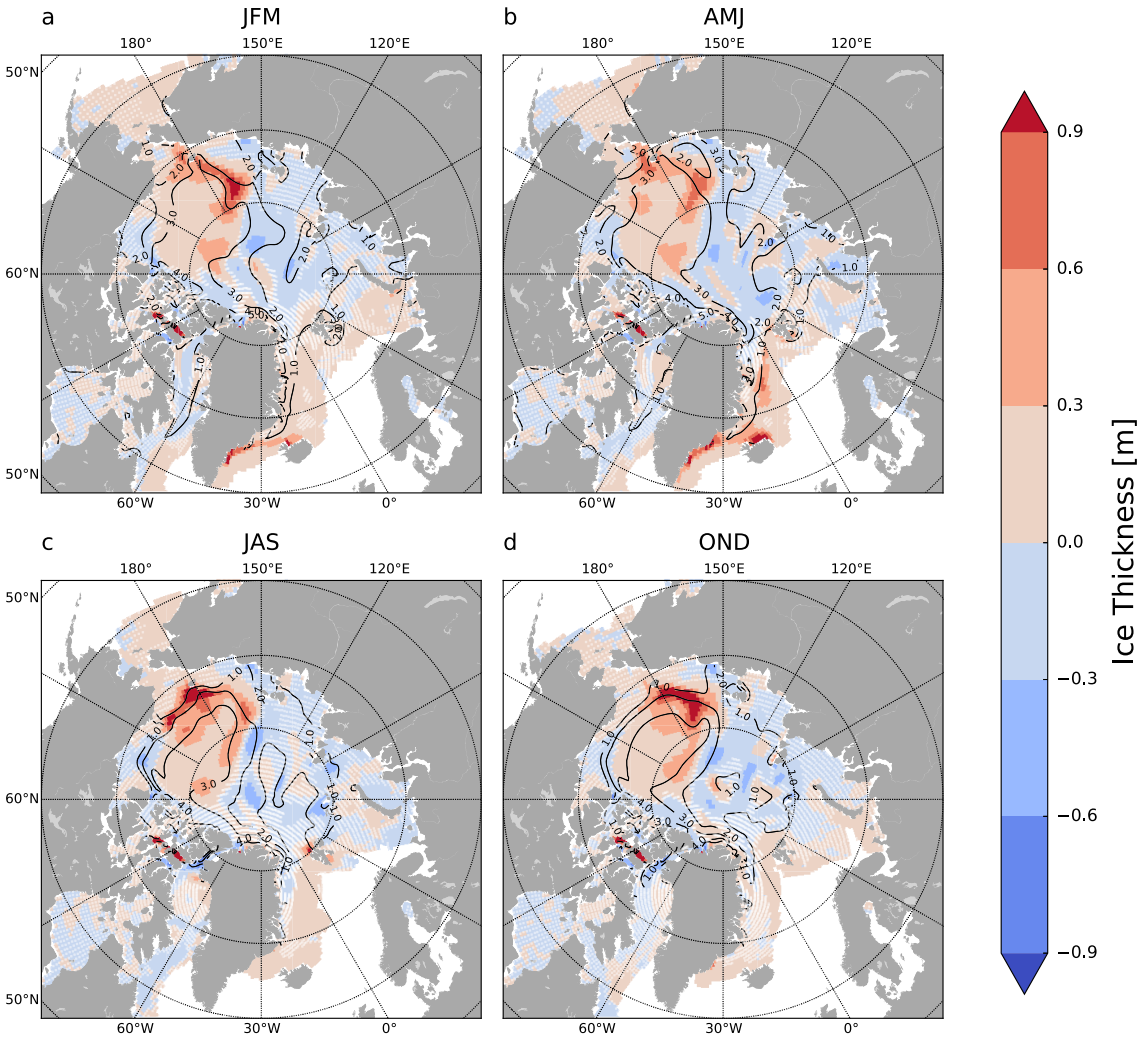

Figure 11. Seasonal mean sea ice thickness anomalies in the 2.0 runoff experiment compared to the control simulation. Ice thickness in the control simulation is shown in black contours (m). White stippling shows areas where the anomaly is not statistically significant at the 95% level. Seasons: JFM is January to March, AMJ is April to June, JAS is July to September, and OND is October to December.

stratification and reduced Bering Strait inflow favor thermodynamic growth, but actual changes in ocean to ice heat flux (not shown) are generally small. Because we used a standalone sea ice-ocean model, the ice area is to a large extent bound by the atmospheric forcing, which remains constant in our simulations. In a fully coupled simulation, atmospheric temperatures would respond to changing sea ice cover and reinforce the ice changes, for example, expanding ice would cool the atmosphere and reduced ice would warm the atmosphere. The large-scale atmospheric circulation would also be affected through thermodynamic coupling (higher pressure over cold ice-covered surface) and dynamic coupling (changing surface momentum exchange depending on the ice area and thickness). Finally, we do not account for sea ice decline due to increased greenhouse gas concentrations.

3.2. Changes in Circulation Within the Arctic Ocean

Under increased runoff, the barotropic flow intensifies in the Eurasian Basin and weakens in the Canada Basin, reflecting changes in the surface and deep circulation (Figure 12a). The stronger barotropic stream function in the Eurasian Basin results from the Arctic-wide strengthening of the cyclonic boundary current circulation in the AW layer (Figure 12c). The weaker barotropic circulation in the Canada Basin is the

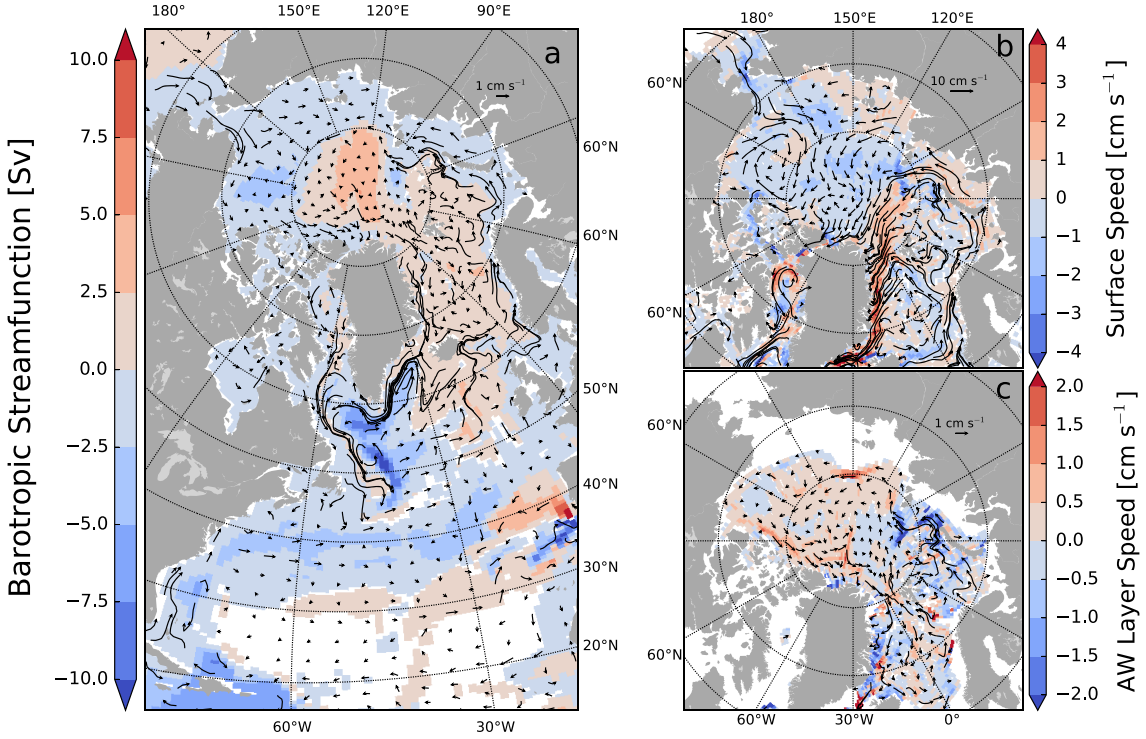

Figure 12. Ocean circulation in the 2.0 runoff experiment (vectors) and anomalies compared to the control simulation (shading): (a) barotropic stream function, (b) surface current speed in model layers 1–2 (approximately 0–50 m depth), and (c) AW layer current speed in model layers 33–45 (approximately 100–1000 m depth). Only anomalies that are significant at the 95% confidence level are plotted. Note that Figures 12b and 12c show the anomalies in current speed (absolute velocity) which is different from Figures 8 and 9 where we show anomalies in the mass transport.

combined result of the opposite responses in the surface (Figure 12b, weaker anticyclonic Beaufort Gyre) and AW layer (Figure 12c, stronger cyclonic) circulation. The weakening of the Beaufort Gyre (Figure 12b) and associated shift in the transpolar drift toward the Eurasian Basin (Figures 8 and 9) are due to a weakening of the sea surface height (SSH) gradient (Figures 14a and 14b) between the Canada Basin and Eurasian Basin.

The intensified flow in the AW layer (Figures 8 and 9, and 12c) is a result of the stronger stratification, which leads to sharper horizontal density gradients [*Spall*, 2013] and reduces the atmospheric (anticyclonic) momentum transfer to the ocean [*Lique et al.*, 2015]. Lighter waters produced at the Barents Shelf weaken the gravity current entering St. Anna trough (Figure 12c). There is also a widening of the boundary current which could indicate stronger eddy momentum transport toward the interior. The widening could, however, be an artifact of the eddy parameterization [*Bentsen et al.*, 2013; *Eden et al.*, 2009; *Eden and Greatbatch*, 2008], which increases horizontal diffusivity when the buoyancy frequency increases as happens with increasing runoff and stronger stratification.

Interestingly, although the AW layer circulation strengthens inside the Arctic Ocean, the net exchange through the gateways generally weakens as seen in section 3.3. From the mass conservation point of view, a stronger boundary current does not require larger AW inflow if there is a reorganization of the circulation. In the 2.0 runoff experiment, we see such a reorganization, with the AW inflow continuing as a boundary current around the Arctic Ocean instead of recirculating within the Eurasian Basin as in the control simulation (Figure 8 and supporting information Figure S3). Qualitatively, the circulation response to increasing river runoff resembles the response to positive AO forcing, with a weaker Beaufort Gyre and a stronger boundary current [*Karcher et al.*, 2012].

3.3. Volume and Heat Exhanges Between Arctic Ocean and Surrounding Basins

The volume exchange through the Arctic gateways generally weakens as the runoff increases. This is true for the net volume transport in the Bering Strait, CAA, and BSO (Figure 13a). There is an increase in net volume transport in the Fram Strait reaching 0.5 Sv (approximately 40%) in the highest runoff case.

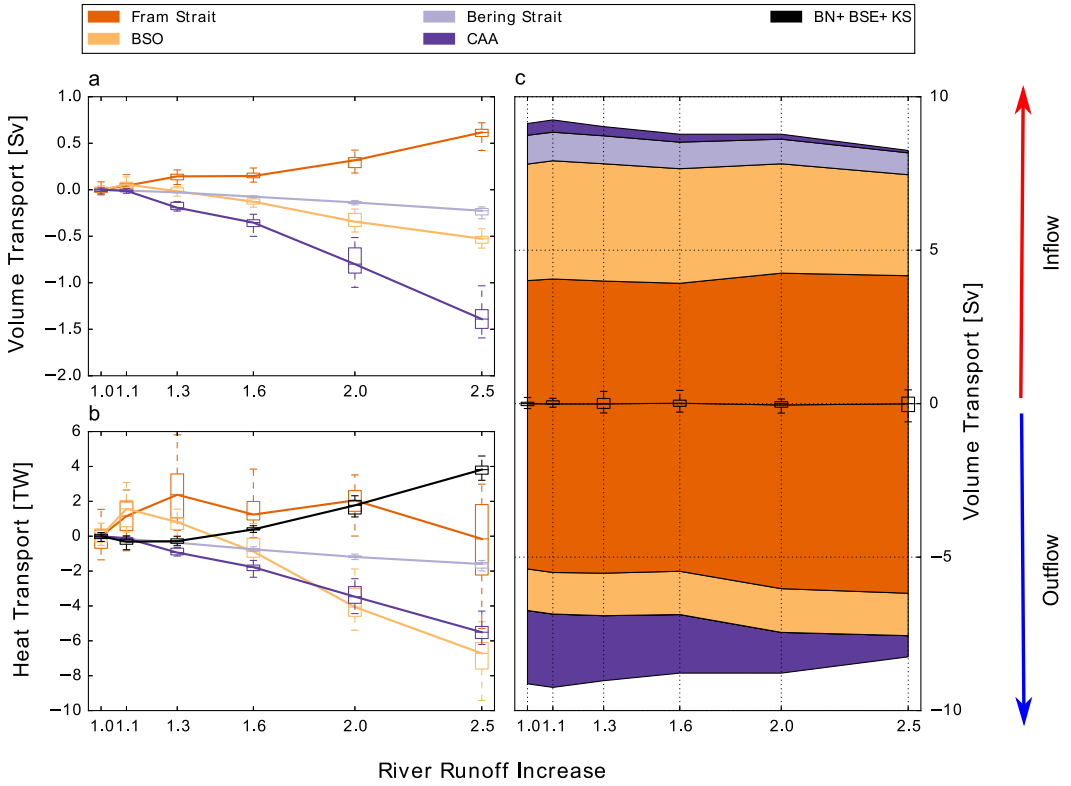

Figure 13. Transport through the Arctic gateways as a function of runoff shown as anomalies relative to the control simulation: (a) net volume transport, (b) net heat transport calculated relative to 0°C, and (c) volume transport components (negative values indicate outflow and positive values indicate inflow to the Arctic Ocean). Whisker-and-box symbols show the extreme and interquartile ranges during the 20 year analysis period, and the solid line connects the medians. The mean volume and heat transport values for the control simulation are given in Table 1. The BN+BSE+KS component is the transport through the northern and eastern end of the Barents Sea. The volume transport is not shown for this section as it matches the volume transport in the BSO; the mean net heat transport (±standard deviation) in the control simulation is −16.02±0.16 TW.

The general weakening of the volume exchanges can be understood in terms of how increasing runoff alters SSH and pressure gradients across the gateways [*McGeehan and Maslowski*, 2012]. With more runoff, the surface freshens and SSH increases inside the Arctic Ocean (Figure 14), thus weakening the pressure gradient that drives the inflow through the Bering Strait. In addition, freshwater accumulates in Baffin Bay, thus weakening the pressure gradient that drives outflow through the CAA. At the same time, changes in the sea surface gradients orient the transpolar drift toward Fram Strait rather than CAA (see section 3.2). As a result, the net volume transports weaken through both the Bering Strait and CAA by 25% and 50%, respectively, in the highest runoff case compared to the control simulation (Figure 13a). The decrease in outflow through the CAA is about 1 Sv larger than the decrease in inflow through the Bering Strait, but the net exchange is balanced by the surface outflow through Fram Strait (Figure 13c).

The inflows through the Fram Strait and Barents Sea are closely coupled because they are both branches of the AW inflow, which divides just upstream of the BSO. The sum of the inflows remains close to constant with increasing runoff (Figure 13c) which is to be expected as there is no large change in the AW inflow (North Atlantic Drift) through the Nordic Seas (Figure 12).

The changes in the net heat transports through the gateways generally follow the changes in volume transports. The heat transport decreases in the Bering Strait, CAA, and BSO with the decreasing volume transport (Figure 13b). Heat transport through the Fram Strait stays close to constant despite an increase in volume transport, because the negative heat transport anomaly due to the colder inflow is compensated by a stronger cold outflow, which is a positive heat transport when referenced to 0°C. More locally, the heat transport through the BSO decreases, but in the northern and eastern exits, it increases due to reduced surface cooling (not shown) and reduced volume transport through the Barents Sea. The overall ocean heat transport to the Arctic Ocean decreases from 97 ± 1.0 to 83 ± 4.5 TW over the 1.0–2.5 runoff experiments.

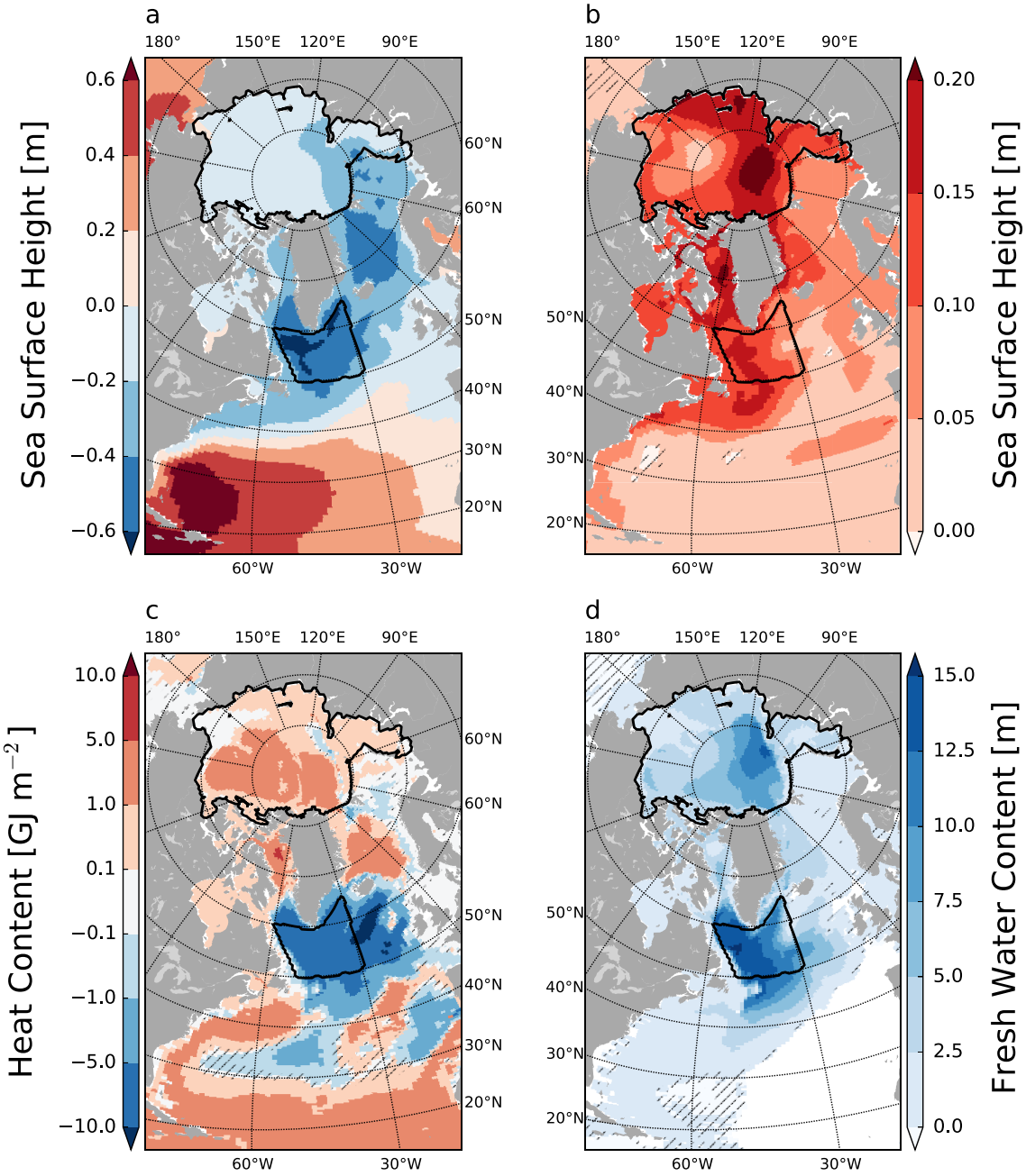

Figure 14. (a) Sea surface height in the control simulation and anomalies in the (b) 2.0 runoff experiment of sea surface height, (c) vertically integrated heat content, and (d) vertically integrated freshwater content. Freshwater content is calculated relative to a salinity of 34.8. Hatching indicates values that are not significantly different from the control simulation at the 95% confidence level. The solid black line indicates the regions in the Arctic and subpolar gyre area which were used to calculate the heat budgets in Figure 16.

3.4. Regional Response Outside the Arctic Ocean Due to Increased Runoff

At large scales in the North Atlantic, the anomalies in freshwater content (Figure 14d) compare well with the (absolute) anomalies in the barotropic stream function (Figure 12a) because the two are coupled via the SSH: changes in freshwater content alter ocean density and SSH gradients, which in turn affect the barotropic circulation. In the Nordic Seas, the increased outflow from Fram Strait generally freshens the basin, especially around the rims, which enhances local SSH gradients (Figure 14b). This strengthens the

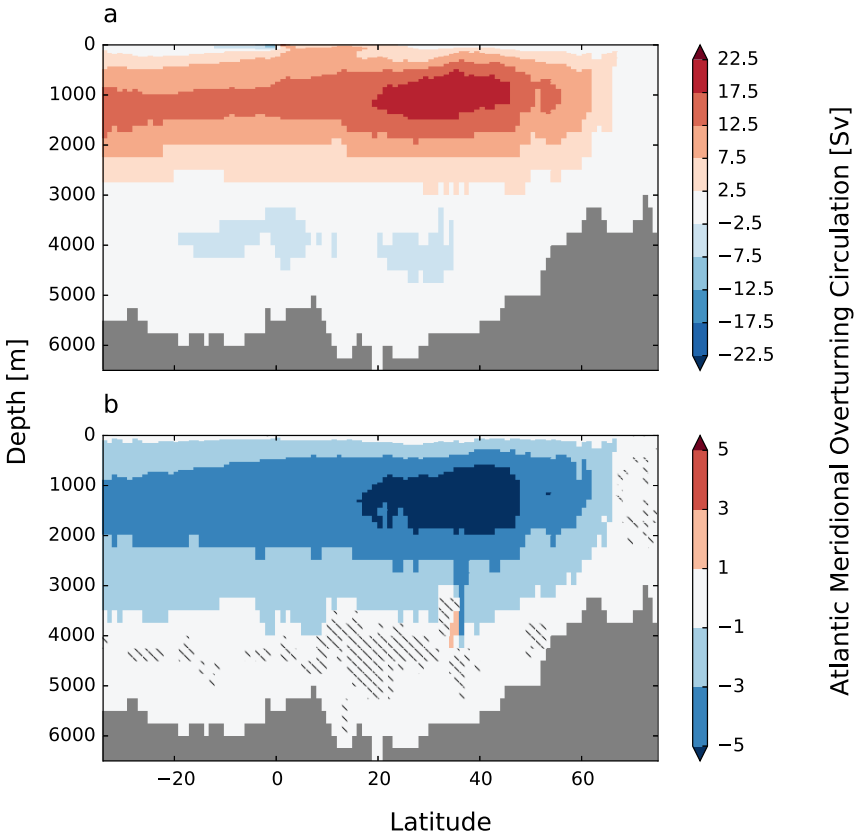

Figure 15. (a) Atlantic Meriodional Overturning Circulation (AMOC) in the control simulation and (b) AMOC anomaly in the 2.0 runoff experiment. AMOC is the stream function calculated in the Atlantic Basin in depth coordinates. Hatching indicates values that are not significantly different from the control simulation at the 95% confidence level.

barotropic circulation and intensifies the East Greenland Current in particular (Figure 12). Further south, the subpolar gyre region freshens as more freshwater is brought in from the Arctic Ocean, and less saline Atlantic Water is brought in from the south. A fresher surface layer leads to lighter convective water masses and weakens the gradients of isopycnal surfaces and SSH between the subpolar gyre and subtropical North Atlantic, leading to flatter isopycnals and a weaker barotropic circulation.

As the water masses produced by convection become increasingly fresher and lighter, they weaken the deep western boundary current and the AMOC. In the 2.0 Arctic runoff experiment, there is a 8 Sv (36%) reduction in the AMOC (Figure 15) by the end of the simulation with a continued trend of approximately 1.5 Sv/decade during the 20 year analysis period. Convection continues in the Labrador Sea throughout the simulation.

Finally, we note that while the large-scale warming in the Arctic Ocean is a result of reduced ocean-to-atmosphere heat loss due to stronger stratification, the subpolar latitudes cool due to reduced heat transport convergence. Within the Arctic, ocean heat transport convergence (HCONV) is relatively stable as a function of runoff (Figure 16a), yet the heat content tendency (dH/dt) and heat content anomaly (ΔH) indicate consistent warming with more runoff. This can only be possible with a reduction in surface heat fluxes (HSFC). Because the atmospheric forcing is fixed, the change in surface heat flux must be due to oceanic changes, namely stronger stratification. In the subpolar gyre region, there is a decrease in ocean heat transport convergence (weaker inflow of warm water from the south) that drives a cooling of the ocean and a decrease in surface heat flux that is a response to reduced temperature difference between the atmosphere and the (cooler) ocean (Figure 16b). In terms of the heat budget changes, the western Nordic Seas are similar to the Arctic Ocean, while the eastern Nordic Seas are similar to the subpolar gyre region (not shown). The heat budget in Figure 16 also reveals that the ocean heat content has not equilibrated as the heat content tendency is nonzero during the analysis period.

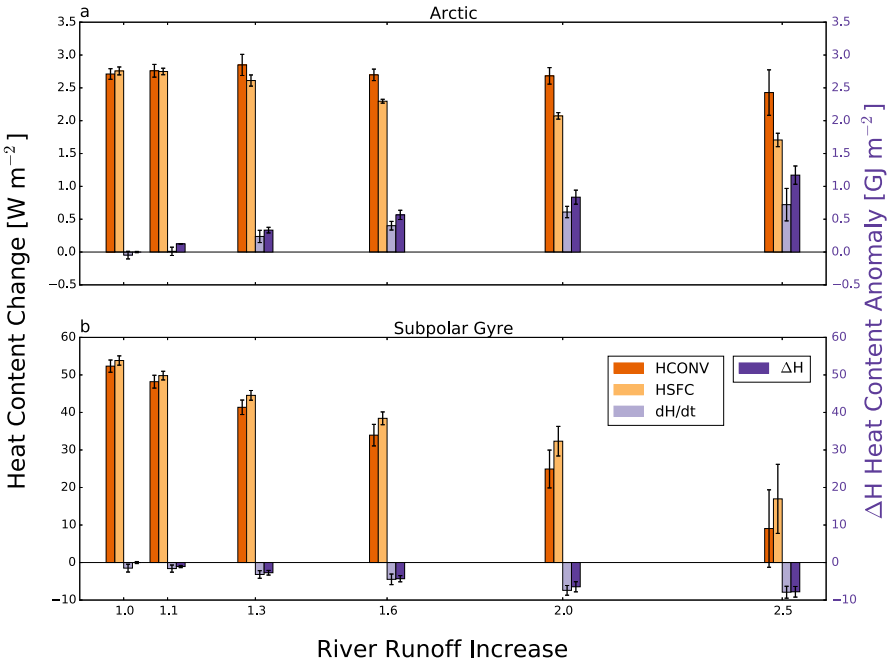

Figure 16. Annual mean heat budget in the (a) Arctic and (b) subpolar gyre region. HCONV (W m^{-2}) is the depth-integrated ocean heat transport convergence, HSFC (W m^{-2}) is the net surface heat flux (positive when ocean is losing heat), dH/dt (W m^{-2}) is the local change in heat content, and ΔH (GJ m^{-2}) is the heat content anomaly relative to the control simulation. The black bars show the standard deviation. Note the different scales on *y* axis in the two plots. See Figure 14 for the boundaries of the Arctic and subpolar gyre region.

4. Discussion

4.1. Local Arctic Response

Within the Arctic, the control simulation and the response to increasing runoff appear reasonable when compared to observations in terms of net exchanges through the Arctic gateways (Table 1) and circulation patterns within the Arctic Ocean (Figure 12 and supporting information Figure S3). The simulated response to increasing Arctic runoff is consistent with accepted theoretical ideas: changes in transports are linked to changes in freshwater content and SSH gradients, and can be explained by barotropic arguments (section 3.3). The changes in heat content can be explained by changes in stratification and ocean heat transport (section 3.4, Figure 16).

The cold halocline is not well represented in the control simulation's basin-wide vertical profiles (Figure 6), but results indicate that some of the related processes are acting correctly. The coldest halocline temperatures in the central Arctic are off the Barents Sea and the Siberian shelves (Figures 10c and 10d), consistent with the local winter convection and flow of cold, dense shelf waters toward the interior Arctic Ocean, as postulated by *Rudels et al*. [1996] and *Steele and Boyd* [1998]. The model is likely producing overly dense shelf waters and mixing them too efficiently with the AW layer, but the fact that the shelf waters are formed in the correct regions and subsequently follow realistic pathways toward the interior gives some confidence that the response to freshwater forcing is qualitatively correct.

The recent observations of warmer AW layer temperatures [*Seidov et al*., 2014] have been linked to warmer AW inflow at Fram Strait [*Beszczynska-Möller et al*., 2012] as well as further south in the Nordic Seas [*Seidov et al*., 2014; *Yashayaev and Seidov*, 2015], rather than to stronger stratification as simulated in our experiments. The warmer inflow is connected to the atmospheric and oceanic conditions in the northern North Atlantic, specifically, the state of the North Atlantic Oscillation and Atlantic Multidecadal Oscillation [*Seidov et al*., 2014; *Yashayaev and Seidov*, 2015]. There could be a role for stronger local stratification in warming the AW layer inside the Arctic Ocean in the future, as discussed by *Polyakov et al*. [2011], although there is not yet any observational support for this. Our simulations suggest that an intensifying warm anomaly inside the Arctic Ocean would be an indication of the local stratification suppressing the vertical heat fluxes.

The strengthening of the AW boundary current with stronger stratification is consistent with previous idealized studies. *Lique et al*. [2015] found that a wider boundary current with a larger transport can be produced by reduced surface stress. *Spall* [2013] suggested that the boundary current is mainly driven by the salinity (density) contrast between the AW and surface layer. In our experiments, increasing runoff enhances the vertical salinity gradients (as in *Spall* [2013]), weakens the Beaufort Gyre (equivalent to reduction in the surface stress in *Lique et al*. [2015]), and produces larger transport in a wider baroclinic boundary current. Recent observations also indicate that the boundary current strength is increasingly controlled by the density gradient-driven baroclinic flow when moving from the Fram Strait toward the interior of the Arctic Ocean [*Pnyushkov et al*., 2015].

4.2. Regional Response Within the Surrounding Oceans

Contrary to the traditional estuarine circulation theory [*Stigebrandt*, 1981], the total exchange between the Arctic and surrounding basins goes down as the runoff increases (Figure 13c). As described in section 3.3, the increased inflow in the Fram Strait results from a reorganization of the Atlantic inflow in the Barents Sea and Fram Strait branches (the total inflow in the two branches remains close to constant over the range of runoff perturbations tested). Due to recirculation in the Fram Strait, the inflow amount is sensitive to the exact location of the cross section over which it is measured, but the response to increasing runoff is similar independent of the location.

While we see no evidence of an estuarine response in our experiments, it could be masked by changes in the overall circulation pattern. In fact, in the smallest runoff case (1.1 runoff experiment), when the circulation changes are also smallest, the model simulates a slight increase in total exchange (Figure 13c), consistent with estuarine circulation theory.

The decrease in the Barents Sea throughflow is explained by freshwater accumulation in the Eurasian Basin (Figure 14). This freshwater accumulation increases the SSH in the Eurasian Basin, which decreases the barotropic pressure gradient over the Barents Sea. This is consistent with the postulated ocean feedback [*Smedsrud et al*., 2013] where rising sea level to the north would decrease AW inflow in the BSO.

The changes in the inflows and outflows have some important consequences for the freshwater accumulation in the subpolar gyre. Earlier observational and high-resolution model studies have shown that mixing from the West Greenland Current (source from Fram Strait via the East Greenland Current) toward the central Labrador sea is much larger than from the Labrador Current (source from CAA) [*Myers*, 2005; *Schmidt and Send*, 2007; *Kawasaki and Hasumi*, 2014]. This implies that a freshwater perturbation flowing out from the Arctic mainly via the Fram Strait (as in our simulations) has a larger impact on the Labrador Sea convection sites, subpolar gyre circulation, and the AMOC, than a freshwater perturbation flowing out via the CAA [see also *Condron and Winsor*, 2012, Figure 2].

The AMOC weakens with increasing runoff despite ongoing convection both in the Labrador and Greenland Seas. Reduction in the AMOC is a well-documented result in North Atlantic hosing experiments [*Manabe and Stouffer*, 1995; *Stouffer et al*., 2006; *Stocker et al*., 2007; *Mignot et al*., 2007; *Roche et al*., 2010] as well as Arctic freshwater perturbations [*Peltier et al*., 2006; *Rennermalm et al*., 2006, 2007]. However, in many of these hosing experiments, the AMOC reduction is associated with a complete shutdown of convection in the North Atlantic, which is not the case in our simulations.

4.3. Limitations of the Study

Our model setup has clear biases in the Arctic. There are large discrepancies in the simulated salinities and AW layer temperature compared with observations (Figures 5 and 6), although we do not expect an exact match because of our idealized atmospheric forcing. However, the simulated large-scale response to increased runoff is consistent over a range of runoff perturbations, providing some confidence in the results despite the biases in the mean state. The mechanisms we identify are similar to those in a number of previous studies using other model systems [*Lique et al*., 2015; *Spall*, 2013], though the details are likely to be model dependent.

A clear limitation of our study is the model resolution (1° horizontal resolution), which is too coarse to properly represent narrow currents and requires subgrid-scale phenomena (such as eddies) to be parameterized. This adds uncertainties to our estimate of runoff sensitivity. For example, the model simulates a broad Arctic boundary current rather than a narrow, bottom-trapped feature, meaning that the gradients are quite

different, and hence their response to increasing runoff could also be quite different. The model also simulates a broader East Greenland Current (EGC) than is observed. This could result in too much freshwater mixing to the interior Nordic Seas and Labrador Sea from the EGC, with implications for convection and water mass transformation. The large grid size also affects the freshwater pathways inside the Arctic, changing the simulated regional response. For example, the model does not resolve coastal currents, which can be important for the freshwater transports [*Janout et al*., 2015; *Whitefield et al*., 2015]. However, we think that while these features are important at regional scales, the simulated basin-wide response is qualitatively robust at multidecadal time scales.

Another consideration is that our atmospheric forcing does not include interannual variability. We chose to force the model with an idealized climatological atmosphere because our aim was to understand the time-averaged ocean and sea ice response to increasing Arctic river runoff. This climatology is close to neutral in terms of the Arctic Oscillation (AO), the primary pattern of variability in the extratropical Northern Hemisphere. Because the AO affects surface circulation, one might expect different AO conditions to result in different pathways for river runoff and hence, different responses to runoff perturbations. We ran an additional sensitivity experiment with doubled runoff for an extremely positive AO year (1989; not shown) and find similar results as in the 2.0 runoff experiment, suggesting that the response is not qualitatively dependent on the atmospheric state. Finally, we have left out any comparison between the strength of the AO-driven interannual variability and the runoff-driven changes, mainly because there is large uncertainty in terms of future changes in AO variability.

5. Conclusions

We have shown that realistic Arctic freshwater perturbations can cause notable changes both inside and outside the Arctic Ocean. The main Arctic response to increased river runoff is a fresher surface and stronger stratification with a warmer halocline and a warmer Atlantic Water layer. In accordance with earlier idealized studies, we find a strengthening of the cyclonic circulation inside the Arctic Ocean Atlantic Water layer. Freshwater accumulates in the Eurasian Basin and raises sea level locally, leading to reduced inflow to the Arctic Ocean through the Bering Strait and the Barents Sea. Freshwater also accumulates and raises sea level in Baffin Bay, leading to reduced outflow through the Canadian Arctic Archipelago. Overall there is a small decrease in the total exchange between the Arctic Ocean and the surrounding seas with increased runoff, contrary to expectations from estuarine circulation theory.

Outside the Arctic Ocean, the additional freshwater affects water mass transformation in the subpolar gyre region. For a doubling of runoff, the gyre circulation slows down by more than 10 Sv (25%) at its maximum, and the Atlantic Meridional Overturning Circulation slows down by about 8 Sv (36%) by the end of the simulations, with a downward trend of approximately 1.5 Sv/decade. Despite considerable freshwater accumulation in the subpolar gyre, there is ongoing convection in the region.

While our results are robust over a range of runoff perturbations in a coupled sea ice-ocean model, the missing atmospheric feedbacks should be assessed in future studies. In particular, a changing sea ice cover affects pressure and wind patterns through thermodynamic and mechanical coupling, and this in turn could influence the sea ice and ocean circulation. Similarly, the changing albedo could affect the global energy balance and hence atmospheric and oceanic circulation on larger scales. Although the atmospheric feedbacks would likely modulate the strength and timing of the simulated responses, a strong freshwater perturbation could still be expected to force an ocean response similar to that documented in this study.

There is a strong model-based evidence that high-latitude freshwater perturbations affect ocean circulation in the North Atlantic and Arctic, though the details of the response can be model dependent. There is also ample observational and paleo proxy evidence suggesting similar linkages. Our results suggest that the response to high-latitude freshwater perturbations can be very different close to the source regions compared with further south at subpolar latitudes. Future work should aim to understand the differences in the regional response to freshwater perturbations in coupled models and in proxy records. It would be highly valuable, although challenging, to reconstruct magnitudes of the past freshwater forcing events and combine those estimates with high-resolution coupled models.

Acknowledgments
We wish to thank M. Bentsen and I. Bethke for help with the model setup and B. Tremblay, L. Renaud-Desjardins, and E. Lambert for insightful discussions and helpful comments. We would also like to thank C. Lique, one anonymous reviewer, and the Editor for useful comments that helped improve the manuscript. We acknowledge the World Climate Research Programme's Working Group on Coupled Modelling, which is responsible for CMIP, for data, and we thank the climate modeling groups (listed in supporting information Table S1 of this paper) for producing and making available their model output. For CMIP, the U.S. Department of Energy's Program for Climate Model Diagnosis and Intercomparison provides coordinating support and led development of software infrastructure in partnership with the Global Organization for Earth System Science Portals. All the data, model setup, and analysis scripts used in this study are available through the corresponding author by e-mail at aleksi.nummelin@uib.no. M. Ilicak is supported by Ice2Ice project that has received funding from the European Research Council under the European Community's Seventh Framework Programme (FP7/2007-2013)/ERC grant agreement 610055. This work was supported by the Bjerknes Centre projects DYNAWARM and BASIC and the Centre for Climate Dynamics (SKD) at the Bjerknes Centre (C. Li).

References

Alkire, M. B., J. Morison, and R. Andersen (2015), Variability in the meteoric water, sea-ice melt, and Pacific water contributions to the central Arctic Ocean, 2000–2014, *J. Geophys. Res. Oceans*, *120*, 1573–1598, doi:10.1002/2014JC010023.

Bauch, D., J. A. Hölemann, A. Nikulina, C. Wegner, M. A. Janout, L. A. Timokhov, and H. Kassens (2013), Correlation of river water and local sea-ice melting on the Laptev Sea shelf (Siberian Arctic), *J. Geophys. Res. Oceans*, *118*, 550–561, doi:10.1002/jgrc.20076.

Bentsen, M., et al. (2013), The Norwegian Earth System Model, NorESM1-M—Part 1: Description and basic evaluation of the physical climate, *Geosci. Model Dev.*, *6*(3), 687–720, doi:10.5194/gmd-6-687-2013.

Beszczynska-Möller, A., E. Fahrbach, U. Schauer, and E. Hansen (2012), Variability in Atlantic water temperature and transport at the entrance to the Arctic Ocean, 1997–2010, *ICES J. Mar. Sci.*, *69*(5), 852–863, doi:10.1093/icesjms/fss056.

Bleck, R., and L. T. Smith (1990), A wind-driven isopycnic coordinate model of the north and equatorial Atlantic Ocean: 1. Model development and supporting experiments, *J. Geophys. Res.*, *95*(C3), 3273–3285, doi:10.1029/JC095iC03p03273.

Bleck, R., C. Rooth, D. Hu, and L. T. Smith (1992), Salinity-driven thermocline transients in a wind- and thermohaline-forced isopycnic coordinate model of the north Atlantic, *J. Phys. Oceanogr.*, *22*(12), 1486–1505, doi:10.1175/1520-0485(1992)022⟨1486:SDTTIA⟩2.0.CO;2.

Condron, A., and P. Winsor (2012), Meltwater routing and the Younger Dryas, *Proc. Natl. Acad. Sci. U.S.A.*, *109*(49), 19,928–19,933, doi:10.1073/pnas.1207381109.

Deshayes, J., R. Curry, and R. Msadek (2014), CMIP5 model intercomparison of freshwater budget and circulation in the North Atlantic, *J. Clim.*, *27*, 3298–3317, doi:10.1175/JCLI-D-12-00700.1.

Dmitrenko, I. A., et al. (2010), Wind-driven diversion of summer river runoff preconditions the Laptev Sea coastal polynya hydrography: Evidence from summer-to-winter hydrographic records of 2007–2009, *Cont. Shelf Res.*, *30*(15), 1656–1664, doi:10.1016/j.csr.2010.06.012.

Droettboom, M., et al. (2015), matplotlib: v1.4.3, doi:10.5281/zenodo.15423.

Eden, C., and R. J. Greatbatch (2008), Towards a mesoscale eddy closure, *Ocean Modell.*, *20*(3), 223–239, doi:10.1016/j.ocemod.2007.09.002.

Eden, C., M. Jochum, and G. Danabasoglu (2009), Effects of different closures for thickness diffusivity, *Ocean Modell.*, *26*(1-2), 47–59, doi:10.1016/j.ocemod.2008.08.004.

Fichot, C. G., K. Kaiser, S. B. Hooker, R. M. W. Amon, M. Babin, S. Bélanger, S. A. Walker, and R. Benner (2013), Pan-Arctic distributions of continental runoff in the Arctic Ocean., *Sci. Rep.*, *3*, 1053, doi:10.1038/srep01053.

Gent, P. R., et al. (2011), The community climate system model version 4, *J. Clim.*, *24*(19), 4973–4991, doi:10.1175/2011JCLI4083.1.

Gerdes, R., W. Hurlin, and S. M. Griffies (2006), Sensitivity of a global ocean model to increased run-off from Greenland, *Ocean Modell.*, *12*(3-4), 416–435, doi:10.1016/j.ocemod.2005.08.003.

Holland, M. M., D. A. Bailey, B. P. Briegleb, B. Light, and E. Hunke (2012), Improved sea ice shortwave radiation physics in CCSM4: The impact of melt ponds and aerosols on Arctic sea ice, *J. Clim.*, *25*(5), 1413–1430, doi:10.1175/JCLI-D-11-00078.1.

Hunter, J. D. (2007), Matplotlib: A 2d graphics environment, *Comput. Sci. Eng.*, *9*(3), 90–95, doi:10.1109/MCSE.2007.55.

Janout, M. A., et al. (2015), Kara Sea freshwater transport through Vilkitsky Strait: Variability, forcing, and further pathways toward the western Arctic Ocean fromamodel and observations Markus, *J. Geophys. Res. Oceans*, *120*, 2331–2349, doi:10.1002/2014JC010632.

Jones, E. P. (2001), Circulation in the Arctic Ocean, *Polar Res.*, *20*(2), 139–146, doi:10.1111/j.1751-8369.2001.tb00049.x.

Karcher, M., F. Kauker, R. Gerdes, E. Hunke, and J. Zhang (2007), On the dynamics of Atlantic Water circulation in the Arctic Ocean, *J. Geophys. Res.*, *112*, C04S02, doi:10.1029/2006JC003630.

Karcher, M., J. N. Smith, F. Kauker, R. Gerdes, and W. M. Smethie (2012), Recent changes in Arctic Ocean circulation revealed by iodine-129 observations and modeling, *J. Geophys. Res.*, *11*, C08007, doi:10.1029/2011JC007513.

Kawasaki, T., and H. Hasumi (2014), Effect of freshwater from the West Greenland Current on the winter deep convection in the Labrador Sea, *Ocean Modell.*, *75*, 51–64, doi:10.1016/j.ocemod.2014.01.003.

Komuro, Y. (2014), The impact of surface mixing on the Arctic river water distribution and stratification in a global ice-ocean model, *J. Clim.*, *27*, 4359–4370, doi:10.1175/JCLI-D-13-00090.1.

Large, W. G., and S. G. Yeager (2004), Diurnal to decadal global forcing for ocean and sea–ice models: The data sets and flux climatologies, NCAR/TN-460+STR Technical note, NCAR, doi:10.5065/D6KK98Q6.

Lehner, F., C. C. Raible, D. Hofer, and T. F. Stocker (2012), The freshwater balance of polar regions in transient simulations from 1500 to 2100 AD using a comprehensive coupled climate model, *Clim. Dyn.*, *39*(1-2), 347–363, doi:10.1007/s00382-011-1199-6.

Lique, C., H. L. Johnson, and P. E. Davis (2015), On the interplay between the circulation in the surface and the intermediate layers of the Arctic Ocean, *J. Phys. Oceanogr.*, *45*, 1393–1409, doi:10.1175/JPO-D-14-0183.1.

Locarnini, R. A., et al. (2013), *World Ocean Atlas 2013, vol. 1, Temperature, NOAA Atlas NESDIS 73*, edited by S. Levitus and A. Mishonov, 40 pp. [Available at http://data.nodc.noaa.gov/woa/WOA13/DOC/woa13_vol1.pdf.]

Manabe, S., and R. Stouffer (1995), Simulation of abrupt climate change induced by freshwater input to the North Atlantic Ocean, *Nature*, *378*, 165–167, doi:10.1038/378165a0.

McGeehan, T., and W. Maslowski (2012), Evaluation and control mechanisms of volume and freshwater export through the Canadian Arctic Archipelago in a high-resolution pan-Arctic ice-ocean model, *J. Geophys. Res.*, *117*, C00D14, doi:10.1029/2011JC007261.

Melling, H., et al. (2008), Fresh-water fluxes via Pacific and Arctic outflows across the Canadian Polar Shelf, in *Arctic–Subarctic Ocean Fluxes*, edited by R. R. Dickson, J. Meincke, and P. Rhines, pp. 193–247, Springer, Dordrecht, Netherlands, doi:10.1007/978-1-4020-6774-7_10.

Mignot, J., A. Ganopolski, and A. Levermann (2007), Atlantic subsurface temperatures: Response to a shutdown of the overturning circulation and consequences for its recovery, *J. Clim.*, *20*(19), 4884–4898, doi:10.1175/JCLI4280.1.

Morison, J., R. Kwok, C. Peralta-Ferriz, M. Alkire, I. Rigor, R. Andersen, and M. Steele (2012), Changing Arctic Ocean freshwater pathways, *Nature*, *481*(7379), 66–70, doi:10.1038/nature10705.

Myers, P. G. (2005), Impact of freshwater from the Canadian Arctic Archipelago on Labrador Sea Water formation, *Geophys. Res. Lett.*, *32*, 1–4, doi:10.1029/2004GL022082.

Nghiem, S. V., D. K. Hall, I. Rigor, P. Li, and G. Neumann (2014), Effects of Mackenzie River discharge and bathymetry on sea ice in the Beaufort Sea, *Geophys. Res. Lett.*, *41//*, 873–879, doi:10.1002/2013GL058956.

Nguyen, A. T., D. Menemenlis, and R. Kwok (2009), Improved modeling of the Arctic halocline with a subgrid-scale brine rejection parameterization, *J. Geophys. Res.*, *114*, C11014, doi:10.1029/2008JC005121.

Nilsson, J., and G. Walin (2010), Salinity-dominated thermohaline circulation in sill basins: Can two stable equilibria exist?, *Tellus, Ser. A*, *62*(2), 123–133, doi:10.1111/j.1600-0870.2009.00428.x.

Nummelin, A., C. Li, and L. H. Smedsrud (2015), Response of Arctic Ocean stratification to changing river runoff in a column model, *J. Geophys. Res. Oceans*, *120*, 2655–2675, doi:10.1002/2014JC010571.

Overeem, I., and J. P. M. Syvitski (2010), Shifting discharge peaks in Arctic Rivers, 1977–2007, *Geogr. Ann., Ser. A*, *92*(2), 285–296, doi:10.1111/j.1468-0459.2010.00395.x.
Peltier, W. R., G. Vettoretti, and M. Stastna (2006), Atlantic meridional overturning and climate response to Arctic Ocean freshening, *Geophys. Res. Lett.*, *33*, L06713, doi:10.1029/2005GL025251.
Pemberton, P., J. Nilsson, M. Hieronymus, and H. M. Meier (2015), Arctic Ocean water mass transformation in S–T coordinates, *J. Phys. Oceanogr.*, *45*(4), 1025–1050, doi:10.1175/JPO-D-14-0197.1.
Peterson, B. J., R. M. Holmes, J. W. McClelland, C. J. Vörösmarty, R. B. Lammers, A. I. Shiklomanov, I. A. Shiklomanov, and S. Rahmstorf (2002), Increasing river discharge to the Arctic Ocean., *Science*, *298*(5601), 2171–2173, doi:10.1126/science.1077445.
Pnyushkov, A. V., I. V. Polyakov, V. V. Ivanov, Y. Aksenov, A. C. Coward, M. Janout, and B. Rabe (2015), Structure and variability of the boundary current in the Eurasian Basin of the Arctic Ocean, *Deep Sea Res., Part I*, *101*, 80–97, doi:10.1016/j.dsr.2015.03.001.
Polyakov, I. V., et al. (2011), Fate of early 2000s Arctic warm water pulse, *Bull. Am. Meteorol. Soc.*, *92*(5), 561–566, doi:10.1175/2010BAMS2921.1.
Rawlins, M. A., et al. (2010), Analysis of the Arctic system for freshwater cycle intensification: Observations and expectations, *J. Clim.*, *23*(21), 5715–5737, doi:10.1175/2010JCLI3421.1.
Rennermalm, A. K., E. F. Wood, S. J. Déry, A. J. Weaver, and M. Eby (2006), Sensitivity of the thermohaline circulation to Arctic Ocean runoff, *Geophys. Res. Lett.*, *33*, L12703, doi:10.1029/2006GL026124.
Rennermalm, A. K., E. F. Wood, A. J. Weaver, M. Eby, and S. J. Déry (2007), Relative sensitivity of the Atlantic meridional overturning circulation to river discharge into Hudson Bay and the Arctic Ocean, *J. Geophys. Res.*, *112*, G04S48, doi:10.1029/2006JG000330.
Rennermalm, A. K., E. F. Wood, and T. J. Troy (2010), Observed changes in pan-Arctic cold-season minimum monthly river discharge, *Clim. Dyn.*, *35*(6), 923–939, doi:10.1007/s00382-009-0730-5.
Roche, D. M., A. P. Wiersma, and H. Renssen (2010), A systematic study of the impact of freshwater pulses with respect to different geographical locations, *Clim. Dyn.*, *34*, 997–1013, doi:10.1007/s00382-009-0578-8.
Rudels, B. (2015), Arctic Ocean circulation, processes and water masses: A description of observations and ideas with focus on the period prior to the International Polar Year 2007–2009, *Prog. Oceanogr.*, *132*, 22–67, doi:10.1016/j.pocean.2013.11.006.
Rudels, B., L. G. Anderson, and E. P. Jones (1996), Formation and evolution of the surface mixed layer and halocline of the Arctic Ocean, *J. Geophys. Res.*, *101*(C4), 8807–8821, doi:10.1029/96JC00143.
Rudels, B., E. P. Jones, U. Schauer, and P. B. Eriksson (2004), Atlantic sources of the Arctic Ocean surface and halocline waters, *Polar Res.*, *23*(2), 181–208, doi:10.1111/j.1751-8369.2004.tb00007.x.
Schauer, U., A. Beszczynska-Möller, W. Walczowski, E. Fahrbach, J. Piechura, and E. Hansen (2008), Variation of measured heat flow through the Fram Strait between 1997 and 2006, in *Arctic–Subarctic Ocean Fluxes*, edited by R. R. Dickson, J. Meincke, and P. Rhines, pp. 65–85, Springer, Dordrecht, Netherlands, doi:10.1007/978-1-4020-6774-7_4.
Schlosser, P., D. Bauch, R. Fairbanks, and G. Bönisch (1994), Arctic river-runoff: Mean residence time on the shelves and in the halocline, *Deep Sea Res., Part I*, *41*(7), 1053–1068, doi:10.1016/0967-0637(94)90018-3.
Schmidt, S., and U. Send (2007), Origin and composition of seasonal Labrador Sea freshwater, *J. Phys. Oceanogr.*, *37*(6), 1445–1454, doi:10.1175/JPO3065.1.
Schmidtko, S., G. C. Johnson, and J. M. Lyman (2013), MIMOC: A global monthly isopycnal upper-ocean climatology with mixed layers, *J. Geophys. Res. Oceans*, *118*, 1658–1672, doi:10.1002/jgrc.20122.
Seidov, D., J. I. Antonov, K. M. Arzayus, O. K. Baranova, M. Biddle, T. P. Boyer, D. R. Johnson, A. V. Mishonov, C. Paver, and M. M. Zweng (2014), Oceanography north of 60 N from World Ocean Database, *Prog. Oceanogr.*, *132*, 153–173, doi:10.1016/j.pocean.2014.02.003.
Smedsrud, L. H., et al. (2013), The role of the Barents Sea in the Arctic climate system, *Rev. Geophys.*, *51*(3), 415–449, doi:10.1002/rog.20017.
Spall, M. A. (2013), On the circulation of Atlantic Water in the Arctic Ocean, *J. Phys. Oceanogr.*, *43*(11), 2352–2371, doi:10.1175/JPO-D-13-079.1.
Steele, M., and T. J. Boyd (1998), Retreat of the cold halocline layer in the Arctic Ocean, *J. Geophys. Res.*, *103*(C5), 10,419–10,435, doi:10.1029/98JC00580.
Steele, M., R. Morley, and W. Ermold (2001), PHC: A global ocean hydrography with a high-quality Arctic Ocean, *J. Clim.*, *14*(9), 2079–2087, doi:10.1175/1520-0442(2001)014⟨2079:PAGOHW⟩2.0.CO;2.
Stigebrandt, A. (1981), A model for the thickness and salinity of the upper layer in the Arctic Ocean and the relationship between the ice thickness and some external parameters, *J. Phys. Oceanogr.*, *11*(10), 1407–1422, doi:10.1175/1520-0485(1981)011⟨1407:AMFTTA⟩2.0.CO;2.
Stocker, T. F., A. Timmermann, M. Renold, and O. Timm (2007), Effects of salt compensation on the climate model response in simulations of large changes of the Atlantic meridional overturning circulation, *J. Clim.*, *20*(24), 5912–5928, doi:10.1175/2007JCLI1662.1.
Stouffer, R., J. Yin, and J. Gregory (2006), Investigating the causes of the response of the thermohaline circulation to past and future climate changes, *J. Clim.*, *19*(8), 1365–1387, doi:10.1175/JCLI3689.1.
Swingedouw, D., C. B. Rodehacke, S. M. Olsen, M. Menray, Y. Gao, U. Mikolajewicz, and J. Mignot (2014), On the reduced sensitivity of the Atlantic overturning to Greenland ice sheet melting in projections: A multi-model assessment, *Clim. Dyn.*, *44*, 3261–3279, doi:10.1007/s00382-014-2270-x.
Whitefield, J., P. Winsor, J. Mcclelland, and D. Menemenlis (2015), A new river discharge and river temperature climatology data set for the pan-Arctic region, *Ocean Modell.*, *88*, 1–15, doi:10.1016/j.ocemod.2014.12.012.
Woodgate, R. A., K. Aagaard, and T. J. Weingartner (2005), Monthly temperature, salinity, and transport variability of the Bering Strait through flow, *Geophys. Res. Lett.*, *32*, L04601, doi:10.1029/2004GL021880.
Yamamoto-Kawai, M., F. A. McLaughlin, E. C. Carmack, S. Nishino, K. Shimada, and N. Kurita (2009), Surface freshening of the Canada Basin, 2003–2007: River runoff versus sea ice meltwater, *J. Geophys. Res.*, *114*, C00A05, doi:10.1029/2008JC005000.
Yashayaev, I., and D. Seidov (2015), The role of the Atlantic Water in multidecadal ocean variability in the Nordic and Barents Seas, *Prog. Oceanogr.*, *132*, 68–127, doi:10.1016/j.pocean.2014.11.009.
Zweng, M. M., et al. (2013), *World Ocean Atlas 2013, vol. 2, Salinity, NOAA Atlas NESDIS 74*, edited by S. Levitus and A. Mishonov, 39 pp. [Available at http://data.nodc.noaa.gov/woa/WOA13/DOC/woa13_vol2.pdf.]

Consequences of Future Increased Arctic Runoff on Arctic Ocean Stratification, Circulation, and Sea Ice Cover

Aleksi Nummelin,[1,2], Mehmet Ilicak[3,2], Camille Li,[1,2] Lars H. Smedsrud,[1,2,4]

Contents of this file

1. Figure S1
2. Figure S2
3. Figure S3
4. Table S1

Introduction This supporting information provides additional comparison between the control simulation and available observational datasets (Figures S1 and S2), and the

[1]Geophysical Institute, University of Bergen, Allégaten 70, 5007 Bergen, Norway

[2]Bjerknes Centre for Climate Research, Bergen, Norway

[3]Uni Research Climate, Allégaten 55, 5007 Bergen, Norway

[4]University Centre in Svalbard (UNIS)

circulation response to increased runoff (Figure S3). It also provides a list of all the names of the modelling centers, models, and the specific ensemble members of the CMIP5 multi–model ensemble that were used to produce Figure 1 (Table S1). The list includes 19 different models and a total of 49 different ensemble members.

Table S1. Details of the CMIP5 multi–model ensemble used to produce Figure 1. Column 1 gives the name of the modelling centers (or groups) that produced the data, column 2 gives the CMIP5 ID of each modelling center, column 3 gives the names of the models run by each modelling center (note that one center might run more than one model), and column 4 gives the names of the ensemble members from each model that we used to produce Figure 1.

References

Locarnini, R. A., A. V. Mishonov, J. I. Antonov, T. P. Boyer, H. E. Garcia, O. K. Baranova, M. M. Zweng, C. R. Paver, J. R. Reagan, D. R. Johnson, M. Hamilton, and D. Seidov (2013), World Ocean Atlas 2013, Volume 1: Temperature., in *NOAA Atlas NESDIS 73*, edited by S. Levitus and A. Mishonov, p. 40.

Schmidtko, S., G. C. Johnson, and J. M. Lyman (2013), MIMOC: A global monthly isopycnal upper-ocean climatology with mixed layers, *Journal of Geophysical Research: Oceans*, *118*(4), 1658–1672, doi:10.1002/jgrc.20122.

Steele, M., R. Morley, and W. Ermold (2001), PHC: A global ocean hydrography with a high-quality Arctic Ocean, *Journal of Climate*, *14*(9), 2079–2087, doi:10.1175/1520-0442(2001)014⟨2079:PAGOHW⟩2.0.CO;2.

Zweng, M. M., J. R. Reagan, J. I. Antonov, R. A. Locarnini, A. V. Mishonov, J. I. Antonov, T. P. Boyer, H. E. Garcia, O. K. Baranova, D. R. Johnson, D. Seidov, and M. M. Biddle (2013), World Ocean Atlas 2013, Volume 2: Salinity., in *NOAA Atlas NESDIS 74*, edited by S. Levitus and A. Mishonov, p. 39.

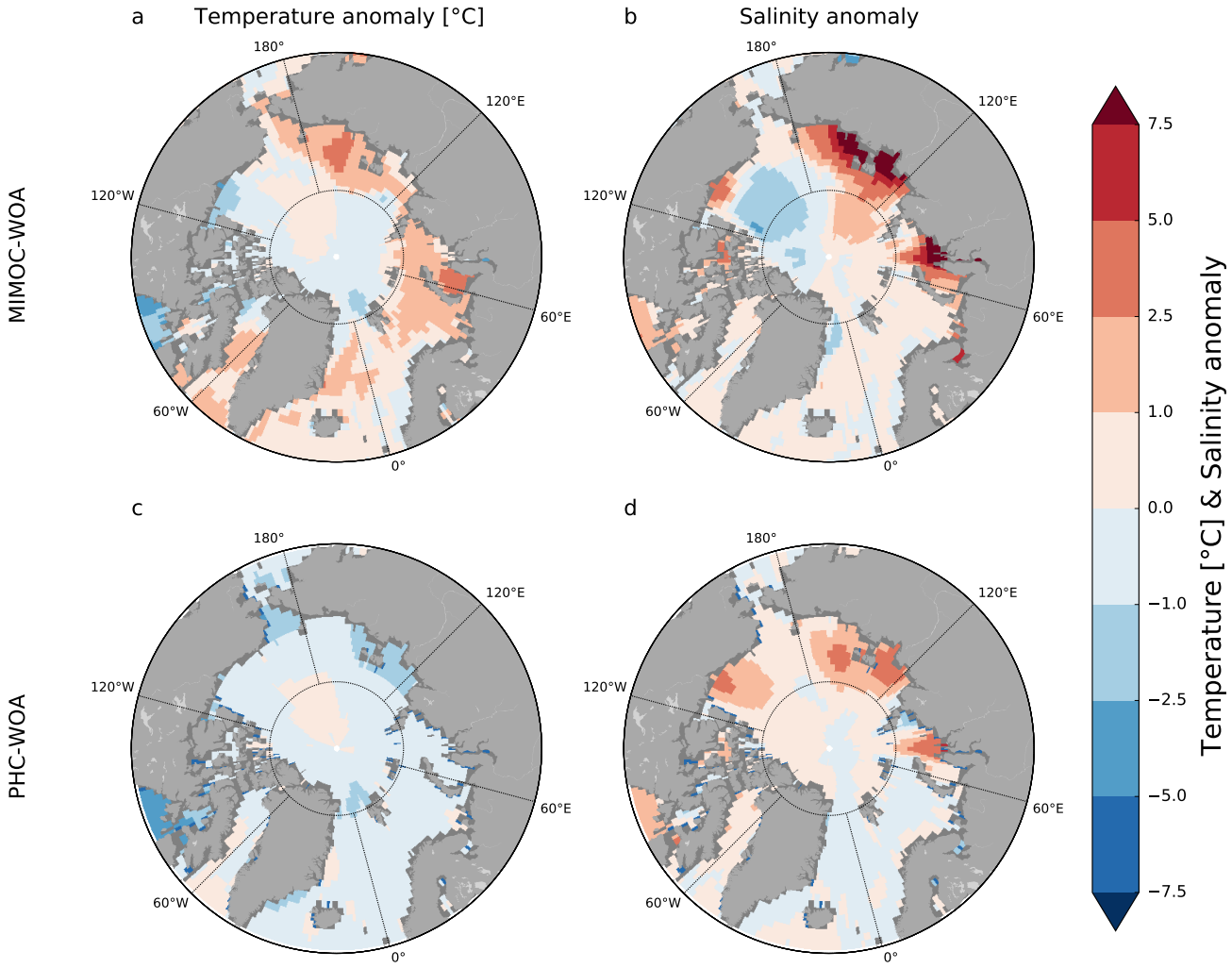

Figure S1. Comparison of the surface temperature and salinity fields between the Monthly Isopycnal & Mixed-layer Ocean Climatology (MIMOC [*Schmidtko et al.*, 2013]) (a-b) and World Ocean Atlas (WOA) 2013 [*Locarnini et al.*, 2013; *Zweng et al.*, 2013], and between the Polar Science Center Hydrographic Climatology (PHC3.0, updated from *Steele et al.* [2001]) (c-d) and WOA. All the panels are limited to 60°N, which is the limit of the PHC3.0 dataset. Note the nonlinear colorbar.

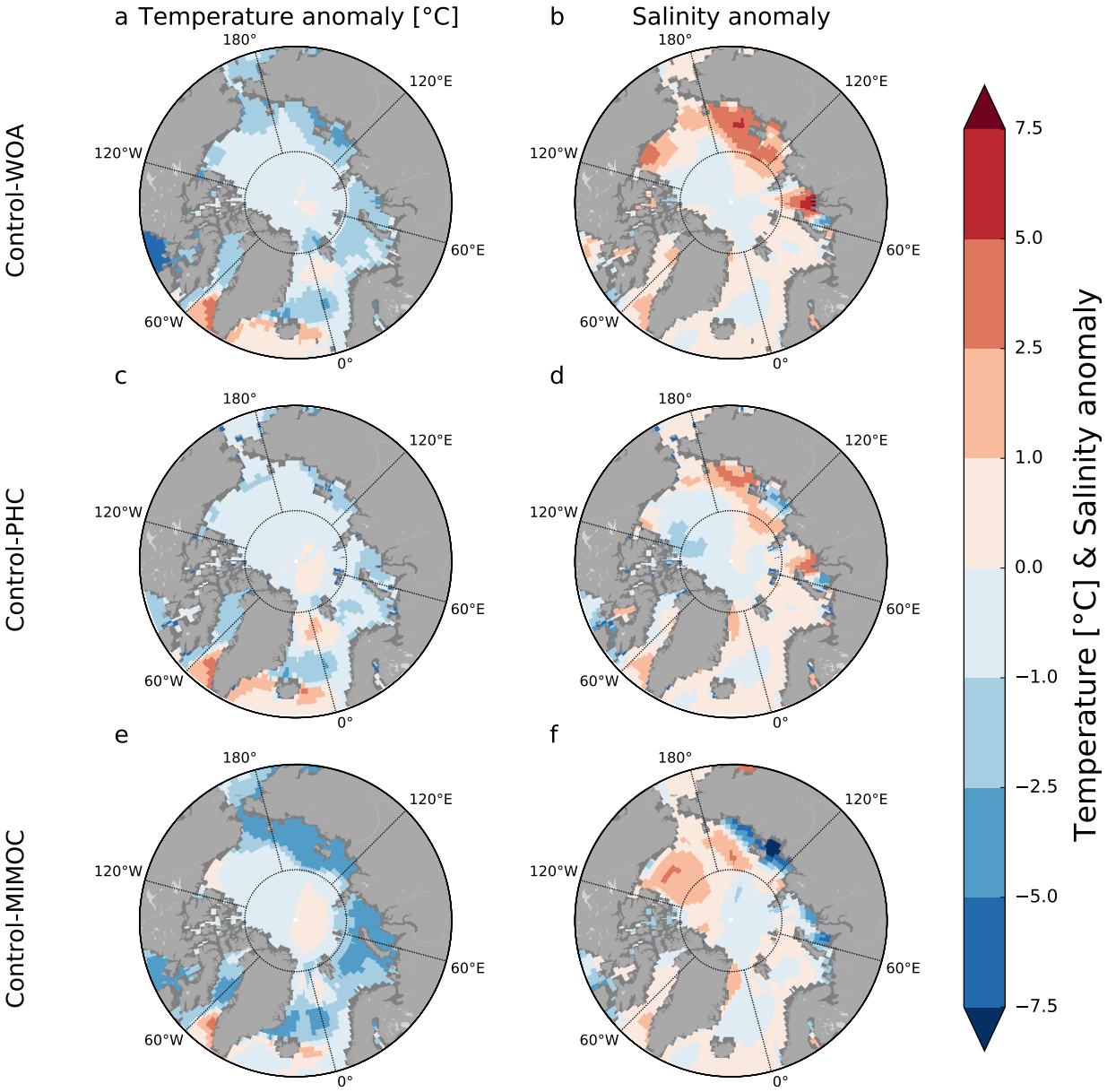

Figure S2. Comparison of the surface temperature and salinity fields between the control simulation (average of the last 20 years of simulation) and the World Ocean Atlas (WOA) 2013 [*Locarnini et al.*, 2013; *Zweng et al.*, 2013] (a-b), the Polar Science Center Hydrographic Climatology (PHC3.0, updated from *Steele et al.* [2001]) (c-d), and the Monthly Isopycnal & Mixed-layer Ocean Climatology (MIMOC [*Schmidtko et al.*, 2013]) (e-f). All the panels are limited to 60°N, which is the limit of the PHC3.0 dataset. Note the nonlinear colorbar.

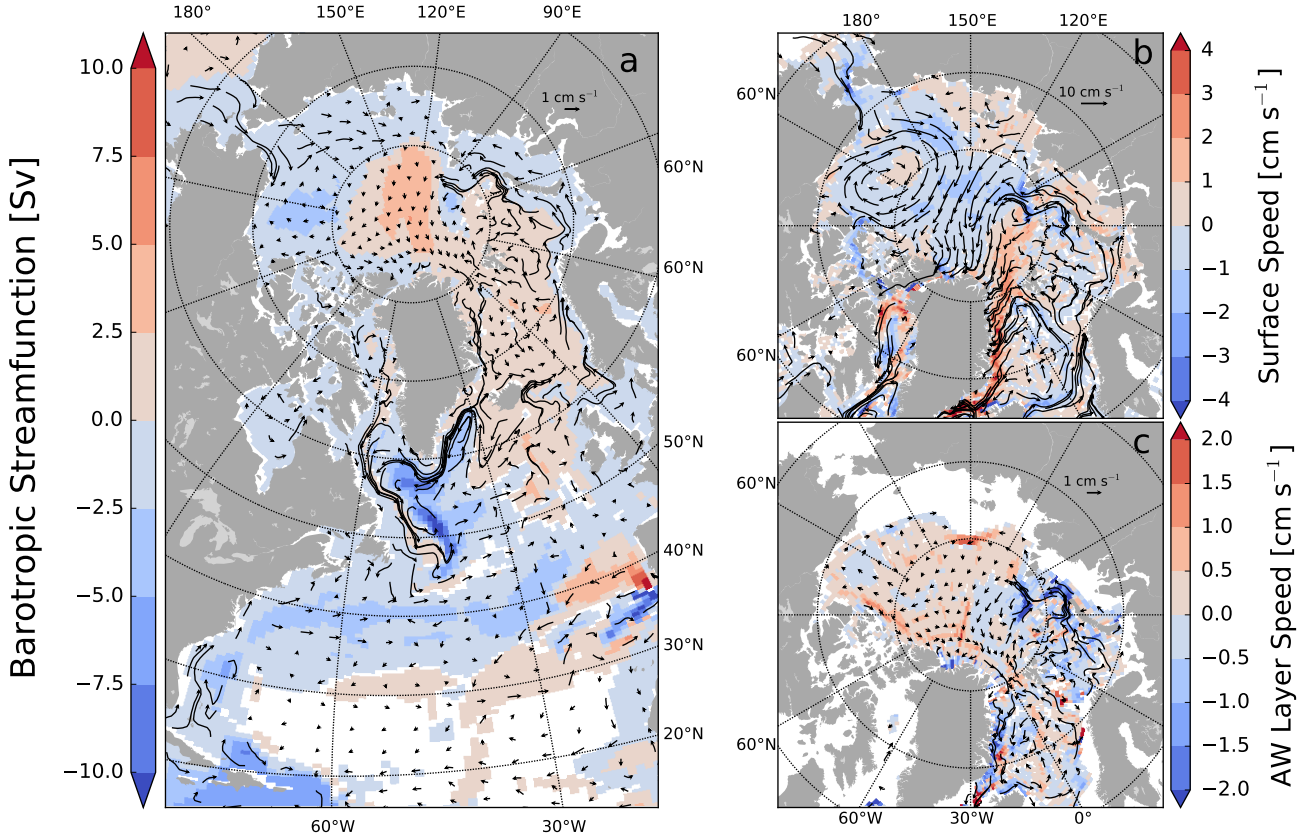

Figure S3. Ocean circulation in the 2.0 runoff experiment (vectors) and anomalies compared to the control simulation (shading): barotropic streamfunction (a), surface current speed in model layers 1–2 (b, approximately 0-50 m depth), and AW layer current speed in model layers 33–45 (c, approximately 100-1000 meters depth). Only anomalies that are significant at the 95% confidence level are plotted.

Modeling Center (or Group)	Institute ID	Model Name	Ensemble Members
Commonwealth Scientific and Industrial Research Organization (CSIRO) and Bureau of Meteorology (BOM), Australia	CSIRO-BOM	ACCESS1.0	r1i1p1
		ACCESS1.3	r1i1p1
National Center for Atmospheric Research	NCAR	CCSM4	r1i1p1, r2i1p1, r3i1p1, r4i1p1, r5i1p1, r6i1p1, r7i1p1
Centre National de Recherches Météorologiques / Centre Européen de Recherche et Formation Avancée en Calcul Scientifique	CNRM-CERFACS	CNRM-CM5	r1i1p1, r2i1p1, r4i1p1, r6i1p1, r10i1p1
Commonwealth Scientific and Industrial Research Organization in collaboration with Queensland Climate Change Centre of Excellence	CSIRO-QCCCE	CSIRO-Mk3.6.0	r1i1p1, r2i1p1, r3i1p1, r4i1p1, r5i1p1, r6i1p1, r7i1p1, r8i1p1, r9i1p1, r10i1p1
NOAA Geophysical Fluid Dynamics Laboratory	NOAA GFDL	GFDL-ESM2G	r1i1p1
		GFDL-ESM2M	r1i1p1
Met Office Hadley Centre (additional HadGEM2-ES realizations contributed by Instituto Nacional de Pesquisas Espaciais)	MOHC (additional realizations by INPE)	HadGEM2-CC	r1i1p1, r2i1p1
		HadGEM2-ES	r1i1p1, r2i1p1, r3i1p1, r4i1p1
Institut Pierre-Simon Laplace	IPSL	IPSL-CM5A-LR	r1i1p1, r2i1p1, r3i1p1, r4i1p1
		IPSL-CM5A-MR	r1i1p1
		IPSL-CM5B-LR	r1i1p1
Japan Agency for Marine-Earth Science and Technology, Atmosphere and Ocean Research Institute (The University of Tokyo), and National Institute for Environmental Studies	MIROC	MIROC-ESM	r1i1p1
		MIROC-ESM-CHEM	r1i1p1
Atmosphere and Ocean Research Institute (The University of Tokyo), National Institute for Environmental Studies, and Japan Agency for Marine-Earth Science and Technology	MIROC	MIROC5	r1i1p1, r2i1p1, r3i1p1, r4i1p1, r5i1p1
Meteorological Research Institute	MRI	MRI-CGCM3	r1i1p1
		MRI-ESM1	r1i1p1
Norwegian Climate Centre	NCC	NorESM1-M	r1i1p1
		NorESM1-ME	r1i1p1

5.2.1 Watermass transformation constraints on the Arctic Ocean circulation

In paper II we briefly discussed the Arctic Ocean circulation from the perspective of watermass transformations. Here we extend this perspective and focus on the estuarine and overturning circulation theories. The following results show that the estuarine circulation strengthens as freshwater is added to the Arctic Ocean, but that the strong decrease in the overturning circulation dominates the decrease in the overall mass exchange between the Arctic Ocean and the surrounding oceans. Our speculations in paper II were qualitatively similar. However, they were not entirely conclusive as we did not separate the contributions from the estuarine and overturning type of watermass transformations. Here, we first describe the estuarine and overturning circulation theories, and then use this framework to analyze the model simulations discussed in detail in paper II.

Definitions

Estuarine circulation is often used to describe circulation within systems where a relatively fresh basin, an estuary, is connected to an ambient, more saline, basin. Steady state salt balance requires that the oceanic salt transport between the two basins compensates for the freshwater input to the estuary. In this framework a strengthening freshwater forcing moves the system towards a new equilibrium with a larger salt transport between the basins. The larger salt transport is achieved as the freshwater forcing freshens the estuary which strengthens the salinity contrast between the two basins and drives a larger geostrophic outflow and a compensating inflow to the estuary.

The overturning circulation is often called a negative estuary. In this framework we consider an overturning basin with a net density gain (buoyancy loss) connected to an ambient ocean basin with a lighter watermass. The watermass flowing into the overturning basin loses buoyancy and flows out of the basin as a denser watermass. In the North Atlantic-Arctic sector the buoyancy loss is due to the heat loss and brine input from the sea ice formation, whereas the net freshwater gain acts against the overturning transformation (but for the estuarine transformation). The outflowing dense waters are colder, but generally fresher than the relatively warm and saline inflow. Since the overturning circulation is driven by the density differences between the inflowing and outflowing watermasses, an increase in the freshwater flux to the overturning basin would be expected to reduce the density of the overturning watermass and therefore hinder the volume exchanges between the two basins.

Here we define the cross-isopycnal watermass transformations that facilitate the two type of circulations as follows: in the estuarine transformation a high density watermass mixes with/entrains into a low density watermass and forms a new relative low density watermass; in the overturning transformation a low density watermass transforms to a high density watermass due to net buoyancy loss.

In the past these two transformations and the connected circulations have been used in idealized frameworks either separately (e.g. *Stigebrandt* (1981); *Stommel* (1961)) or as a combined system (e.g. *Eldevik and Nilsen* (2013); *Lambert et al.* (2016); *Rudels* (2010)). Here we expand the use of the combined system to understand the ocean circulation response to a freshwater perturbation seen in paper II and Arctic volume exchanges under greenhouse warming.

Arctic Ocean circulation response to a freshwater forcing in the light of watermass transformations

We begin by comparing the inflows and outflows at the gateways surrounding the Arctic Ocean in density space. We define the separation point between the estuarine and overturning components as the densest point at which the integrals of the inflow and the outflow (in regard to density) cross each other (Figure 5.1a). Note that it is fully possible that some of the lightest inflow turns into the densest outflow, but assuming that on average the transformations are those with the least work, then the inflow transforms preferentially to its nearest neighboring density classes. Such an analysis reveals that most of the inflow goes through the overturning type of transformation (7 Sv, 74%) in the control case, while roughly 24 % (2.2 Sv) goes through the estuarine type of transformation (Figure 5.1a). We speculate that this division between the transformation supports the least work framework: most of the inflow to the Arctic is already relatively dense and close to the densities of the overturning watermasses, whereas the inflowing watermasses are much denser than the outflowing light watermasses, which means that the estuarine transformation requires more work than the overturning transformation.

Diagnosing the overturning and estuarine components for all of the freshwater perturbation cases of paper II reveals that the estuarine circulation increases with the river runoff up until doubling of the runoff (Figure 5.1b). Such a response is in line with the estuarine circulation theory. The reduced estuarine response at the largest freshwater perturbation could be an indication of a mixing limited regime (*Nilsson and Walin*, 2010). In such a case the increase in stratification due to freshwater forcing limits the entrainment of inflowing watermass to the surface layer and the estuarine transformation weakens.

Despite the increase in the estuarine circulation, the net response is dominated by the decreasing overturning circulation. The additional freshwater acts against any transformation towards denser classes. Interestingly, the circulation response up to 10% increase in the runoff seems to be an exception. In this regime, both the estuarine and the overturning components increase (Figure 5.1b,d). Additional diagnostics of the heat and salt transports suggest active salt-advection feedback (*Lambert et al.*, 2016; *Stommel*, 1961); the increasing estuarine transport drags in more salty water to the Arctic Ocean, which in turn strengthens the overturning type of transformation.

The transient response of the two components to increasing freshwater forcing (Figure 5.1c,d) shows comparable features in all cases. Initially, both the estuarine and the overturning branches strengthen until the decrease in overturning takes over. It is also clear that the largest freshwater perturbation (2.5 times the control river runoff) has not stabilized by the end of the simulations.

As such the results show that the watermass transformation framework can be a useful tool to understand the ocean circulation response to a freshwater forcing. However we note that the division to the estuarine and the overturning type of transformations is prone to be somewhat artificial and diagnostic at best, at least in an Eulerian framework. We simply do not know which type of paths the individual water parcels take in the density space and we can only infer these changes at watermass level.

Arctic Ocean circulation under greenhouse warming in the light of watermass transformations

Here we widen our perspective from the idealized freshwater forcing simulations of paper II to more complete climate model simulations. We analyze exchanges between Arctic and the surrounding oceans using the Coupled Model Intercomparison Project (CMIP5, (*Collins et al.*, 2013)) representative concentration pathway 8.5 (RCP8.5) simulations of the Norwegian Earth System model (NorESM1-M). Note that the ocean and sea-ice components of this fully coupled model are identical to the ones used in paper II. We assume 10 years response timescale for the two transformations and filter the results with a 10 year low-pass filter. Recall that precipitation (*Haine et al.*, 2015) and river runoff (Figure 1, paper II), both increase over time reaching roughly 30% increase by year 2100 in the RCP8.5 simulations.

The results of the RCP8.5 simulations are comparable to the freshwater perturbation simulations. The estuarine transformation acts to increase the volume exchanges between the Arctic Ocean and the surrounding oceans, while weakening overturning transformation dominates the overall trend (Figure 5.2). The magnitudes of the responses are somewhat larger in RCP8.5 simulation than in the idealized simulations of paper II. This is partly expected because the RCP8.5 includes also increasing precipitation which was not included in paper II. It might also be that other factors, such as changing surface temperature and wind forcing, contribute to the changing volume transports which then manifest themselves in our watermass transformation framework (recall that all of the transport is assigned with either estuarine or overturning transformation).

Summary and perspectives

Our additional analysis has shown that we can understand exchanges between Arctic and the surrounding basins in the framework of freshwater affected isopycnal transformations. However, we are still left with a gap in our understanding, namely a theory that combines the understanding of isopycnal transformations with our understanding of the sea surface height driven net exchanges. To illustrate this point we plot the net volume transport anomaly between the Arctic Ocean and the surrounding oceans (North Atlantic and North Pacific) against the respective sea surface height anomalies in Figure 5.3. As expected from a purely barotropic flow, the net inflow through Bering Strait decreases linearly as a function of the decreasing sea surface height difference across the Bering Strait. In contrast, the sea surface height anomaly between the Arctic and the Atlantic seems to relate to a square root of the net volume transport, which is expected in a two layer system where the lower layer is at rest (*Rudels*, 2010). Relating the sea level gradient driven changes in the net exchanges to the isopycnal framework that explains the changes in the inflow and outflow, should be the next step towards a more complete understanding of the Arctic Ocean circulation.

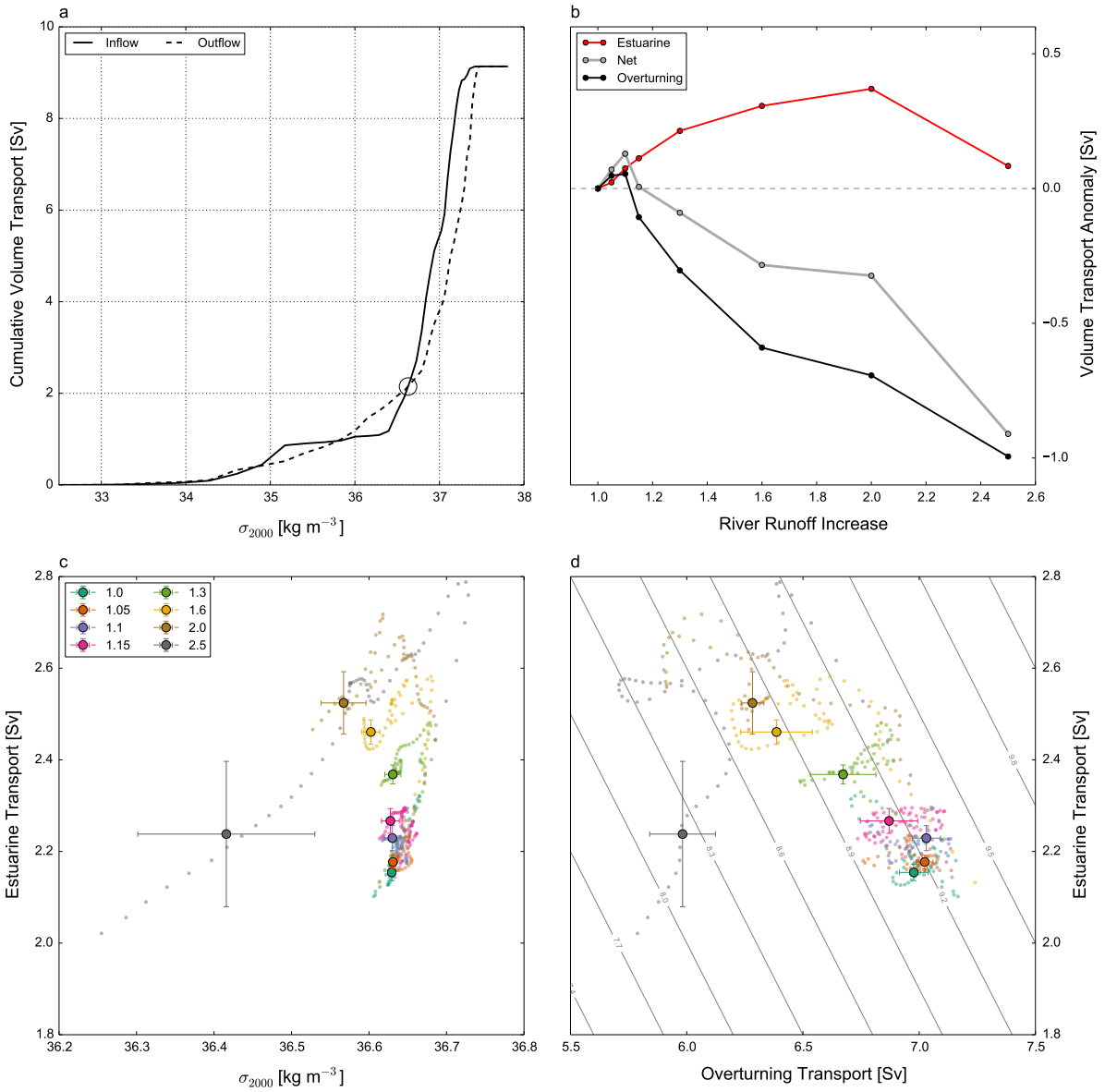

Figure 5.1: Separation of the inflow and outflow into estuarine and overturning components. (a) Cumulative volume transports flowing in and out of the Arctic Ocean in the last 20 years of the control simulation, with a circle illustrating the point which we consider to be separating the estuarine and the overturning components, (b) the estuarine and the overturning components averaged over the last 20 years of the simulations against increase in the river runoff, (c) movement of the separation point in density space for the whole simulation period (60 years), and (d) the estuarine and overturning components for the whole simulation period. In (c) and (d) the results are first filtered with a 10 year low pass filter before separating the individual components, and the large circles show the mean, with the errorbars illustrating standard deviation, over the last 20 years of the simulations.

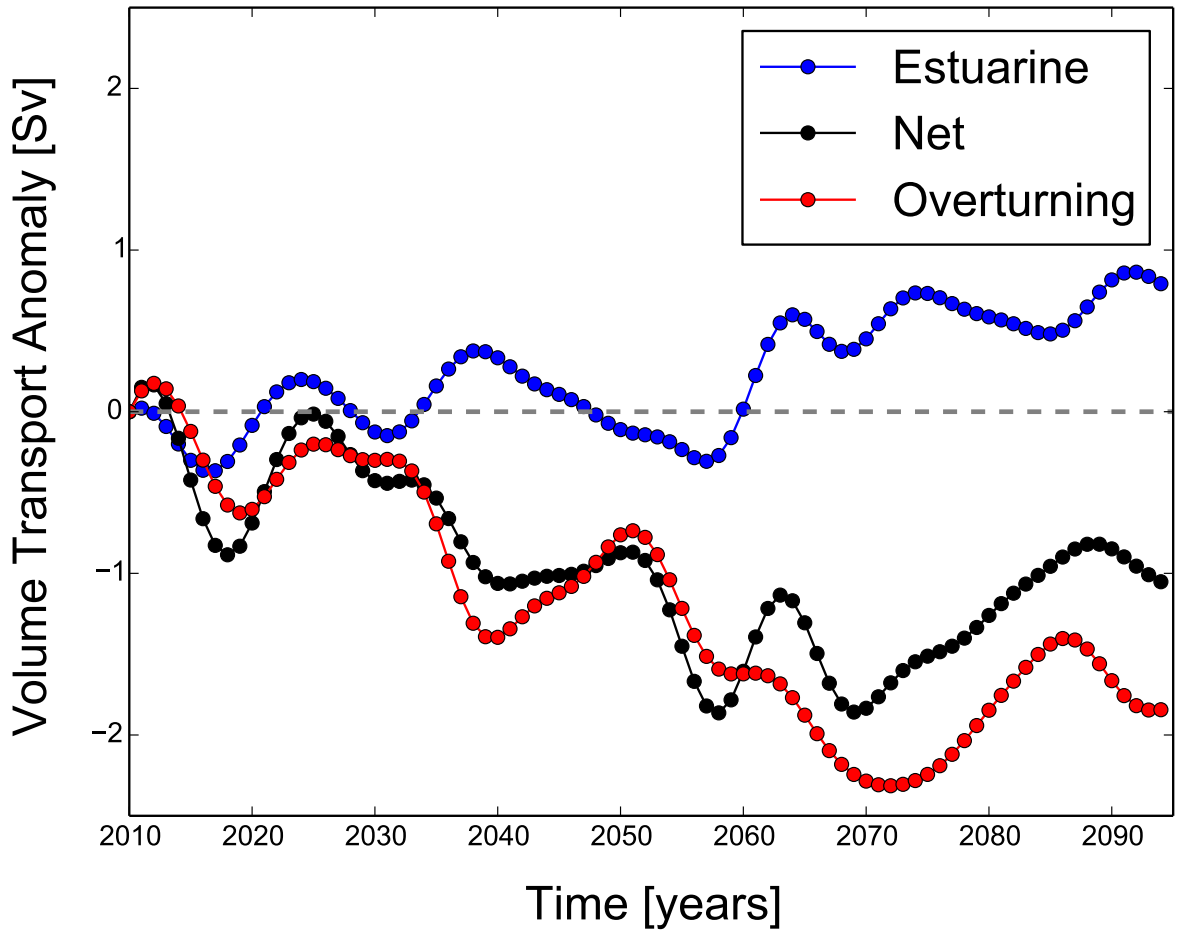

Figure 5.2: Separation of the inflow and outflow into estuarine and overturning components in NorESM1-M RCP8.5 simulation. The results are first filtered with a 10 year low pass filter before the separation into the individual components.

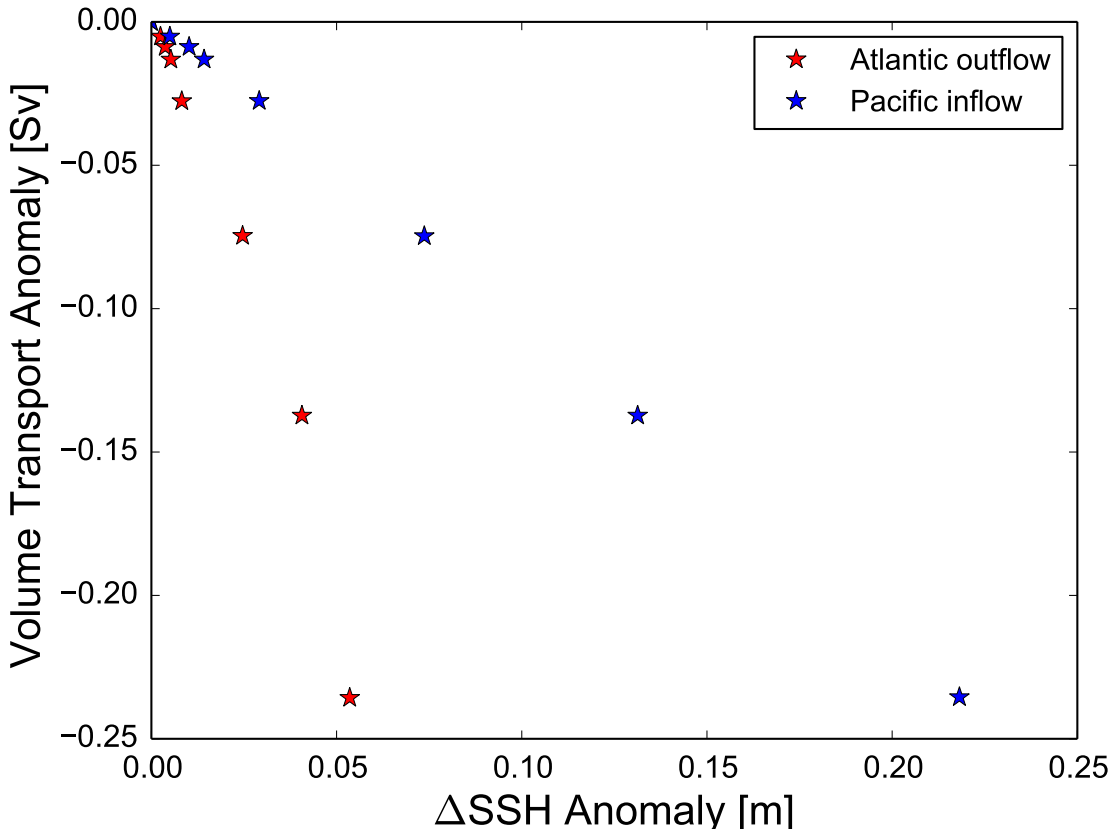

Figure 5.3: Net volume transport between the Pacific Ocean and the Arctic Ocean (inflow to the Arctic), and the Arctic Ocean and the Atlantic Ocean (outflow to the North Atlantic) against the respective sea surface heigth differences in the river runoff perturbation simulations of paper II. All variables are shown as anomalies from the control simulation. ΔSSH is calculated as an average difference of the mean sea surface height in the Arctic and in the North Atlantic and North Pacific (north of 40°N) basins for the last 20 years of the simulations. Note that ΔSSH is defined so that a positive value implies a decreasing gradient.

Bibliography

Alexeev, V. A., P. L. Langen, and J. R. Bates (2005), Polar amplification of surface warming on an aquaplanet in "ghost forcing" experiments without sea ice feedbacks, *Climate Dynamics*, *24*(7-8), 655–666, doi:10.1007/s00382-005-0018-3. 1.1.2

Armour, K. C., I. Eisenman, E. Blanchard-Wrigglesworth, K. E. McCusker, and C. M. Bitz (2011), The reversibility of sea ice loss in a state-of-the-art climate model, *Geophysical Research Letters*, *38*(16), L16,705, doi:10.1029/2011GL048739. 1.1.2

Årthun, M., T. Eldevik, L. H. Smedsrud, Skagseth, and R. B. Ingvaldsen (2012), Quantifying the Influence of Atlantic Heat on Barents Sea Ice Variability and Retreat, *Journal of Climate*, *25*(13), 4736–4743, doi:10.1175/JCLI-D-11-00466.1. 1.1.1

Bathiany, S., D. Notz, T. Mauritsen, G. Raedel, and V. Brovkin (2016), On the potential for abrupt Arctic winter sea-ice loss, *Journal of Climate*, pp. JCLI–D–15–0466.1, doi:10.1175/JCLI-D-15-0466.1. 1.1.2

Belkin, I. M. (2004), Propagation of the "Great Salinity Anomaly" of the 1990s around the northern North Atlantic, *Geophysical Research Letters*, *31*(8), 4–7, doi:10.1029/2003GL019334. 1.3.1

Belkin, I. M., S. Levitus, J. Antonov, and S. A. Malmberg (1998), 'Great Salinity Anomalies' in the North Atlantic, *Progress in Oceanography*, *41*(1), 1–68, doi:10.1016/S0079-6611(98)00015-9. 1.3.1

Bentsen, M., I. Bethke, J. B. Debernard, T. Iversen, A. Kirkevåg, Ø. Seland, H. Drange, C. Roelandt, I. a. Seierstad, C. Hoose, and J. E. Kristjánsson (2013), The Norwegian Earth System Model, NorESM1-M – Part 1: Description and basic evaluation of the physical climate, *Geoscientific Model Development*, *6*(3), 687–720, doi:10.5194/gmd-6-687-2013. 2

Bitz, C., P. Gent, R. Woodgate, M. Holland, and R. Lindsay (2006), The Influence of Sea Ice on Ocean Heat Uptake in Response to Increasing CO2, *Journal of Climate*, *19*, 2437. 2

Bitz, C. M., M. M. Holland, E. C. Hunke, and R. Moritz (2005), Maintenance of the sea-ice edge, *Journal of Climate*, *18*(15), 2903–2921. 1.1.1

Björk, G. (1989), A one-dimensional time-dependent model for the vertical stratification of the upper Arctic Ocean, *Journal of Physical Oceanography*, *19*, 52–67, doi:10.1175/1520-0485(1989)019<0052:AODTDM>2.0.CO;2. 2

Björk, G. (1992), On the response of the equilibrium thickness distribution of sea ice to ice export, mechanical deformation, and thermal forcing with application to the Arctic Ocean, *Journal of Geophysical Research*, *97*(C7), 11,287–11,298, doi: 10.1029/92JC00814. 2

Björk, G. (1997), The relation between ice deformation, oceanic heat flux, and the ice thickness distribution in the Arctic Ocean, *Journal of Geophysical Research*, *102*(C8), 18,681–18,698, doi:10.1029/97JC00789. 2

Björk, G., L. G. Anderson, M. Jakobsson, D. Antony, B. Eriksson, P. B. Eriksson, B. Hell, S. Hjalmarsson, T. Janzen, S. Jutterström, J. Linders, L. Löwemark, C. Marcussen, K. Anders Olsson, B. Rudels, E. Sellén, and M. Sølvsten (2010), Flow of Canadian basin deep water in the Western Eurasian Basin of the Arctic Ocean, *Deep-Sea Research Part I: Oceanographic Research Papers*, *57*(4), 577–586, doi: 10.1016/j.dsr.2010.01.006. 1.2

Böning, C. W., E. Behrens, A. Biastoch, K. Getzlaff, and J. L. Bamber (2016), Emerging impact of Greenland meltwater on deepwater formation in the North Atlantic Ocean, *Nature Geoscience*, *9*(June), 523–528, doi:10.1038/NGEO2740. 1.1.3

Born, A., and A. Levermann (2010), The 8.2 ka event: Abrupt transition of the subpolar gyre toward a modern North Atlantic circulation, *Geochemistry, Geophysics, Geosystems*, *11*(6), 1–8, doi:10.1029/2009GC003024. 1.3

Born, A., and T. F. Stocker (2013), Two Stable Equilibria of the Atlantic Subpolar Gyre, *Journal of Physical Oceanography*, *44*, 246–264, doi:10.1175/JPO-D-13-073.1. 1.3

Born, A., T. F. Stocker, C. C. Raible, and A. Levermann (2013), Is the Atlantic subpolar gyre bistable in comprehensive coupled climate models?, *Climate Dynamics*, *40*(11-12), 2993–3007, doi:10.1007/s00382-012-1525-7. 1.3

Buckley, M. W., and J. Marshall (2015), Observations , inferences , and mechanisms of the Atlantic Meridional Overturning Circulation : A review, *Reviews of Geophysics*, doi:10.1002/2015RG000493. 4

Burkholder, K. C., and M. S. Lozier (2011), Subtropical to subpolar pathways in the North Atlantic: Deductions from Lagrangian trajectories, *Journal of Geophysical Research: Oceans*, *116*(7), 1–12, doi:10.1029/2010JC006697. 4

Burkholder, K. C., and M. S. Lozier (2014), Tracing the pathways of the upper limb of the North Atlantic Meridional Overturning Circulation, *Geophysical Research Letters*, pp. 4254–4260, doi:10.1002/2014GL060226. 4

Carmack, E., I. Polyakov, L. Padman, I. Fer, E. Hunke, J. Hutchings, J. Jackson, D. Kelley, R. Kwok, C. Layton, H. Melling, D. Perovich, O. Persson, B. Ruddick, M.-L. Timmermans, J. Toole, T. Ross, S. Vavrus, and P. Winsor (2015), Toward Quantifying the Increasing Role of Oceanic Heat in Sea Ice Loss in the New Arctic, *Bulletin of the American Meteorological Society*, *96*(12), 2079–2105, doi: 10.1175/BAMS-D-13-00177.1. 1.2.1

Chelton, D. B., R. a. DeSzoeke, M. G. Schlax, K. El Naggar, and N. Siwertz (1998), Geographical Variability of the First Baroclinic Rossby Radius of Deformation, *Journal of Physical Oceanography*, *28*(3), 433–460, doi:10.1175/1520-0485(1998)028<0433:GVOTFB>2.0.CO;2. 1.2.2

Collins, M., R. Knutti, J. Arblaster, J.-L. Dufresne, T. Fichefet, P. Friedlingstein, X. Gao, W. J. Gutowski, T. Johns, G. Krinner, M. Shongwe, C. Tebaldi, A. J. Weaver, and M. Wehner (2013), Long-term Climate Change: Projections, Commitments and Irreversibility, in *Climate Change 2013: The Physical Science Basis. Contribution of Working Group I to the Fifth Assessment Report of the Intergovernmental Panel on Climate Change*, edited by T. Stocker, D. Qin, G.-K. Plattner, M. Tignor, S. Allen, J. Boschung, A. Nauels, Y. Xia, V. Bex, and P. Midgley, pp. 1029–1136, Cambridge University Press, Cambridge, United Kingdom and New York, NY, USA., doi:10.1017/CBO9781107415324.024. 1.1.3, 2, 5.2.1

Czaja, A., and J. Marshall (2015), Why is there net surface heating over the Antarctic Circumpolar Current?, *Ocean Dynamics*, *65*(5), 751–760, doi:10.1007/s10236-015-0830-1. 1.1.1

Day, J. J., J. C. Hargreaves, J. D. Annan, and A. Abe-Ouchi (2012), Sources of multi-decadal variability in Arctic sea ice extent, *Environmental Research Letters*, *7*(3), 034,011–, doi:10.1088/1748-9326/7/3/034011. 1.2

Deshayes, J., R. Curry, and R. Msadek (2014), CMIP5 Model Intercomparison of Freshwater Budget and Circulation in the North Atlantic, *Journal of Climate*, *1995*, 3298–3317, doi:10.1175/JCLI-D-12-00700.1. 1.3

Dickson, R. R., J. Meincke, S. A. Malmberg, and A. J. Lee (1988), The "great salinity anomaly" in the Northern North Atlantic 1968-1982, *Progress in Oceanography*, *20*(2), 103–151, doi:10.1016/0079-6611(88)90049-3. 1.3.1

Ding, Y., J. A. Carton, G. A. Chepurin, M. Steele, and S. Hakkinen (2016), Seasonal heat and freshwater cycles in the Arctic Ocean in CMIP5 coupled models, *Journal of Geophysical Research : Oceans*, *121*, 1–14, doi:10.1002/2015JC011124. 1.2.1

Donohoe, A., K. C. Armour, A. G. Pendergrass, and D. S. Battisti (2014), Shortwave and longwave radiative contributions to global warming under increasing CO 2, *Proceedings of the National Academy of Sciences*, *111*, 16,700–16,705, doi:10.1073/pnas.1412190111. 1.1.2

Dosser, H. V., and L. Rainville (2015), Dynamics of the Changing Near-Inertial Internal Wave Field in the Arctic Ocean, *Journal of Physical Oceanography*, *46*(2), 395–415, doi:10.1175/JPO-D-15-0056.1. 1.2

Drijfhout, S., S. Bathiany, C. Beaulieu, V. Brovkin, M. Claussen, C. Huntingford, M. Scheffer, G. Sgubin, and D. Swingedouw (2015), Catalogue of abrupt shifts in Intergovernmental Panel on Climate Change climate models, *Proceedings of the National Academy of Sciences*, *112*(43), E5777–E5786, doi:10.1073/pnas.1511451112. 1.1.2

Eisenman, I., and J. S. Wettlaufer (2009), Nonlinear threshold behavior during the loss of Arctic sea ice., *Proceedings of the National Academy of Sciences*, *106*(1), 28–32, doi:10.1073/pnas.0806887106. 1.1.2

Eldevik, T., and J. E. Ø. Nilsen (2013), The Arctic-Atlantic Thermohaline Circulation, *Journal of Climate*, *26*(21), 8698–8705, doi:10.1175/JCLI-D-13-00305.1. 5.2.1

Fer, I. (2009), Weak vertical diffusion allows maintenance of cold halocline in the central Arctic, *Atmospheric and Oceanic Science Letters*, *2*(3), 148–152, doi:10.1080/16742834.2009.11446789. 1.2

Ferrari, R., and C. Wunsch (2009), Ocean Circulation Kinetic Energy: Reservoirs, Sources, and Sinks, *Annual Review of Fluid Mechanics*, *41*(1), 253–282, doi:10.1146/annurev.fluid.40.111406.102139. 1.2.2

Forster, P. M. (2016), Inference of Climate Sensitivity from Analysis of Earth's Energy Budget, *Annual Review of Earth and Planetary Sciences*, *44*(1), doi:10.1146/annurev-earth-060614-105156. 1.1.2

Foukal, N. P., and M. S. Lozier (2016), No inter-gyre pathway for sea-surface temperature anomalies in the North Atlantic., *Nature Communications*, *7*, 11,333, doi:10.1038/ncomms11333. 4

Gallaher, S. G., T. P. Stanton, W. J. Shaw, S. T. Cole, J. M. Toole, J. P. Wilkinson, T. Maksym, and B. Hwang (2016), Evolution of a Canada Basin ice-ocean boundary layer and mixed layer across a developing thermodynamically forced marginal ice zone, *Journal of Geophysical Research: Oceans*, doi:10.1002/2016JC011778. 1.2.1

Gerdes, R., W. Hurlin, and S. M. Griffies (2006), Sensitivity of a global ocean model to increased run-off from Greenland, *Ocean Modelling*, *12*(3-4), 416–435, doi:10.1016/j.ocemod.2005.08.003. 1.3.2

Glessmer, M., T. Eldevik, and K. Våge (2014), Atlantic origin of observed and modelled freshwater anomalies in the Nordic Seas, *Nature Geoscience*, (7), 801–805, doi:10.1038/NGEO2259. 1.3.1

Haine, T. W., B. Curry, R. Gerdes, E. Hansen, M. Karcher, C. Lee, B. Rudels, G. Spreen, L. de Steur, K. D. Stewart, and R. Woodgate (2015), Arctic freshwater export: Status, mechanisms, and prospects, *Global and Planetary Change*, *125*, 13–35, doi:10.1016/j.gloplacha.2014.11.013. 1.2, 1.3.2, 5.2.1

Haine, T. W. N. (2016), Ocean science: Vagaries of Atlantic overturning, *Nature Geoscience*, *9*, 479–480, doi:10.1038/ngeo2748. 1.1.3

Häkkinen, S. (1993), An Arctic source for the great salinity anomaly: A simulation of the Arctic ice-ocean system for 1955–1975, *Journal of Geophysical Research*, *98*(C9), 16,397, doi:10.1029/93JC01504. 1.2, 1.3.1

Hattermann, T., P. E. Isachsen, W. J. Von Appen, J. Albretsen, and A. Sundfjord (2016), Eddy-driven recirculation of Atlantic Water in Fram Strait, *Geophysical Research Letters*, *43*(7), 3406–3414, doi:10.1002/2016GL068323. 1.2.2, 4

Holland, M. M., C. M. Bitz, and B. Tremblay (2006), Future abrupt reductions in the summer Arctic sea ice, *Geophysical Research Letters*, *33*(23), 1–5, doi: 10.1029/2006GL028024. 1.1.2

Ilicak, M., H. Drange, Q. Wang, R. Gerdes, Y. Aksenov, D. A. Bailey, M. Bentsen, A. Biastoch, A. Bozec, C. Böning, C. Cassou, E. Chassignet, A. C. Coward, B. Curry, G. Danabasoglu, S. Danilov, E. Fernandez, P. G. Fogli, Y. Fujii, S. M. Griffies, D. Iovino, A. Jahn, T. Jung, W. G. Large, C. Lee, C. Lique, J. Lu, S. Masina, A. J. G. Nurser, B. Rabe, C. Roth, D. Salas y Mélia, B. L. Samuels, P. Spence, H. Tsujino, S. Valcke, A. Voldoire, X. Wang, and S. G. Yeager (2016), An assessment of the Arctic Ocean in a suite of interannual CORE-II simulations. Part III: Hydrography and fluxes, *Ocean Modelling*, *99*, 86–109, doi:10.1016/j.ocemod.2015.12.009. 1.2.2

Jackson, J. M., S. E. Allen, F. a. McLaughlin, R. a. Woodgate, and E. C. Carmack (2011), Changes to the near-surface waters in the Canada Basin, Arctic Ocean from 1993–2009: A basin in transition, *Journal of Geophysical Research*, *116*(C10), C10,008, doi:10.1029/2011JC007069. 1.2.1

Jackson, L. C., K. A. Peterson, C. D. Roberts, and R. A. Wood (2016), Recent slowing of Atlantic overturning circulation as a recovery from earlier strengthening, *Nature Geoscience*, *9*, 518–522, doi:10.1038/ngeo2715. 1.1.3

Kawasaki, T., and H. Hasumi (2014), Effect of freshwater from the West Greenland Current on the winter deep convection in the Labrador Sea, *Ocean Modelling*, *75*, 51–64, doi:10.1016/j.ocemod.2014.01.003. 4

Koenigk, T., and L. Brodeau (2013), Ocean heat transport into the Arctic in the twentieth and twenty-first century in EC-Earth, *Climate Dynamics*, *42*(11), 3101–3120, doi:10.1007/s00382-013-1821-x. 2

Laîné, A., M. Yoshimori, and A. Abe-Ouchi (2016), Surface Arctic Amplification Factors in CMIP5 Models: Land and Oceanic Surfaces, Seasonality., *Journal of Climate*, *29*, 3297–3316, doi:10.1175/JCLI-D-15-0497.1. 1.1.2

Lambert, E., T. Eldevik, and P. Haugan (2016), Thermohaline circulation with 3 stable regimes of flow, *in revision for Tellus A*. 1.3, 2, 5.2.1, 5.2.1

Langen, P. L., and V. A. Alexeev (2007), Polar amplification as a preferred response in an idealized aquaplanet GCM, *Climate Dynamics*, *29*(2-3), 305–317, doi:10.1007/s00382-006-0221-x. 1.1.2

Levitus, S., J. I. Antonov, T. P. Boyer, O. K. Baranova, H. E. Garcia, R. A. Locarnini, A. V. Mishonov, J. R. Reagan, D. Seidov, E. S. Yarosh, and M. M. Zweng (2012), World ocean heat content and thermosteric sea level change (0-2000m), 1955-2010, *Geophysical Research Letters*, *39*(10), 1–5, doi:10.1029/2012GL051106. 1.1.3

Lique, C., H. L. Johnson, and P. E. Davis (2015), On the interplay between the circulation in the surface and the intermediate layers of the Arctic Ocean, *Journal of Physical Oceanography*, *45*(5), 1393–1409, doi:10.1175/JPO-D-14-0183.1. 1.2.2

Little, C. M., C. G. Piecuch, and A. H. Chaudhuri (2016), Quantifying Greenland freshwater flux underestimates in climate models, *Geophyscial Research Letters*, pp. 5370–5377, doi:10.1002/2016GL068878. 1.3.2

Lozier, M. S. (2012), Overturning in the North Atlantic, *Annual Review of Marine Science*, *4*(1), 291–315, doi:10.1146/annurev-marine-120710-100740. 4

Ma, X., P. Chang, R. Saravanan, R. Montuoro, J.-S. Hsieh, D. Wu, X. Lin, L. Wu, and Z. Jing (2015), Distant Influence of Kuroshio Eddies on North Pacific Weather Patterns?, *Scientific Reports*, *5*, 17,785, doi:10.1038/srep17785. 4

Mahlstein, I., and R. Knutti (2011), Ocean Heat Transport as a Cause for Model Uncertainty in Projected Arctic Warming, *Journal of Climate*, *24*(5), 1451–1460, doi:10.1175/2010JCLI3713.1. 1.1.2

Margold, M., K. N. Jansson, A. P. Stroeven, and J. D. Jansen (2011), Glacial Lake Vitim, a 3000-km^3 outburst flood from Siberia to the Arctic Ocean, *Quaternary Research*, *76*(3), 393–396, doi:10.1016/j.yqres.2011.06.009. 1.3.2

Marshall, J., K. C. Armour, J. R. Scott, Y. Kostov, U. Hausmann, D. Ferreira, T. G. Shepherd, and C. M. Bitz (2014), The ocean's role in polar climate change: asymmetric Arctic and Antarctic responses to greenhouse gas and ozone forcing., *Philosophical transactions. Series A, Mathematical, physical, and engineering sciences*, *372*, 20130,040, doi:10.1098/rsta.2013.0040. 2

Marshall, J., J. R. Scott, K. C. Armour, J. M. Campin, M. Kelley, and A. Romanou (2015), The ocean's role in the transient response of climate to abrupt greenhouse gas forcing, *Climate Dynamics*, *44*(7-8), 2287–2299, doi:10.1007/s00382-014-2308-0. 2

McCarthy, G. D., I. D. Haigh, J. J. Hirschi, J. P. Grist, and D. A. Smeed (2015), Ocean impact on decadal Atlantic climate variability revealed by sea-level observations, *Nature*, *521*(7553), 508—-510, doi:10.1038/nature14491. 1.1.3

Mignot, J., a. Ganopolski, and a. Levermann (2007), Atlantic subsurface temperatures: Response to a shutdown of the overturning circulation and consequences for its recovery, *Journal of Climate*, *20*(19), 4884–4898, doi:10.1175/JCLI4280.1. 1.3, 1.3.2

Miles, M. W., D. V. Divine, T. Furevik, E. Jansen, M. Moros, and A. E. J. Ogilvie (2014), A signal of persistent atlantic multidecadal variability in arctic sea ice, *Geophysical Research Letters*, *41*(2), 463–469, doi:10.1002/2013GL058084. 1.2

Miller, G. H., R. B. Alley, J. Brigham-Grette, J. J. Fitzpatrick, L. Polyak, M. C. Serreze, and J. W. C. White (2010), Arctic amplification: Can the past constrain the future?, *Quaternary Science Reviews*, *29*(15-16), 1779–1790, doi:10.1016/j.quascirev.2010.02.008. 1.1.2

Morison, J., R. Kwok, C. Peralta-Ferriz, M. Alkire, I. Rigor, R. Andersen, and M. Steele (2012), Changing Arctic Ocean freshwater pathways., *Nature*, *481*(7379), 66–70, doi:10.1038/nature10705. 1.3.1

Munk, W. H. (1950), On the Wind-Driven Ocean Circulation, doi:10.1175/1520-0469(1950)007<0080:OTWDOC>2.0.CO;2. 1.3

Muschitiello, F., F. S. R. Pausata, J. E. Watson, R. H. Smittenberg, A. A. M. Salih, S. J. Brooks, N. J. Whitehouse, A. Karlatou-Charalampopoulou, and B. Wohlfarth (2015), Fennoscandian freshwater control on Greenland hydrolcimate shifts at the onset of the Younger Dryas, *Nature Communications*, *6*, 1–8, doi:10.1038/ncomms9939. 1.3.2

Muschitiello, F., J. M. Lea, S. L. Greenwood, F. M. Nick, L. Brunnberg, A. Macleod, and B. Wohlfarth (2016), Timing of the first drainage of the Baltic Ice Lake synchronous with the onset of Greenland Stadial 1, *Boreas*, *45*(2), 322–334, doi:10.1111/bor.12155. 1.3.2

Nilsson, J., and G. Walin (2010), Salinity-dominated thermohaline circulation in sill basins: can two stable equilibria exist?, *Tellus A*, *62*(2), 123–133, doi:10.1111/j.1600-0870.2009.00428.x. 5.2.1

Notz, D. (2009), The future of ice sheets and sea ice: between reversible retreat and unstoppable loss., *Proceedings of the National Academy of Sciences*, *106*(49), 20,590–5, doi:10.1073/pnas.0902356106. 1.1.2

Nurser, A. J. G., and S. Bacon (2014), The Rossby radius in the Arctic Ocean, *Ocean Science*, *10*(6), 967–975, doi:10.5194/os-10-967-2014. 1.2.2

Onarheim, I. H., L. H. Smedsrud, R. B. Ingvaldsen, and F. Nilsen (2014), Loss of sea ice during winter north of Svalbard, *Tellus, Series A: Dynamic Meteorology and Oceanography*, *66*(1), 1–9, doi:10.3402/tellusa.v66.23933. 1.1.1, 1.2

Onarheim, I. H., T. Eldevik, M. Årthun, R. B. Ingvaldsen, and L. H. Smedsrud (2015), Skillful prediction of Barents Sea ice cover, *Geophysical Research Letters*, *42*(13), 5364–5371, doi:10.1002/2015GL064359. 1.1.1, 1.2.1

Palter, J. B., M. S. Lozier, and K. L. Lavender (2008), How Does Labrador Sea Water Enter the Deep Western Boundary Current?, *Journal of Physical Oceanography*, *38*(5), 968–983, doi:10.1175/2007JPO3807.1. 4

Peltier, W. R., G. Vettoretti, and M. Stastna (2006), Atlantic meridional overturning and climate response to Arctic Ocean freshening, *Geophysical Research Letters*, *33*(6), L06,713, doi:10.1029/2005GL025251. 1.3.2

Pithan, F., and T. Mauritsen (2014), Arctic amplification dominated by temperature feedbacks in contemporary climate models, *Nature Geoscience*, *7*, 181–184, doi:10.1038/NGEO2071. 1.1.2

Proshutinsky, A., D. Dukhovskoy, M.-l. Timmermans, R. Krishfield, J. L. Bamber, and A. Proshutinsky (2015), Arctic circulation regimes, *Philosophical Transactions of the Royal Society of London A: Mathematical, Physical and Engineering Sciences*, *373*(2052), doi:10.1098/rsta.2014.0160. 1.3.1

Rennermalm, A. K., E. F. Wood, S. J. Déry, A. J. Weaver, and M. Eby (2006), Sensitivity of the thermohaline circulation to Arctic Ocean runoff, *Geophysical Research Letters*, *33*(12), L12,703, doi:10.1029/2006GL026124. 1.3.2

Rennermalm, A. K., E. F. Wood, A. J. Weaver, M. Eby, and S. J. Déry (2007), Relative sensitivity of the Atlantic meridional overturning circulation to river discharge into Hudson Bay and the Arctic Ocean, *Journal of Geophysical Research*, *112*(G4), G04S48, doi:10.1029/2006JG000330. 1.3.2

Reynolds, R. W., N. A. Rayner, T. M. Smith, D. C. Stokes, and W. Wang (2002), An improved in situ and satellite SST analysis for climate, *Journal of Climate*, *15*(13), 1609–1625, doi:10.1175/1520-0442(2002)015<1609:AIISAS>2.0.CO;2. 1.4

Ridley, J. K., J. A. Lowe, and H. T. Hewitt (2012), How reversible is sea ice loss?, *Cryosphere*, *6*(1), 193–198, doi:10.5194/tc-6-193-2012. 1.1.2

Rippeth, T. P., B. J. Lincoln, Y.-D. Lenn, J. a. M. Green, A. Sundfjord, and S. Bacon (2015), Tide-mediated warming of Arctic halocline by Atlantic heat fluxes over rough topography, *Nature Geoscience*, *8*, 191–194, doi:10.1038/ngeo2350. 1.2

Robson, J., P. Ortega, and R. Sutton (2016), A reversal of climatic trends in the North Atlantic since 2005, *Nature Geoscience*, *9*, 1–15, doi:10.1038/ngeo2727. 1.1.3

Roche, D. M., A. P. Wiersma, and H. Renssen (2010), A systematic study of the impact of freshwater pulses with respect to different geographical locations, *Climate Dynamics*, *34*, 997–1013, doi:10.1007/s00382-009-0578-8. 1.3.2

Rudels, B. (2010), Constraints on exchanges in the Arctic Mediterranean-do they exist and can they be of use?, *Tellus A*, *62*(2), 109–122, doi:10.1111/j.1600-0870.2009.00425.x. 1.3, 5.2.1, 5.2.1

Rudels, B. (2015), Arctic Ocean circulation, processes and water masses: A description of observations and ideas with focus on the period prior to the International Polar Year 2007-2009, *Progress in Oceanography*, *132*, 22–67, doi:10.1016/j.pocean.2013.11.006. 1.2.1

Rudels, B. (2016), Arctic ocean stability: The effects of local cooling, oceanic heat transport, freshwater input, and sea ice melt with special emphasis on the nansen basin, *Journal of Geophysical Research: Oceans*, doi:10.1002/2015JC011045. 1.2

Rudels, B., L. G. Anderson, and E. P. Jones (1996), Formation and evolution of the surface mixed layer and halocline of the Arctic Ocean, *Journal of Geophysical Research*, *101*(C4), 8807–8821, doi:10.1029/96JC00143. 1.2

Rudels, B., G. Björk, R. D. Muench, and U. Schauer (1999), Double-diffusive layering in the Eurasian Basin of the Arctic Ocean, *Journal of Marine Systems*, *21*(1-4), 3–27, doi:10.1016/S0924-7963(99)00003-2. 1.2

Rudels, B., M. Korhonen, G. Budéus, A. Beszczynska-Möller, U. Schauer, A. Nummelin, D. Quadfasel, and H. Valdimarsson (2012), The East Greenland Current and its impacts on the Nordic Seas: observed trends in the recent decades, *ICES Journal of Marine Science*, *69*(5), 841–851, doi:10.1093/icesjms/fss079. 2

Schmidtko, S., G. C. Johnson, and J. M. Lyman (2013), MIMOC: A global monthly isopycnal upper-ocean climatology with mixed layers, *Journal of Geophysical Research: Oceans*, *118*(4), 1658–1672, doi:10.1002/jgrc.20122. 1.4

Serreze, M. C., and R. G. Barry (2011), Processes and impacts of Arctic amplification: A research synthesis, *Global and Planetary Change*, *77*(1-2), 85–96, doi:10.1016/j.gloplacha.2011.03.004. 1.1.2

Serreze, M. C., M. M. Holland, and J. C. Stroeve (2007), Perspectives on the Arctic's shrinking sea-ice cover., *Science*, *315*(5818), 1533–6, doi:10.1126/science.1139426. 1.2

Siqueira, L., and B. P. Kirtman (2016), Atlantic near-term climate variability and the role of a resolved Gulf Stream, *Geophysical Research Letters*, *43*, 3964—-3972, doi:10.1002/2016GL068694. 4

Sirevaag, A., and I. Fer (2012), Vertical heat transfer in the Arctic Ocean: The role of double-diffusive mixing, *Journal of Geophysical Research: Oceans*, *117*(7), 1–16, doi:10.1029/2012JC007910. 1.2

Smedsrud, L. H., A. Sorteberg, and K. Kloster (2008), Recent and future changes of the Arctic sea-ice cover, *Geophysical Research Letters*, *35*(20), L20,503, doi:10.1029/2008GL034813. 2

Soden, B., and I. Held (2006), An Assessment of Climate Feedbacks in Coupled Ocean – Atmosphere Models, *Journal of Climate*, *19*(2003), 3354–3360, doi:10.1175/JCLI9028.1. 1.1.2

Spall, M. A. (2013), On the Circulation of Atlantic Water in the Arctic Ocean, *Journal of Physical Oceanography*, *43*(11), 2352–2371, doi:10.1175/JPO-D-13-079.1. 1.2.2, 1.3

Spielhagen, R. F., H. Erlenkeuser, and C. Siegert (2005), History of freshwater runoff across the Laptev Sea (Arctic) during the last deglaciation, *Global and Planetary Change*, *48*, 187–207, doi:10.1016/j.gloplacha.2004.12.013. 1.3.2

Spielhagen, R. F., K. Werner, S. A. Sørensen, K. Zamelczyk, E. Kandiano, G. Budeus, K. Husum, T. M. Marchitto, and M. Hald (2011), Enhanced Modern Heat Transfer to the Arctic by Warm Atlantic Water, *Science*, *331*, 450–453, doi:10.1126/science.1197397. 2

Steele, M., and T. J. Boyd (1998), Retreat of the cold halocline layer in the Arctic Ocean, *Journal of Geophysical Research*, *103*(C5), 10,419–10,435, doi:10.1029/98JC00580. 1.2

Stigebrandt, A. (1981), A Model for the Thickness and Salinity of the Upper Layer in the Arctic Ocean and the Relationship between the Ice Thickness and Some External Parameters, *Journal of Physical Oceanography*, *11*(10), 1407–1422, doi:10.1175/1520-0485(1981)011<1407:AMFTTA>2.0.CO;2. 1.3, 2, 5.2.1

Stommel, H. (1948), The westward intensification of wind-driven ocean currents, *Transactions, American Geophysical Union*, *29*(2), 202, doi:10.1029/TR029i002p00202. 1.3

Stommel, H. (1961), Thermohaline Convection with Two Stable Regimes of Flow, *Tellus*, *13*(2), 224–230, doi:10.1111/j.2153-3490.1961.tb00079.x. 1.3, 5.2.1, 5.2.1

Stouffer, R., J. Yin, and J. Gregory (2006), Investigating the Causes of the Response of the Thermohaline Circulation to Past and Future Climate Changes, *Journal of Climate*, *19*(8), 1365–1387, doi:10.1175/JCLI3689.1. 1.3, 1.3.2

Stroeve, J. C., M. C. Serreze, M. M. Holland, J. E. Kay, J. Malanik, and A. P. Barrett (2011), The Arctic's rapidly shrinking sea ice cover: a research synthesis, *Climatic Change*, *110*(3-4), 1005–1027, doi:10.1007/s10584-011-0101-1. 1.2, 1.2.1

Stroeve, J. C., V. M. Kattsov, A. P. Barrett, M. C. Serreze, T. V. Pavlova, M. M. Holland, and W. N. Meier (2012), Trends in Arctic sea ice extent from CMIP5, CMIP3 and observations, *Geophysical Research Letters*, *39*(16), doi:10.1029/2012GL052676. 1.2

Sverdrup, H. U. (1947), Wind-Driven Currents in a Baroclinic Ocean; with Application to the Equatorial Currents of the Eastern Pacific., *Proceedings of the National Academy of Sciences*, *33*(1), 318–326, doi:10.1073/pnas.33.11.318. 1.3

Swärd, H., M. O'Regan, L. Ampel, R. Ananyev, D. Chernykh, T. Floden, S. L. Greenwood, M. E. Kylander, C. M. Mörth, P. Preto, and M. Jakobsson (2015), Regional deglaciation and postglacial lake development as reflected in a 74 m sedimentary record from Lake Vättern, southern Sweden, *Gff*, *5897*(February 2016), 1–19, doi:10.1080/11035897.2015.1055510. 1.3.2

Swingedouw, D., P. Braconnot, P. Delecluse, E. Guilyardi, and O. Marti (2007), The impact of global freshwater forcing on the thermohaline circulation: Adjustment of North Atlantic convection sites in a CGCM, *Climate Dynamics*, *28*, 291–305, doi:10.1007/s00382-006-0171-3. 1.3.2

Tandon, N. F., and P. J. Kushner (2015), Does External Forcing Interfere with the AMOC's Influence on North Atlantic Sea Surface Temperature?, *Journal of Climate*, *28*(16), 6309–6323, doi:10.1175/JCLI-D-14-00664.1. 1.1.3

Tarasov, L., and W. R. Peltier (2005), Arctic freshwater forcing of the Younger Dryas cold reversal., *Nature*, *435*, 662–665, doi:10.1038/nature03617. 1.3.2

Taylor, K. E., R. J. Stouffer, and G. a. Meehl (2012), An Overview of CMIP5 and the Experiment Design, *Bulletin of the American Meteorological Society*, *93*(4), 485–498, doi:10.1175/BAMS-D-11-00094.1. 1.1.3

Thomson, J., and W. E. Rogers (2014), Swell and sea in the emerging Arctic Ocean, *Geophysical Research Letters*, *41*(9), 3136–3140, doi:10.1002/2014GL059983. 1.2

Tietsche, S., D. Notz, J. H. Jungclaus, and J. Marotzke (2011), Recovery mechanisms of Arctic summer sea ice, *Geophysical Research Letters*, *38*(2), L02,707, doi:10.1029/2010GL045698. 1.1.2

Timmermans, M. L. (2015), The impact of stored solar heat on Arctic sea ice growth, *Geophysical Research Letters*, *42*(15), 6399–6406, doi:10.1002/2015GL064541. 1.2.1

Timmermans, M.-L., and C. Garrett (2006), Evolution of the Deep Water in the Canadian Basin in the Arctic Ocean, *Journal of Physical Oceanography*, *36*(5), 866–874, doi:10.1175/JPO2906.1. 1.2

Timmermans, M. L., C. Garrett, and E. Carmack (2003), The thermohaline structure and evolution of the deep waters in the Canada Basin, Arctic Ocean, *Deep-Sea Research Part I: Oceanographic Research Papers*, *50*(10-11), 1305–1321, doi:10.1016/S0967-0637(03)00125-0. 1.2

van den Berk, J., and S. Drijfhout (2014), A realistic freshwater forcing protocol for ocean-coupled climate models, *Ocean Modelling*, *81*, 36 – 48, doi:http://dx.doi.org/10.1016/j.ocemod.2014.07.003. 1.3.2

Vihma, T., R. Pirazzini, I. Fer, I. A. Renfrew, J. Sedlar, M. Tjernström, C. Lüpkes, T. Nygård, D. Notz, J. Weiss, D. Marsan, B. Cheng, G. Birnbaum, S. Gerland, D. Chechin, and J. C. Gascard (2014), Advances in understanding and parameterization of small-scale physical processes in the marine Arctic climate system: A review, *Atmospheric Chemistry and Physics*, *14*(17), 9403–9450, doi:10.5194/acp-14-9403-2014(REF). 1.2.2

von Appen, W.-J., U. Schauer, T. Hattermann, and A. Beszczynska-Möller (2016), Seasonal cycle of mesoscale instability of the West Spitsbergen Current, *Journal of Physical Oceanography*, pp. JPO–D–15–0184.1, doi:10.1175/JPO-D-15-0184.1. 1.2.2

Wagner, T. J., and I. Eisenman (2015), How Climate Model Complexity Influences Sea Ice Stability, *Journal of Climate*, (1984), 150310071401,001, doi:10.1175/JCLI-D-14-00654.1. 1.1.2

Wang, Q., M. Ilicak, R. Gerdes, H. Drange, Y. Aksenov, D. A. Bailey, M. Bentsen, A. Biastoch, A. Bozec, C. Böning, C. Cassou, E. Chassignet, A. C. Coward, B. Curry, G. Danabasoglu, S. Danilov, E. Fernandez, P. G. Fogli, Y. Fujii, S. M. Griffies, D. Iovino, A. Jahn, T. Jung, W. G. Large, C. Lee, C. Lique, J. Lu, S. Masina, A. J. G. Nurser, B. Rabe, C. Roth, D. Salas y Mélia, B. L. Samuels, P. Spence, H. Tsujino, S. Valcke, A. Voldoire, X. Wang, and S. G. Yeager (2016), An assessment of the Arctic Ocean in a suite of interannual CORE-II simulations. Part I: Sea ice and solid freshwater, *Ocean Modelling*, *99*, 86–109, doi:10.1016/j.ocemod.2015.12.009. 1.2

Winton, M. (2006), Amplified Arctic climate change: What does surface albedo feedback have to do with it?, *Geophysical Research Letters*, *33*(3), 1–4, doi:10.1029/2005GL025244. 1.1.2

Yang, J., A. Proshutinsky, and X. Lin (2016), Dynamics of an idealized Beaufort Gyre: 1. The effect of a small beta and lack of western boundaries, *Journal of Geophysical Research : Oceans*, *121*, 1249–1261, doi:10.1002/2015JC011296. 1.2, 1.2.2

Yeager, S. G., A. R. Karspeck, and G. Danabasoglu (2015), Predicted slowdown in the rate of atlantic sea ice loss, *Geophysical Research Letters*, *42*(24), 10,704–10,713, doi:10.1002/2015GL065364, 2015GL065364. 1.2

Yoshimori, M., M. Watanabe, A. Abe-Ouchi, H. Shiogama, and T. Ogura (2014), Relative contribution of feedback processes to Arctic amplification of temperature change in MIROC GCM, *Climate Dynamics*, *42*(5-6), 1613–1630, doi:10.1007/s00382-013-1875-9. 1.1.2

Yu, L., Y. Gao, and O. H. Otterå (2015), The sensitivity of the Atlantic meridional overturning circulation to enhanced freshwater discharge along the entire , eastern and western coast of Greenland, *Climate Dynamics*, *46*(5), 1351–1369, doi:10.1007/s00382-015-2651-9. 1.3.2

Zhang, R. (2015), Mechanisms for low-frequency variability of summer Arctic sea ice extent., *Proceedings of the National Academy of Sciences*, *112*(15), 4570–5, doi:10.1073/pnas.1422296112. 1.1.1, 1.2